Universiteit Utrecht

‘Mapping changing groundwater levels in Northeast Thailand throughout the 21st century considering climate change conditions’

- A modelling study using iMOD –

01 July 2019

Utrecht University
Faculty of Geosciences
Earth Surface and Water
Hydrology

‘Mapping changing groundwater levels in Northeast Thailand throughout the 21st century considering climate change conditions’

- A modelling study using iMOD –

01 July 2019

Wouter Sebastiaan Goofers
Studentnumber: 4062809
Earth Surface and Water

In loving memory of my grandfather, without whom I would not be where I am today.

Wouter Janse, 1926 - 2017

Abstract

English

The north-eastern region of Thailand, referred to as "Isan", experiences the most extensive droughts when compared to the rest of the country. Increasing water demands due to population growth and agricultural development has resulted in more frequent and severe water shortages. It is expected that during the 21st century Global Climate Change will be putting more strain on the limited fresh water resources.

During droughts the, mostly rural, population are more reliant on already declining groundwater resources. While excessive groundwater extraction could leave residents without drinking water during a prolonged dry season, a dropping water table could also further increase the regions problems with salt water intrusion.

To aid in decision-making processes, when considering water resource management in Isan, the areas where the biggest changes in groundwater level are expected for the year 2050 and 2100 were identified. To account for the effects of climate change, delta changes derived from three climate models (GFDL-ESM2M, IPSL-CM5A-LR, MPI-ESM-MR) were imposed on meteorological observations. Subsequently, the expected change in groundwater recharge was calculated and used as an input for a one-layered steady-state finite-element groundwater model. The relative differences between the modelled historic and future periods were then calculated for two climate change scenarios (RCP 4.5 and 8.5) and two pumping scenarios.

The annual RCM climate modelling results show, although systematically underestimated and less so for extreme values, a similar distribution as the observations. A decrease in the hydraulic head is predicted for all scenarios at the end of the 21st century. While groundwater extraction exerts more influence locally, climate change causes a more evenly spread decline of the groundwater head over the entire north-east of Thailand. In general, taking into consideration the hydrological model's limitations, the most remarkable changes in groundwater elevation are located the furthest from riparian areas and coincide with the location most effected by groundwater extraction. These areas, besides Buriram, are all situated in the Chi watershed and include for the most part the provinces of Chaiyaphum Mahasarakham, Roi Et and Nong Bua Lamphu.

With the already expected decline of groundwater head defined within this study throughout all of Isan because of climate change, a continued intensification of groundwater extraction could lead to an increase in saltwater intrusion and eventually the unavailability of the groundwater resources for domestic purposes. Because of its importance for the livelyhood of the region during water shortages, it is advised not to expand upon groundwater utilization for irrigational purposes, especially for those regions defined in this research to be most affected during the 21st century, to keep the resource available as a safeguard throughout periods of drought.

Dutch
Het noordoosten van Thailand, ook wel Isaan genoemd, ondervindt de meest wijdverspreide droogtes in verhouding tot de rest van het land. Vanwege de bevolkingsgroei en landbouwontwikkelingen heeft een toename in de watervraag ertoe geleid dat watertekorten steeds nijpender worden. Naar verwachting zal klimaatverandering tijdens de 21ste eeuw nog meer druk zetten op de nu al gelimiteerde zoetwater voorraad.
De voornamelijk agrarische bevolking is in tijden van droogte in toenemende mate aangewezen op de afnemende hoeveelheid beschikbaar grondwater. Door de overmatige onttrekking van grondwater daalt de grondwaterspiegel waardoor er drinkwater tekorten kunnen ontstaan en er verdere intrusie van zout water kan plaatsvinden.

Met als doel behulpzaam te zijn bij het maken van beslissingen met betrekking tot het managen van grondwater in Isaan zijn de gebieden waar de grootste veranderingen in de grondwaterspiegel optreden in kaart gebracht voor het jaar 2050 en 2100. Klimaatverandering is hierbij in acht genomen door een delta change te onttrekken uit drie klimaatmodellen (GFDL-ESM2M, IPSL-CM5A-LR, MPI-ESM-MR) en deze toe te passen op meteorologische observaties. Vervolgens is de verwachte verandering in de jaarlijkse hoeveelheid water beschikbaar voor het aanvullen van het grondwater berekend en gebruikt voor het doorrekenen van de toekomstige grondwaterstanden in een enkel-laags statisch grondwater model voor een stabiele toestand. De relatieve verschillen tussen de gemodelleerde historische en toekomstige periodes zijn daarna doorgerekend voor twee klimaatscenario's (RCP4.5 en RCP8.5) en voor twee scenario's waarin de intensiteit van de grondwateronttrekking wordt gevarieerd.

De op jaarbasis gemodelleerde resultaten laten een systematische onderschatting zien en extreme waarden worden minder goed gerepresenteerd, maar over het algemeen wordt eenzelfde distributie getoond als geconstateerd bij de metingen. Een afname in de stijghoogte aan het eind van de 21ste eeuw wordt voorspeld door alle scenario's. Terwijl de invloed van grondwateronttrekkingen lokaal een grotere invloed uitoefent, zorgt klimaatverandering voor een meer gelijkmatig verspreide daling van de grondwaterspiegel over de gehele noordoostelijke regio van Thailand.
Met in achtname van de limitaties van het hydrologisch model, zijn de meest opmerkelijke veranderingen in de grondwaterstanden over het algemeen te vinden daar waar ze het verst verwijderd zijn van de invloedssfeer van de rivieren én overlappen met de gebieden die het meest worden beïnvloed door grondwater extractie. Deze gebieden, behalve Buriram, bevinden zich, zo goed als allemaal, in het stroomgebied van de Chi rivier en omvatten voornamelijk de provincies Chaiyaphum, Mahasarakham, Roi Et en Nong Bua Lamphu.

Met de in dit onderzoek reeds vastgestelde verwachtte daling van de grondwaterspiegel voor heel Isaan, kan een verdere intensivering van grondwater extractie er toe leiden dat grondwater op bepaalde momenten niet meer beschikbaar zal zijn voor huishoudelijk gebruik en zout water intrusie een groter probleem zal worden.
Vanwege het belang van grondwater voor de leefbaarheid van de omgeving tijdens watertekorten wordt dan ook aanbevolen om het gebruik van grondwater voor irrigatiedoeleinden niet verder uit te breiden, om zo de beschikbaarheid ervan voor huiselijk gebruik te kunnen blijven waarborgen in tijden van droogte. Dit geldt in het bijzonder voor de gebieden die in dit onderzoek zijn geïdentificeerd als het meest beïnvloed tijdens de 21ste eeuw.

Thai
ภาคตะวันออกเฉียงเหนือของประเทศไทยเรียกว่า"อีสาน"ประสบภัยแล้งที่กว้างขวางที่สุดเมื่อเทียบกับส่วนที่เหลือของประเทศซึ่งมีความต้องการน้ำที่เพิ่มขึ้นเนื่องจากการเติบโตของประชากรและการพัฒนาการเกษตรส่งผลให้เกิดการขาดแคลนน้ำบ่อยครั้งและรุนแรงขึ้นคาดว่าในช่วงศตวรรษที่21การเปลี่ยนแปลงสภาพภูมิอากาศโลกจะส่งผลกระทบต่อแหล่งน้ำจืดที่จำกัดมากขึ้น
ในช่วงฤดูแล้งประชากรในชนบทส่วนใหญ่พึ่งพาทรัพยากรน้ำใต้ดินที่ลดลงอยู่แล้วในขณะที่การสกัดน้ำใต้ดินมากเกินไปอาจทำให้ผู้อยู่อาศัยไม่มีน้ำดื่มในช่วงฤดูแล้งที่ยาวนานตารางน้ำหยดอาจช่วยเพิ่มปัญหาในภูมิภาคด้วยการรุกล้ำของน้ำเค็ม

เพื่อช่วยในกระบวนการตัดสินใจเมื่อพิจารณาการจัดการทรัพยากรน้ำในภาคอีสานพื้นที่ที่คาดว่าจะมีการเปลี่ยนแปลงระดับน้ำบาดาลที่ใหญ่ที่สุดในปี2050และ2100เพื่ออธิบายถึงผลกระทบของการเปลี่ยนแปลงสภาพภูมิอากาศได้มีการกำหนดการเปลี่ยนแปลงเดลต้าจากแบบจำลองภูมิอากาศสามแบบ(GFDL-ESM2M, IPSL-CM5A-LR, MPI-ESM-MR)ในการสังเกตการณ์ทางอุตุนิยมวิทยา
จากนั้นการคำนวณการเปลี่ยนแปลงที่คาดหวังในการเติมน้ำใต้ดินจะถูกคำนวณและใช้เป็นข้อมูลสำหรับแบบจำลองน้ำใต้ดินอันมีค่าคงที่แบบองค์ประกอบเดียวจากนั้นคำนวณความแตกต่างสัมพัทธ์ระหว่างช่วงเวลาในอดีตและอนาคตที่จำลองไว้สำหรับสถานการณ์การเปลี่ยนแปลงของสภาพภูมิอากาศสองสถานการณ์(RCP4.5และ8.5)และสถานการณ์การปั๊มสองสถานการณ์

ผลการสร้างแบบจำลองสภาพภูมิอากาศRCMประจำปีแสดงให้เห็นว่าแม้จะประเมินต่ำกว่าความเป็นระบบและมีค่าน้อยมากการคาดการณ์การลดลงของหัวไฮดรอลิกสำหรับทุกสถานการณ์ในปลายศตวรรษที่21ในขณะที่การสกัดน้ำบาดาลมีอิทธิพลต่อท้องถิ่นมากขึ้นการเปลี่ยนแปลงภูมิอากาศทำให้หัวน้ำใต้ดินลดลงอย่างสม่ำเสมอทั่วภาคตะวันออกเฉียงเหนือของประเทศไทยโดยทั่วไปเมื่อคำนึงถึงข้อจำกัดของตัวแบบอุทกวิทยาการเปลี่ยนแปลงที่น่าทึ่งที่สุดในการยกระดับน้ำใต้ดินจะอยู่ห่างจากพื้นที่ชายฝั่งและใกล้เคียงกับตำแหน่งที่ได้รับผลกระทบมากที่สุดจากการสกัดน้ำใต้ดินพื้นที่เหล่านี้นอกเหนือจากบุรีรัมย์ที่ตั้งอยู่ในพื้นที่ลุ่มน้ำชีและส่วนใหญ่เป็นจังหวัดชัยภูมิมหาสารคามร้อยเอ็ดและหนองบัวลำภู

อย่างไรก็ตามด้วยความคาดหวังที่ลดลงของหัวน้ำใต้ดินที่กำหนดไว้ในการศึกษานี้ตลอดทั้งภาคอีสานเนื่องจากการเปลี่ยนแปลงสภาพภูมิอากาศการสกัดน้ำใต้ดินที่เข้มข้นอย่างต่อเนื่องอาจนำไปสู่การเพิ่มขึ้นของการรุกล้ำของน้ำเค็มและในที่สุดเนื่องจากมีความสำคัญต่อความมีชีวิตชีวาของภูมิภาคในระหว่างการขาดแคลนน้ำจึงไม่ควรขยายการใช้น้ำบาดาลเพื่อวัตถุประสงค์ในการชลประทานโดยเฉพาะอย่างยิ่งสำหรับภูมิภาคที่กำหนดไว้ในการวิจัยนี้จะได้รับผลกระทบมากที่สุดในช่วงศตวรรษที่21เป็นการป้องกันตลอดช่วงฤดูแล้ง

Expression of gratitude

Hereby I would like to make use of the opportunity to explicitly thank all parties that made the realization of this research report possible.

Starting with Mr Robin Brown, Mr Justin Lefty Formby, Ms Chelsea Lynn and especially Ms Suphansa Nilnoree for helping to establish first contact with the Royal Irrigation Department (RID), giving a foothold to kick-start the project.

From the RID, I would like to express my gratitude towards Ms Supinda Wattanakarn and Mr Adisorn Champathong for their assistance in communicating with the Thai Meteorology Department (TMD) and the Department of Groundwater Resources (DGR), but also their time and effort spend on listening to my proposition and their input regarding the aim of the research project were much appreciated.

From the DGR, I would like to thank Ms Ocpasorn Occarach and her staff for their assistance with the collection of contiguous subsurface data.

From Ramkhamhaeng University's RU-CORE department, I would like to thank assistant professor Mr Dr Jerasorn Santisirisomboon and his staff for helping to obtain to necessary climate data and for their invitation to join the SARCCIS conference.
Also working at the Ramkhamhaeng University (RU), I want to show my appreciation towards both Ms Sirikamol Sirisumpan and Ms Pakul Hathairattanakool for helping to develop a better understand of the Thai language.

From Utrecht University, I would like to thank: both Mr Maarten Zeylmans van Emmichoven MSc for his technical support and Mr Dr Rens van Beek as the second corrector for this research paper. Furthermore, special thanks goes out to the research project supervisor Mr Dr Niko Wanders, who had welcome ideas on how to improve the quality of this research report and was able to provide motivation and support throughout.

Last, but not least, I would like to thank my father, Mr Michiel Goofers, for his input regarding the paper's textual demeanour and Ms Wanassa Srisawat for helping me with Thai translations and improving my Thai language proficiency. I would also like to express my gratitude towards my mother, Ms Kitty Jaspers and especially my girlfriend, Ms Jumjee Nammungkun, for the support she provided during the time spend in Thailand.

Some final words, in both figurative and literal sense, seem appropriate here to commemorate my late friend and colleague diving instructor Tanguy Metz, who passed away during the writing of this report.

'Tanguy, I very much enjoyed all our good times together. It is with pain in my heart that I have to say farewell to you so soon. I am forever sorry that I will not be able to come and visit you as we had once planned.

It gives me great solace that, at the time, I know you were following your dreams. You never compromised on what was important to you, even if that meant risking an uncertain future. For this I admire you.

Your untimely departure came as a lightning strike from a blue sky and both as my diving buddy and as my friend you will be missed. May you rest in peace my friend.'

Wouter Goofers, Utrecht, July 2019

Prelude

Being the culmination of the received education so far, a reflection upon the process of writing this masterthesis seems appropriate. The experiences it has brought, and the lessons learned, will not be forgotten anytime soon.

The freedom to choose your own research subject can be both a blessing and a curse. Although overwhelmed by the possibilities at first, it also gave the opportunity to pursue personal interests.
Wanting to gain experience working abroad in a non-western country, it very soon became clear that Thailand would be the country of choice. Having been there several times before, the awareness of the differences in diet and the language barrier were already present. Also, previously established friendships would prove invaluable in establishing contact with the relevant governmental departments.
Taking part in a master's that has a focus on hydrology and having a background in environmental sciences, the decision was quickly made to pick a subject that would combine the knowledge of both studies. After reading into the country's situation regarding its water related challenges, it became evident that a groundwater model, that would take climate change into consideration for the 21st century would be of added value.

As soon as the choice was made to perform the masterthesis in Thailand, the first challenge already presented itself. How to establish communications with the foreign authorities concerned with the topic of choice?
In this matter the importance of networking became very apparent. Through a long, and at times unlikely, chain of contacts, communications were established with Ms Suphansa Nilnoree, a young Thai woman with altruïsm at her core. With her aid, and a lot of patience, an audience was arranged at the Royal Irrigation Department (RID), who showed an interest in hearing the ideas for the masterthesis presented in this document.

Not wanting to dive in nose first without having any guarantee on a successful endeavour, acquaintances were made with the RID during the summer holidays to establish the possibility of acquiring the necessary data to commence the research project.
Fortune favours the bold, as the reception by Ms Supinda and Mr Champatong from the RID was most hospitable. They provided a listening ear and were very helpful during the remainder of the quest for the required data.
Sequentially visitations were also made at the Thai Meteorological Department (TMD) and the Department of Groundwater Resources (DGR). Having established the benevolence of the parties involved, sufficient confidence was gained to move forward with the research project.
With time to spare, the opportunity arose to travel through the region in question, providing even more incentive to write the research report.

Having returned home, enough material was gathered to write a research proposal that was able to convince both the project supervisor Mr Dr Niko Wanders and the University of Utrecht (UU) to greenlight the project.
Before flying back to Bangkok, further preparations were made to get more of an edge in my communications upon my return in Thailand. I started Thai language lessons under the supervision of Ms Wanassa Srisawat, who taught me a great many things that turned out to be more than helpful in establishing relations.
Also, on a technical level, preparations had to be made. Being able to work with a Geographical Information System (GIS) was required to processes the spatial information that would be provided by the Thai. Partaking in a GIS-course to acquire the necessary skills, introductions were made with Mr

Maarten Zeylmans van Emmichoven MSc, who proved to be not only most helpful as a teacher, but also as an advisor later on, during the more technical stages of the research project.
Besides learning the basics of the Thai language and the necessary computer skills, having the financial resources to facilitate a prolonged stay in Bangkok (three months) was also a major obstacle that needed to be resolved. Having chosen a country that is not only outside of the European Union, but also has little to no ties with the UU, financial sacrifices had to be made according to my priorities.

With all preparation finished, the research project started at the beginning of December 2018. On arrival, one week was set-aside for finding an accommodation that was reasonably priced, but also close to the public transport system and clean. This turned out to be quite the challenge, but after a lot of phone calls and running around a vacant studio-apartment that fitted the description was found. After settling down in the apartment, a couple of days were left (and needed) to explore the neighbourhood and adjust to the new surroundings.
Full of energy, contacts established during the summer holidays were visited, starting at the RID. Not having forgotten the research proposal presentation in August, the desired attention was received. The RID then followed up by providing the necessary documentation to procure the desired meteorological data from the Thai Meteorology Department (TMD) and opened the doors at the Department of Groundwater Resources (DGR) for further discussion. The DGR gave a warm welcome as well and provided support with the analysis of subsurface data.

According to the schedule constructed when writing the research-proposal, the KNMI-climate explorer would be used to consider a change in the meteorological variables. However, during the analysis of the GCM records, it became clear that the model resolution with a meridian arc of 2.5 degrees would not suffice when compared to the measurements from the TMD's AWSs. Therefore, substitute climate models with a higher resolution were required.
Luckily, the Ramkhamhaeng University Centre Of regional climate change and Renewable Energy (RU-CORE), which was literally around the corner, just started distributing their dynamically downscaled GCMs. Their models' resolution was good enough to calculate the changes for the individual AWSs and after a quick visit, explaining the research intentions, an invitation was procured for the "training workshop of access and utilization of regional climate downscaled data of Southeast Asia Regional Climate Change Information System (SARCCIS)".
Meanwhile, being at the Ramkhamhaeng (RU), wanting to make the most of the opportunity, contact was established with two young language professors who were teaching at the university. Both Ms Sirikamol Sirisumpan and Ms Pakul Hathairattanakool agreed to a language exchange that would benefit both parties.

After about a month, the heat (on average 35 degrees Celsius) became much more tolerable and the body had not only adjusted to the change in diet, but also the wide variety of delicious Thai dishes made every meal something to look forward to!
Progressions became visible in the analysis of the data that was being collected and, equally important, activities other than work were revitalizing, as was the opportunity to return to the research area in question.

Although enjoying the experience, it wasn't all fun and games. More than once, it was quite the opposite. Having to pick up how to write R-script to obtain the required information from netCDF-files supplied by the RU-core and having to learn how to use IMOD, without any support, was sometimes very frustrating. Also, balancing expenses and making ends meet was not an easy task within the budget that was at hand.
Furthermore, not being able to express oneself in the nuances only possible in the native tongue, or not being able to be understood in a foreign language, can really get on one's nerves. With only few people around that spoke proper-English, let alone Dutch, it was, at times, lonely. Moral even reached

an all-time low when the news came that a good friend, and colleague diving instructor, had passed away in a motorcycle accident. Thankfully, loved ones are never far away when needed.

Nearing the end, Bangkok felt like a home, making the return journey one with mixed feelings. Life in Bangkok was much enjoyed and there was still so much to see and do, but the missing computational requirements and the necessity to converse with Mr Dr Wanders about the research results and structure became ever more pressing.

Back home, the work pace had to be picked up a notch. Being able to ask questions regarding computer technical issues, computational progress became a lot quicker. Having done a lot of data preparation beforehand, the hydrological computer model was running in no time and results started pouring in. Making a clear overview of all the data proved to be a major challenge. Debugging, writing and re-writing, all tedious at best, resulted in long days. But, he who perseveres wins, and after six months and a lot of effort, the masterthesis was completed.

Looking back, there are a couple of subjects that deserve to be underlined.
First, without a social network, the entire project would have never gotten off the ground. Having the right contacts was not only important to establish business relations, but it was also of great value on a personal level. When something like the passing of a friend occurs, it proved equally important to have a network of supportive people during such difficult times.
Secondly, both (a lot of) patience and a having a keen eye on the future needs were significant factors in gaining timely results. Unfortunately, not all that information that was needed was known from the start. Preparation is key and knowing what and how you want it needs to be clear before any meeting to prevent missed opportunities. Although there might have been extra resources that, when added, could have resulted in a better thesis, data flaws and shortcomings only became apparent when finishing up processing back home. Not being able to request or receive additional data in time to enhance the research, a point was reached at which the resources at hand just had to suffice. The fact that improvements can always be made led to the realisation that, in the end, it is all about creating the best result with the information available, which sometimes, leads to concessions.
Finally, it is not only the available resources, but also the available time that was of major importance. The difficulties of time management became very prominent when opportunities were encountered to enhance the research report. Making a schedule is one thing but sticking to it is something else entirely. An example of a consideration between quality and time-management was the use of the KNMI-Climate explorer to calculate a future change in the temporal dynamics of meteorological variables. Due to its coarse resolution, spatial variation would have been impossible to capture. By keeping eyes and ears open, implementing the climate data from the RU-CORE made the project much better for it, but at the cost of a significant amount of time. With every opportunity, the question must be asked what is there to be gained and how much time does it cost?

To conclude this retrospective, probably the most important is taking the time to enjoy it all. Being so far from home, experiencing cultural differences in an altogether gorgeous scenery makes everything worthwhile. Witnessing shared struggles and seeing the differences in how to cope with them is fascinating. The privileges of Western society, but also its shortcomings, are laid bare, especially when comparing social constructs and there is lots to be learned from it.
I have experienced the Thai as a hospitable, but proud people whom are both tolerant and patient with foreigners, and I would return in a heartbeat, being for business or otherwise.

It took a leap of faith to start this project. With many uncertainties down the road it was a real challenge, but a fun one at that and never did it lead to regret. The final challenge to conclude this master's program will be an internship. Wanting to see the more of the world and the opportunities it presents, efforts are now being made to collaborate with foreign entities and work together on giving ourselves, and the generations to come, a more sustainable future.

Table of Contents

Glossary and abbreviations

Glossary:	Meaning:
Homogeneous	Properties of a medium are different depending on the direction, but the same for different locations.
Isotropic	Properties of a medium are the same in a certain direction, but different per location.
Isotropic homogeneous	Medium properties are the same in every direction and for every location.
Permeability	Intrinsic property of a medium describing its pore space interconnectivity.
Hydraulic conductivity	A rate at which water flows through a porous medium, while considering fluid properties.
Transmissivity	The transmissivity is the hydraulic conductivity multiplied by the aquifer thickness.
Watershed	A system of surface and subsurface water that converges to a single outlet.
Systematic bias	A systematic error that has the tendency to produce a specific result.
Recharge	The water that, after infiltrating the soil, percolates to the groundwater table.
Riparian area	The area directly affected by the presence of a river.
Hydraulic head	The potential surface elevation of the water table.

Abbreviations:	Meaning:
RID	Royal Irrigation Department
TMD	Thai Meteorology Department
DGR	Department of Groundwater Resources
GCM	Global Circulation Model
GIS	Geographical Information System
RCM	Regional Climate Model
GCC	Global Climate Change
pr	precipitation
tas	average temperature
tasmax	maximum temperature
tasmin	minimum temperature
rh	relative humidity
sh	sunshine hours
et	pan-evaporation
evspsbl	actual evaporation including sublimation and transpiration
MODFLOW	Modular Three-Dimensional Finite-Difference Groundwater Flow Model
IPF	iMOD Point File
IDF	iMOD Data File
CRAE	Complementary Relationship Areal Evapotranspiration
RMSE	Root Mean Square Error
netCDF	network Common Data Form
RCP	Representative Concentration Pathway
Ens	Ensemble
GFDL-ESM2M (GFDL)	Geophysical Fluid Dynamics Laboratory – Earth System Model 2M
IPSL-CM5A-LR (IPSL)	Institute Pierre Simon Laplace - Climate Model 5A – Low Resolution
MPI-ESM-MR (MPI)	Max Planck Institute – Earth System Model - MR

1. Introduction

1.1 Context

In May 2019, Thailand's department of disaster prevention and mitigation declared the provinces Phitsanulok, Roi Et, Sisaket, Mahasarakham, Nakhon Ratchasima, Trat, Chon Buri drought disaster zones, implying that these provinces had severe shortages of fresh water (Kemtong & Angskul, 2019). Four out of seven of these provinces: Roi et, Sisaket, Mahasarakham and Nakhon Ratchasima are situated in the Northeast of Thailand, a region that experiences the most extensive droughts of the country (Chitradon et al, 2009).

The north-eastern region, referred to as "Isan", is part of the Mekong basin (figure 1). Covering roughly 18% of the Mekong's catchment area, its contribution to the Mekong river's discharge (6%) is rather small compared to its size and corresponds with the relatively dry nature of the region (Toda et al., 2004).

Isan, comprised of 19 provinces (appendix, A1), houses approximately one-third (20 million people) of Thailand's population and has, compared to the rest of Thailand, the highest percentage of land dedicated to agricultural practices, with paddy rice as the main cultivated crop (Floch & Molle, 2008). Most of its inhabitants are farmers, who constitute the poorest class of people in Thailand and are getting poorer (Sanyu Consultants Inc., 2010).

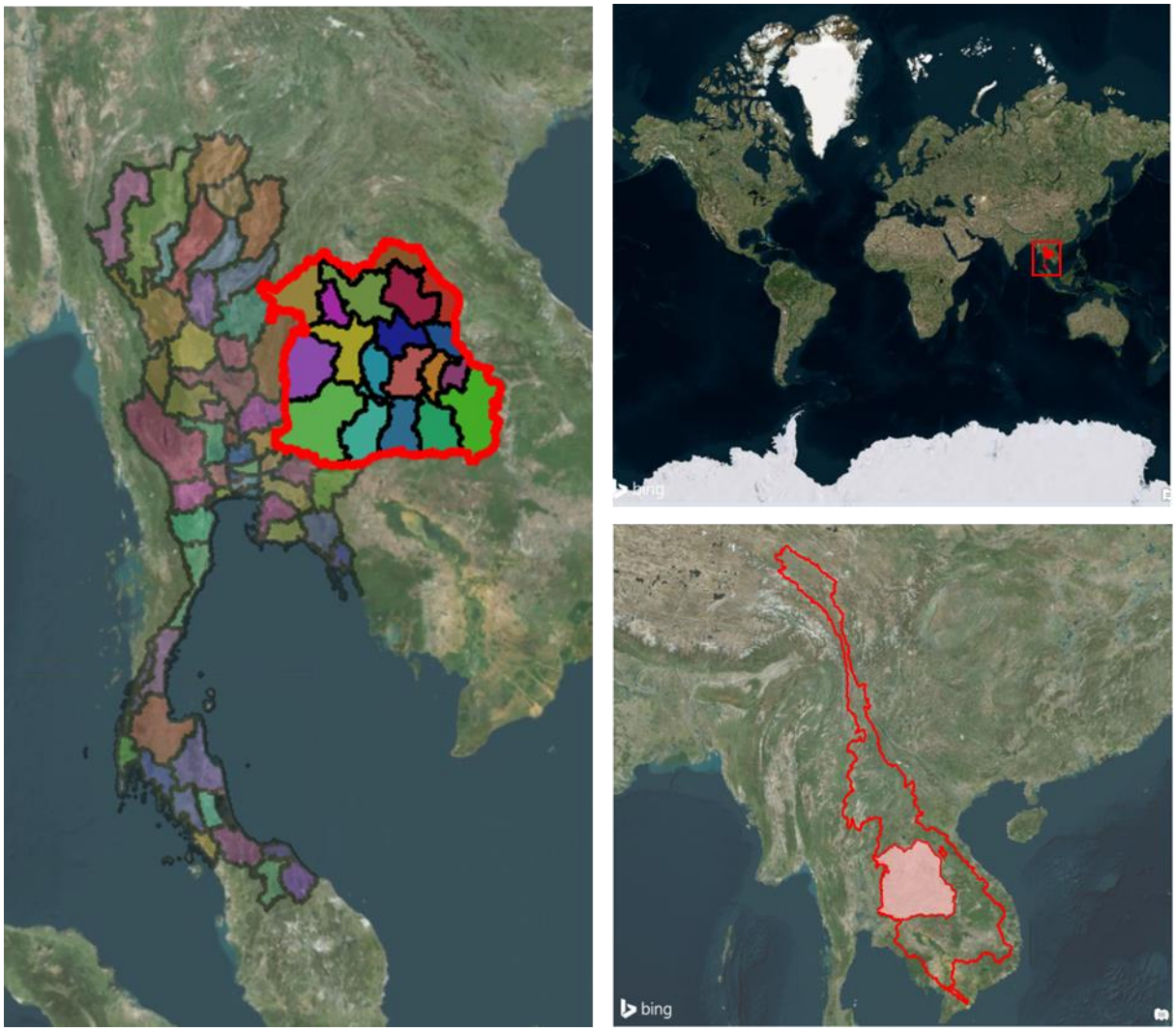

Figure 1: Highlighted in the top right corner is Thailand's location on the globe. On the left, the relative position of the north-eastern region and, in the bottom right, Isan's position within the Mekong watershed (Bing Maps Aerial, 2019).

Although it is the largest agricultural area by size, it is not the most productive. The region has relatively low productivity, due to its infertile and saline soils and a lack of water storage and resources (Floch & Molle, 2008; Fornés & Pirarai, 2014). However, contributing 45% to Thailand's total rice harvest, Isan is not only of major importance in Thailand's role as the second largest exporter of rice in the world (33%), which is a major contributor to the roughly 12% of the country's Gross Domestic Product (GDP) earned with the export of agricultural products, but also provides employment for roughly 35% of the population (Sanyu Consultants Inc., 2010).

1.2 Problem definition

1.2.1 Drought

Starting in 1950, Thailand's population had tripled in size by the end of the millennium and only has begun to level off in recent years (Worldometers.info, 2019). While urbanisation has been increasing rapidly, in 2009, around two-thirds of the population still lived in rural areas (FAO, 2016; Worldometers.info, 2019). Coinciding with this population growth was large scale deforestation to benefit agricultural and economic development (Marks, 2011; Thailand Country Report, 2009). With roughly 90% of the available water resources being used for agriculture, this change in land-use led to an increased water demand, which initiated a now emerging water shortage (FAO, 2016).

Thailand has three distinct seasons, a wet season, from May until October, a (relatively) cool dry season from October until February and a hot dry season during March and April (FAO, 2016). It is especially during the (later) dry season that water shortages are most prominent. Several studies have investigated Isan's drought sensitivity and underlined the regional consequences of the increasingly more frequent and severe water shortages (Chitradon et al, 2009; Krittasudthacheewa et al., 2012; Mongkolsawat et al., 2009; Thailand Country Report, 2009 & 2016).

1.2.2 Management

Although being dry and marginal land with low runoff, Isan has been a rural area long before it was part of Thailand. When Thai rule became more present in the beginning of the 20th century, irrigation schemes were constructed for several reasons: to stabilize crop production, for dry season cultivation, to combat rural poverty, to ensure food security with rapid population growth, to fight against communism and to win voters (Floch and Molle, 2008).

In 2001, roughly 25% (12000 km^2) of all public irrigation schemes in Thailand were situated in Isan (Boonlue, 2005; Floch & Molle, 2008; Sethaputra et al., 2001). Irrigation is primarily used as a supplement during the rainy season, but already experiences shortages during that period, with 79% of the areas equipped for irrigation actually watered (FAO, 2016). During the dry season, even less water is available, only facilitating irrigation for less than 5% dry season cropping (Floch & Molle, 2008). Water storage is needed to capture the irregular runoff which can then be used for irrigation. Also, river water from the Mekong is diverted and vital for irrigation development. Many small, medium and large-scale irrigation projects were realised to supply water to the region's vast agricultural lands, but due to a lack of a general distribution network the combined irrigation efforts cover only 9% of the arable land (Floch & Molle, 2008).

Considering the future, potentially irrigated area estimations fluctuate considerably and reach a maximum of approximately 30% of the cultivated lands (Boonlue, 2005; Floch & Molle, 2008). However, investment returns have been very limited due to unsuccessful dry season cropping (Floch & Molle, 2008; NEDECO, 1988; Palanisami & Apinantara, 1984). Furthermore, all sites most ideally suited for irrigation practices have already been exploited in early development stages (Molle, 2003), making expending upon irrigation systems, economically speaking, not very lucrative (Floch & Molle, 2008).

Besides finding irrigation sites whose development costs are proportional to its economic returns, irrigation development faces many more difficulties in Isan. Undulating topography makes it difficult to construct storage sites and low water holding capacity of sandy soils causes rapid infiltration (Bell & Seng, 2004; Floch & Molle, 2008; Fukai et al., 1995). Also, salt bearing sediments have already affected 10% of all irrigated areas by making the water used for irrigation saline (FAO, 2016; Floch & Molle, 2008). Together with low commodity prices (Prapertchob, 2001) and the necessity of forced resettlement for large scale projects (Lightfoot, 1981) irrigation schemes have a hard time coming of the ground (Floch & Molle, 2008).

Although there has been a general movement towards less water-demanding crops, the focus for decreasing the water stress should be on increasing efficiency in the agricultural sector or moving away from agricultural dominance altogether (FAO, 2016; Floch & Molle, 2008).
Instead, increased development of, especially, dry season cropping has created higher water demands, making the region more vulnerable to droughts, and has led to agricultural underperformance (Bell & Seng, 2004; FAO, 2016).

1.2.3 Climate change

The possibility of Thailand to be adversely affected by climate change is very present (Ecktein et al., 2019). Because irrigation only covers a relatively small percentage of the agricultural area present, most of Isan is dependent on precipitation to sustain its crops (Sanyu Consultants Inc., 2010). It is expected that Global Climate Change will result in an increase in temperature and more intense, less frequent rainfall, creating longer lasting droughts (Limsakul et al., 2019). The regions high evaporation rates (KKU-Ford, 1982; Limpinuntana, 2001) are only expected to increase with the predicted rise in temperature, causing even more extreme droughts, especially during El Niño events when temperature rise further still (Thailand Country Report, 2009). Therefore, it can be expected that the strain on the already limited water resources will intensify, making water shortages more common in the future and especially problematic for those farmers who do not have access to irrigation waters.

1.2.4 Groundwater extraction

Nowadays, water demands are met for the most part by applying surface water (83%), while the remainder is supplied through groundwater extraction (17%) (FAO, 2016). Unfortunately, the water demand far exceeds renewable sources, which account for only 22% of the total demand (Fornés & Pirarai, 2014).
The majority of the population in Isan uses groundwater to compensate for water shortages, especially during dry season. Most of these wells have a low yield (around 48m^3/day) and are used for domestic consumption (Floch & Molle, 2008; Fornés & Pirarai, 2014).
Even so, groundwater extraction rates surpass the natural recharge capacity, resulting in a lowering of the water table (Fornés & Pirarai, 2014). Considering an increase in both water demand because of irrigation and in droughts because of climate change, it is not unrealistic to assume an increased strain on the groundwater resources. Furthermore, due to large parts of Isan having saline soils, a lowering of the groundwater table is increasing the distribution of saline groundwater (appendix, A2), effecting the livelyhood of the region (Patamatmkul, 2001; Pholkern et al., 2018; Srisuk, 1997; Wongsomsak, 1986).

1.2.5 Problem definition

An increase in population, agricultural development and irrigation schemes have led to higher water demands in Isan, an area that has limited water resources and high evaporation rates. As a result, water shortages are currently emerging. These shortages are expected to increase with global warming due to an increase in temperature, leading to more frequent and severe droughts. It can be assumed

that during these droughts the population will be more reliant on already declining groundwater resources. However, increased pumping could have considerable consequences for the livelyhood of the region. While depletion of fresh groundwater would leave residents without drinking water, a dropping water table could also further increase the regions expanding saline groundwater areas.

So far, there seems to be no plan regarding the impact of climate change and action has been mostly reactive (Friend & Thinphanga, 2018). Therefore, it would benefit long-term decision making if the impact that climate change will have on groundwater resources is known. To be able to take effective prevention and mitigation measures, areas were groundwater levels are expected to be most affected need to be identified first, thus leading to the following research question and objective.

1.3 Research question

To what extent will climate change and groundwater extraction affect the groundwater levels in Isan throughout the 21st century?

1.4 Research objective and scope

The research objective will be to calculate the expected change in the meteorological variables according to climate model scenarios and use them as an input for a steady-state groundwater model to compute groundwater fluctuations for the 21st century considering a changing climate.

Surface water changes, as well as changes in land-use during this time will be outside the scope of this research.

1.5 Hypothesis

Under the consensus of Global Circulation Models (GCMs) predicting an intensification of the hydrological cycle, it is expected that higher temperatures will lead to more evapotranspiration, while precipitation becomes more variable within the year. With these drier conditions a lowering of the water table is expected, especially during the dry season, because of the population's dependence on groundwater during these times. The biggest drops in groundwater heads are then anticipated to be away from riparian areas.

The following chapters will continue to explain the methodology used to calculate the expected changes in the meteorological variables and will describe how the hydrological model was constructed. Consequently, results are presented and discussed before answering the proposed research question in the conclusion.

2. Methods

2.1 Overview

To take into consideration the effects of climate change throughout the 21st century, three Regional Climate Models (RCMs), created by dynamically downscaling three GCMs, were used to represent the future temporal dynamics of the meteorological variables available. Climate model results were then compared to an observed record to calculate the relative changes.
However, not all meteorological variables have observational records of equal length. Therefore, when possible, the observational records were extrapolated, resulting in a "synthetic record". The combined results of the synthetic, observed and RCM records are referred to as the meteorological time-series. (figure 2).

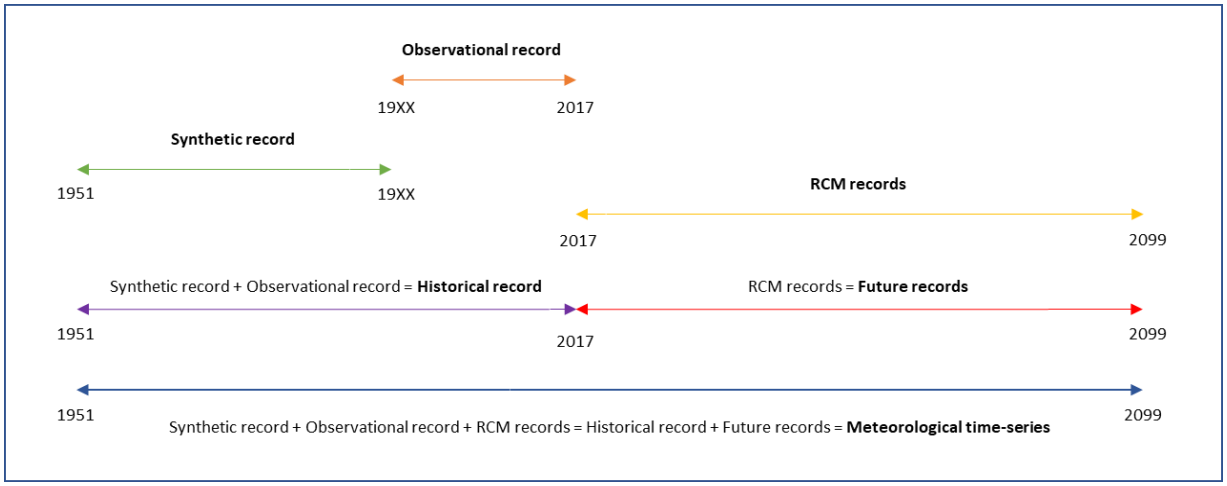

Figure 2: Abstract representation of the components that were combined to create the meteorological time-series. The XX's in 19XX indicate a variable necessity for extrapolation, depending on the length of the variable's observed records.

The relative changes suggested by the meteorological time-series were used as the input for the hydrological model constructed to compute groundwater fluctuations. A detailed overview of the methodology is schematically presented in a flowchart (figure 3).
Following this overview, the methodology used to create the meteorological time-series and the hydrological model set-up are discussed in detail below.

2.2 Meteorological time-series

2.2.1 Observational record

In total 28 available Thai Meteorological Department (TMD) Automated Weather Stations (AWSs) are present within the research area, of which 17 stations contained records of sufficient length to consider within the scope of this research (figure 4).

Measurements from these 17 TMD AWSs include daily values for the variables: precipitation (pr), pan-evaporation (et), average temperature (tas), minimum temperature (tasmin), maximum temperature (tasmax), relative humidity (rh) and sunshine hours (sh). The length of the observations ranges between 1951 – 2017, depending on the variable (appendix, B1).
Suggested TMD station locations were non-sensical and therefore adjusted using Bing Maps aerial photography (Bing Maps Aerial, 2019) to fit the nearest airport location. If no airport was nearby, the nearest city hall was used as a reference. Both the original and adjusted coordinates used are present in the appendix (B2).

Missing values were substituted with the averages for that particular month or, in some cases, year for that specific location. Minimal missing values were encountered, with all locations having 1% missing values on average (appendix, B3).

2.2.2 Synthetic record

Pan-evaporation measurements were not of equal length compared to those of the precipitation measurements and were therefore extrapolated to create the longest possible historical record. To calculate daily evaporation, Morton's CRAE method (Morton, 1983) was implemented using a slightly altered version of the WREVAP program (Morton et al., 1985) by McMahon et al. (2013). This method was selected due to its limited data requirements, considering there is no historical wind data available, but also because it is an independently tested method for calculating evaporation on a regional scale for land environments, showing accurate results (Hobbins et al., 2001a; McMahon et al., 2013; Szilagyi, J., 2001).

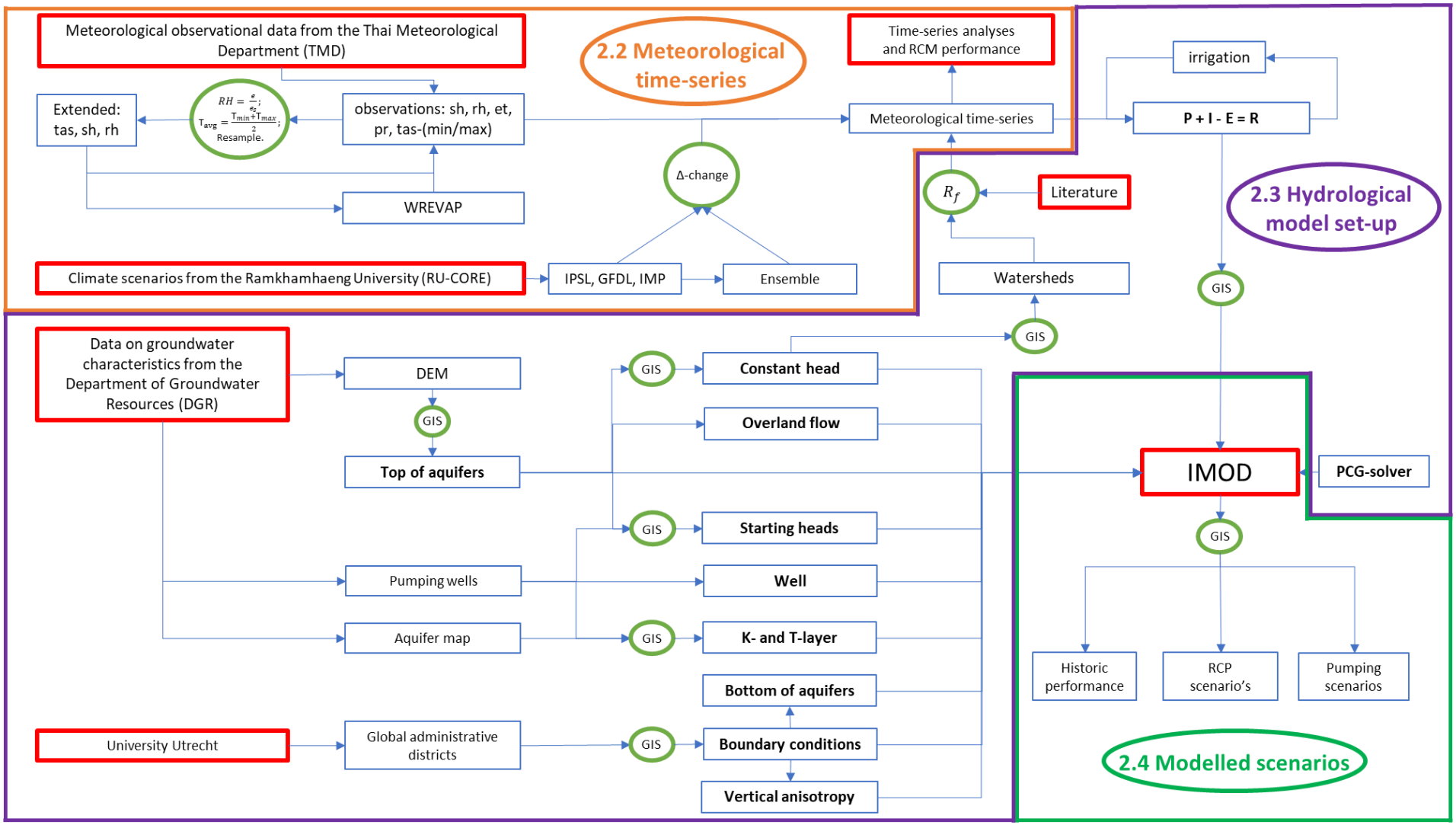

Figure 3: A flowchart providing an abstract representation of all the methodology components. The numbers 2.2, 2.3 and 2.4 refer to the method's section wherein the corresponding methodology components (colour-coded) are discussed in more detail.

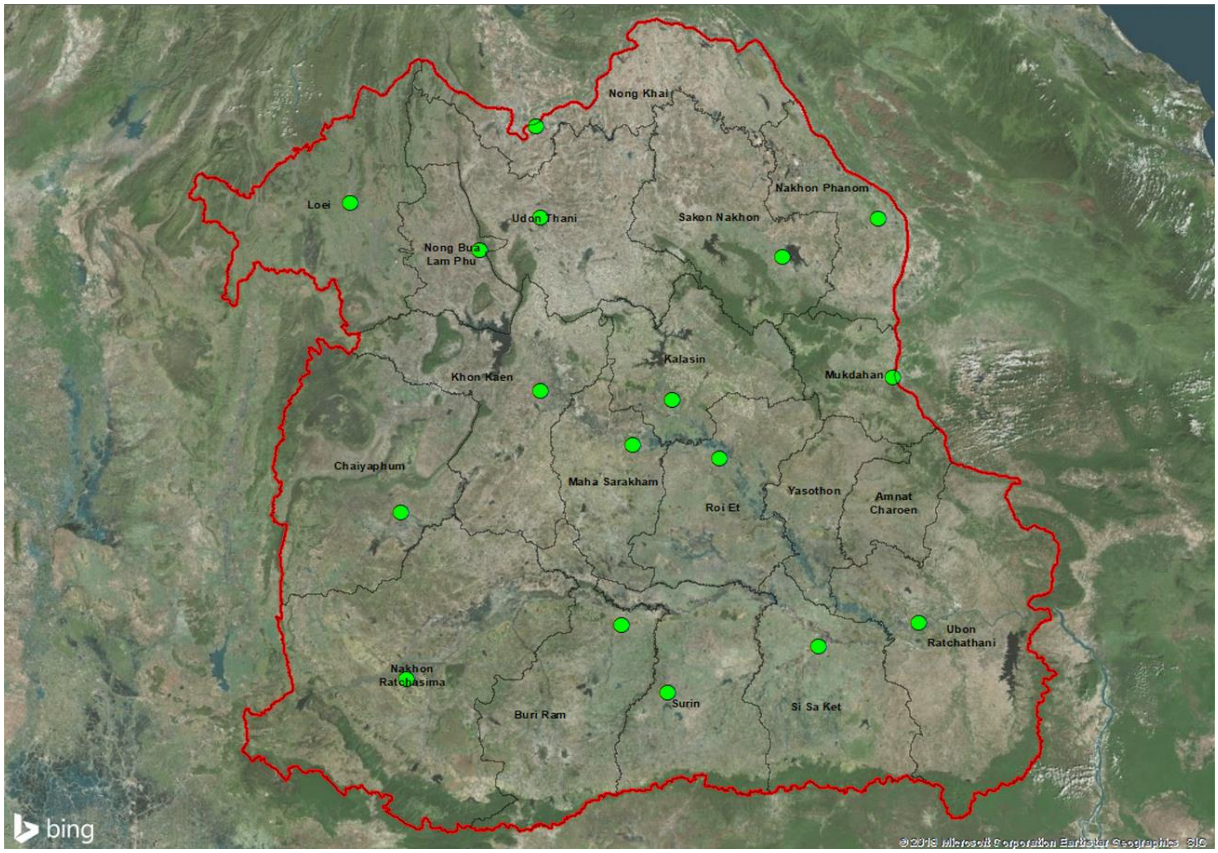

Figure 4: A spatial representation of the locations of the TMD AWSs (green dots) relative to the different provinces within the research area, which is outlined in red (Bing Maps Aerial, 2019).

The input data to run the program consists of the following variables: latitude, elevation, month number, mean annual precipitation, mean daily air temperature, mean daily relative humidity and mean daily sunshine hours. A worked example and a listing of the slightly modified version of the Fortran 90 version of Morton's WREVAP program can be found in the "Supplementary Material to paper 'Estimating actual, potential, reference crop and pan evaporation using standard meteorological data: A pragmatic synthesis'" (McMahon et al., 2013).

To run WREVAP for the longest possible potential evaporation record, the variables: tas, rh and sh had to be extrapolated as well.
Firstly, average temperatures for Mahasarakham, Kalasin, Buriram, Sisaket and Nong Bua Lamphu were extended by calculating the averages from minimum and maximum temperatures and performing a systematic bias correction.
Secondly, to create a relative humidity timeseries of equal duration to that of the temperature records for all stations, the empirical formula: $e_s = 6.1078\, e^{(\frac{17.269 T_{dew}}{T_{dew}+237.3})}$ was used (e.g. Eccel, 2012; Holbo, 1981; WMO, 1979), assuming, that during night time, the daily tasmin is equal to the dew point temperature (T_{dew}).

Thirdly, previous values for daily sunshine hours where randomized as an input for missing years. For those locations with missing daily sunshine hours, data was used from the closest possible location within the same watershed, under the assumption that this variable would not be significantly different, with minimal distance between locations for such a relatively flat area as the Khorat plateau. The locations that were used as a substitute for other locations, and for how long, has been registered in appendix (B4).

The observational record, together with the calculated synthetic record for tas, rh and sh were used to complete two WREVAP model runs. The first run, with all the observational data from 1990-2017 acting as a control, and a second run, using the entire historical record (1951-2017). The final product is a combination of the model output for the years 1951-1989 and the measurements for the years 1990 – 2017.

2.2.3 RCM records

Projections for the 21st century were derived from three dynamically downscaled GCMs, being: GFDL-ESM2M (GFDL), IPSL-CM5A-LR (IPSL) and MPI-ESM-MR (MPI) with a 25 km x 25 km grid resolution (SEACLID-CORDEX, 2018; Cruz et al., 2017; Juneng et al., 2016; Ngo-Duc et al., 2017; Tangang et al., 2018)[1].

All three, now referred to as "RCMs", contained daily data for the historical period of 1970 until 2005 and daily data for Representative Concentration Pathway (RCP) scenario's RCP4.5 and RCP8.5 for the period 2005 until 2100.
Using "R", yearly sums and averages were extracted from the netCDF-files for the RCMs output variables provided by the RU-CORE department from the Ramkhamhaeng University (RU-CORE, 2019), being daily: pr, tas, tasmin, tasmax, rh, sh and actual evapotranspiration (evspsbl). These variables are not bias corrected. Information was only extracted for those cells in which the concerning TMD station was located. An example raster of an RCM output and the relevant cell extracted for each individual TMD station is presented in the appendix, C1a, b. The R-code used for the data extraction is available in the appendix (C2).

A simple delta change method was then applied to make future projections for all RCM variables. First, the variables' averages were calculated for the historical RCM period 1970-2005. Secondly, the values for consequent years from 2005 up until 2100 were compared to the calculated historical RCM average to extract the relative (delta) change. Finally, the resulting delta change was imposed on the same period within the historical record (1970-2005), to create a time-series until the end of the 21st century. The results of all three RCMs were combined to form an ensemble mean model.

To evaluate the RCM accuracy, both the historic performance (1970 – 2005) and future performance (2006 – 2017) were compared to the observational records for the variable precipitation. Precipitation was chosen, because it, besides evaporation, is the most important meteorological variable used as an input for modelling hydraulic head. Also, compared to evaporation, precipitation has the longest observational records available (1990 – 2017 versus 1951-2017, respectively).

2.2.4 Meteorological time-series analysis

To assess the relative change in the temporal dynamics of the meteorological variables, a time-series analysis was performed. Comparing the historical record with the future records to evaluate possible shifting trends throughout 1951 – 2099, yearly averages of all variables were calculated to capture the annual fluctuations. Monthly averages were computed for the variables precipitation and evaporation to investigate interannual fluctuations corresponding to the change in seasons (wet and dry season).

First, a Probability Density Function (PDF) and Cumulative Normal Distribution (CND) were constructed for the yearly averages to assess a possible shift in the mean and variability for both the variables precipitation and evaporation.

[1] "The downscaled data is a product of the SEACLID/CORDEX Southeast Asia Project which is funded by the Asia-Pacific Networks for Global Change Research (APN) (ARCP2015-04CMY-Tangang)".

Second, because not only the amount of precipitation is important, but also the timing, changes in the interannual variation of average precipitation were also considered. Coinciding, a frequency analysis was performed on the average monthly precipitation for all locations. To determine the relative change in the interannual temporal dynamics during the observational period, the periods 1951-1984 and 1985 – 2017 were compared.

Furthermore, to evaluate the possibility of obtaining accurate results when extending the interannual analysis with data from the RCM records, the historical and future RCM timeseries, for both precipitation and evaporation, were compared with one another to identify a shift in seasonal patterns.

2.3 Hydrological model set-up

To quantify and map groundwater fluctuations, a one-layer finite difference hydrological model was set up using iMOD, the MODFLOW Graphical User Interface (GUI) developed by Deltares (Vermeulen et al., 2018). The iMOD hydrological model required several modules to run calculations on hydraulic heads, which are discussed in detail below.

Top of aquifers (TOP) & Overland flow package (OLF)

The TOP module is described as "the top level of the permeable part of each model layer" (Vermeulen et al., 2018) and was assumed to be equal to surface level. A (Digital Elevation Model) DEM provided by the DGR was used as the TOP module (appendix, D1). However, the DEM first had to be adjusted for proper drainage. Due to the relative flatness of the area and DEM imperfections, rivers were displaced at some locations. Therefore, one major flaw was corrected by manually rerouting the river. Using Bing Maps Aerial photography (Bing Maps Aerial, 2019) as a reference, the Mun river was "burned" into the DEM by lowering the elevation with one meter on average, correcting the river's flow path (figure 5). Thereafter, a sink fill function was used (Planchon & Darboux, 2002) to smooth out stagnant cells and create a surface fit for hydrological modelling. As a result, there was a serious redistribution of the corresponding watersheds (figure 6), which were grouped into the Mun, Chi and Mekong watershed as suggested by the FAO (FAO, 2016).

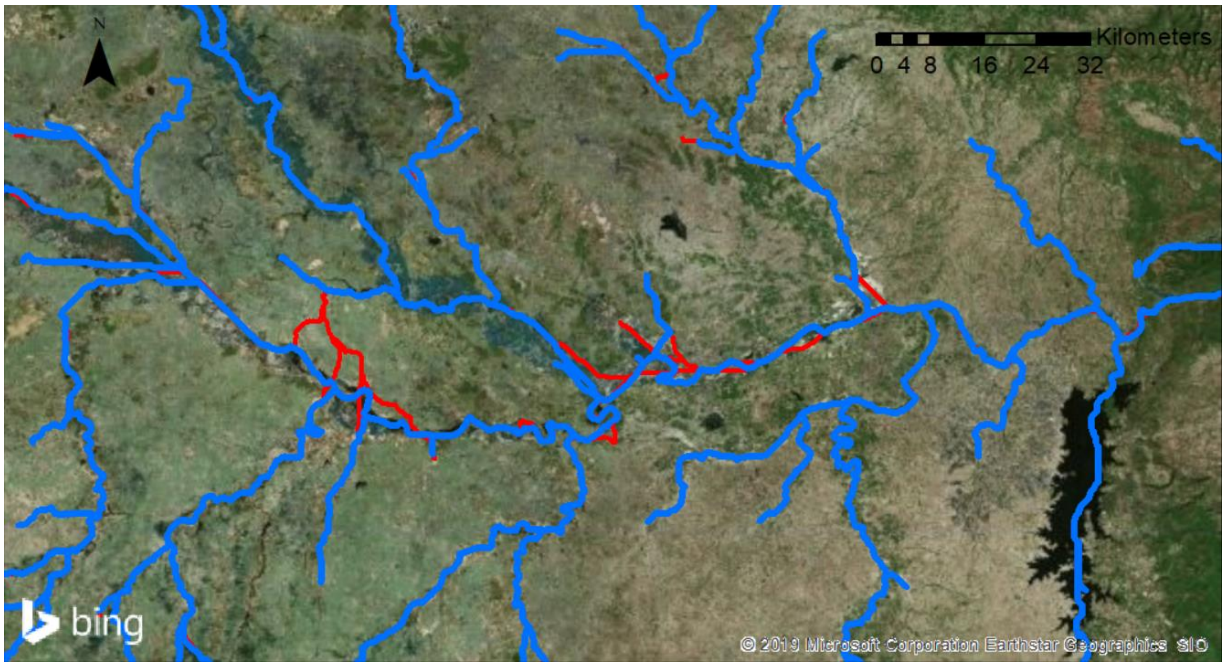

Figure 5: The red lines show the old river flow path; the blue lines show the river flow path after adjusting the DEM. The backdrop is an aerial photo showing the rivers actual flow path (Bing Maps Aerial, 2019).

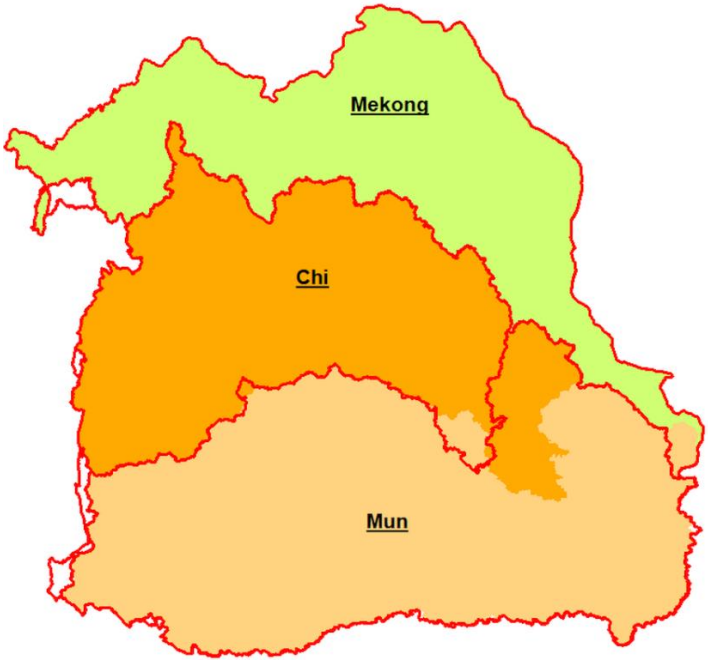

Figure 6: The old watershed delineation is visible (outlined in red), whereas the new watershed delineation is colour-coded. After adjusting the Mun river flow path, there was a redistribution of the total surface area appointed to the Mun and Chi watersheds.

Consequently, the adjusted DEM was used for the overland flow module, which "defines the elevation above which outflow of groundwater will occur" (Vermeulen et al., 2018), thereby, removing the water from the model as overland flow whenever it exceeds the surface level. Furthermore, it needs to be noted that "The OLF elevation may be determined at a few centimetres above ground elevation to represent shallow ponding, caused by small obstructions against outflow. The flow rate of the OLF package is calculated assuming a fixed resistance against the outflow of 1 day" (Vermeulen et al., 2018).

Constant head package (CHD)

"The constant head package defines the elevation of groundwater heads at cells where the BND value < 0 by one IDF (or a constant value)" (Vermeulen et al., 2018).

Flow direction and accumulation were calculated according to the methodology described in (Jenson & Domingue, 1988). A selection was made from the resulting flow accumulation raster, selecting only those cells with the flow contribution of at least 200,000 other cells. Consequently, the binary raster was vectorised and used to extract the values of the corresponding cells from the DEM, minus one meter, to prevent drainage problems on the relatively flat surface. The resulting river raster was set as a constant head boundary, assuming the river's head does not change throughout the year. The final river flow path can be found in appendix D2.

Bottom of aquifers (BOT)

The BOT is described as "the bottom level of the permeable part of each model layer" (Vermeulen et al., 2018). The Bottom was set at an elevation of zero meters, which corresponds to the DEM's reference level.

Boundary conditions (BND)

The BND "denotes areas that are part of the simulation, groundwater flow goes through them and the heads are computed" (Vermeulen et al., 2018) and was made to be equal to the global administrative areas (Global Administrative Areas, 2015).

Starting heads (SHD) & Well package (WEL)

The starting heads "specify for each cell the initial head to start the model simulation with" (Vermeulen et al., 2018).

A raster portraying the initial hydraulic head for the research area was constructed using data from 2396 pumping wells collected in 2001, provided by the DGR (appendix, D3). To create the SHD, the surface elevation for each well's location was extracted from the adjusted DEM. Consequently, the Static Water Level (SWL) of each well was subtracted from the surface elevation to obtain the hydraulic head. These points were then ANUDEM (v.5.3) interpolated (Hutchinson, 1988; Hutchinson et al., 2011).

The same wells were used for the well package, which "defines the groundwater abstractions for each model layer" (Vermeulen et al., 2018). Each well had a specific yield assigned to it. However, out of 2396 wells, 759 had no data concerning the amount of water extracted. Therefore, the median from all wells was calculated (72 m^3/day) and used to fill the data gaps to get an estimate of the impact of the pumping wells in the research area.

Recharge package (RCH)

"The recharge package defines the quantity of water from precipitation that percolates to the groundwater by one IDF (or a constant value)" (Vermeulen et al., 2018).

Recharge, being one of the most important variables in groundwater modelling, was calculated using the entire meteorological time-series. Assuming that for this historical period there was no change in storage, recharge was considered equal to precipitation minus actual evaporation ($P - E_{act} = R$).

The historical average precipitation and potential evaporation (E_{pot}) for each TMD-station were calculated from the year 1951 up to and including 2017. Whenever the extent of the time-series was not available from 1951, the oldest possible date available for that TMD-station was used to calculate the historical average. Thereafter, future averages for the remainder of the 21st century were computed using the yearly averages calculated by imposing the delta change method extracted from the RCMs on the historical record.

The E_{pot} was converted to actual evapotranspiration (E_{act}) with the aid of a reduction factor (R_f). Assuming precipitation minus the potential runoff (R_{pot}) values suggested by Sanyu Consultants Inc. (2010), to be equal to the E_{act}, the R_f was calculated by dividing the E_{act} by the E_{pot} derived from the TMD AWSs (equation 1):

$$R_f = \frac{P - R_{pot}}{E_{pot}} = \frac{E_{act}}{E_{pot}} \qquad \textit{(eq. 1)}$$

resulting in three distinct R_f's: Mekong = 0.71, Chi=0.60 and Mun =0.58 (table 1).

	Mekong	Chi	Mun
Rpot [Mm³]	25,600	14,200	25,000
Area [km²]	46,460	49,480	69,700
Rpot [mm]	$25{,}600*10^6/46{,}460*10^6$=551	$14{,}200*10^6/49{,}480*10^6$=287	$25{,}000*10^6/69{,}700*10^6$=359
Precipitation [mm]	1,593	1,279	1,314
P – R = Eact [mm]	1593 – 551 = 1042	1279 – 287 = 992	1314 – 359 = 955
Epot [mm]	1476	1642	1646
Rf = Eact / Epot [-]	1042/ 1476 = **0.71**	992/1642 = **0.60**	955/1646 = **0.58**

Table 1: R_f calculations per watershed.

Finally, because of the importance of irrigation in the area and the lack of available data thereof, the lowest negative recharge value in the observational record was used to estimate the amount of

average yearly irrigation (I), which was assumed to be evenly spread over the entire research area ($(P+I)-E_{act}=R$). By doing so, all negative recharge values from the observational record were eliminated. This approach led to an estimated average yearly irrigation of 440 mm.
To gain insight into the relative wetness of each watershed, an ensemble was created combining all three watersheds to be able to compare each watershed to the research area's average.

As an input for the RCH, the average value for recharge per AWS was calculated for 3 periods: historic 1951 – 2001 (corresponding with the year the starting heads were measured), future 2002-2050 and future 2051-2099. These averages were then prepared within a GIS and interpolated again using the ANUDEM method (Hutchinson, 1988; Hutchinson et al., 2011). A negative average value for recharge was encountered only twice in the future record. Both occurrences, suggested by the GFDL-model, were contributed to the AWS located in Chaiyaphum and were set to zero accordingly.

Horizontal permeabilities (KHV) and transmissivity (KDW)
"The transmissivity and the horizontal permeability of each model layer is defined by one IDF (or a constant value)" (Vermeulen et al., 2018). Data from the same wells used to calculate the starting heads were combined with a 2-D aquifer map, also provided by the DGR (appendix, D4).

However, only 421 out of the 2396 wells could be used for connecting horizontal permeability (K) and transmissivity (T) values to their respective aquifers.
First, because the aquifer-id was missing from the well data, the more general "hydro-unit" description had to be used. There were 389 wells bearing the same hydro-unit as those present on the aquifer map (appendix, D5).
Second, for those aquifers that did not have wells with corresponding hydro-units, the (32) wells that were located within the boundary of that aquifer were used (appendix, D6).
Finally, for four hydro-units neither a name-based, nor a location-based approach deemed viable. Therefore, they were merged with their neighbouring aquifer. The calculated median of these wells was used as the average K and T value for the KHV and KDW iMOD module.

An overview of the (combined) aquifers, the number of wells involved and their K- and T-values and Standard Deviation (SD) is presented in appendix D7 and C8 as well as the resulting K- and T-layers used as model input (appendix, D9 and 10).

Vertical anisotropy for aquifers (KVA)
"The vertical anisotropy (-) of each model layer is defined by one IDF (or a constant value). The vertical anisotropy is multiplied with the horizontal permeability to calculate the vertical permeability in the permeable part of a modellayer" (Vermeulen et al., 2018).
No information concerning the vertical resistance was available. Therefore, the KVA was set to one. Because of iMOD's multiplication of the vertical anisotropy with the horizontal permeability, a KVA of one makes the aquifer effectively homogenous isotropic.

Preconditioned conjugate gradient (PCG) solver
To run the model, the single core PCG solver was used on default settings. These include: 150 outer iterations and 30 inner iterations and took about 12 hours to run for a 30*30-meter resolution on a computer with an intel-i7 processor, using approximately 28GB of virtual memory (appendix, D11).

2.4 Modelled scenarios

With these initial values and predicted changes described above, a one-layer steady-state model was created for calculating the hydraulic heads for 3 timesteps: historic 2001 and future 2050 and 2100.

The starting heads, based on measurements taken in 2001, were compared to the historic model run to validate model performance.
After model performance assessment, the relative differences between the modelled historic period and both the future RCP4.5 and RCP8.5 scenarios were assessed spatially to locate those areas that would be most affected by climate change.
Consequently, two pumping scenarios were constructed, comparing a scenario without pumping with a scenario where pumping is at regular capacity (100%) and with pumping at double capacity (200%).

3. Results

3.1 Overview

First, the meteorological time-series is set-out. Thereafter, the implementation of the RCM data results, as an input for the hydrological model, is discussed and the groundwater model performance is validated. Finally, the impact of the climate scenarios and the pumping scenarios are presented.

3.2 Validation of the meteorological time-series

The meteorological time-series is discussed in chronological order. Thus, first the synthetic record, second, the observational record and lastly, the RCM records. The results of all three components of the meteorological time-series are then combined and analysed on an annual and interannual basis.

3.2.1 Synthetic data reconstruction

The synthetic record consists of an extended average temperature, relative humidity and daily sunshine hours. The results for these three meteorological variables will be discussed (in that order) before continuing with their culmination in the WREVAP model, concluding with the extended potential evaporation results.

3.2.1.1 Average Temperature

Using minimum and maximum temperature to extend average temperature records results in a general overestimation of average temperatures. However, when systematic bias is removed, the calculated average temperature reflects both the annual fluctuation of the measured average temperature for the control period and the interannual cycle (appendix, E1a, b).
All but one location (Kalasin) showed acceptable results, with an average annual Root Mean Square Error (RMSE) of 0.23 and R^2 between 0.83 and 1.00, suggesting that the model deviation is on average within 1% of the measured values and has a good fit (appendix, E2).

3.2.1.2 Relative Humidity

Although modelling results for relative humidity prove to be less accurate than those for average temperature, the methodology used still captures a similar annual pattern and seasonal cycle as suggested by the measurement data. However, it becomes apparent that the relative humidity model has a lessened ability to simulate extreme values (appendix, E3, 4).
Model performance shows an average annual RMSE of 1.58 (2.2%) and an average interannual RMSE of 2.85 (4%) (appendix, E5). Although, model accuracy, at times, may be questionable, the impact of adding the extrapolated values to the average for all stations causes little disturbance within the averaged seasonal cycle (appendix, E6). Therefore, the results are deemed viable to be used as input for the WREVAP evaporation simulation.

3.2.1.3 Daily sunshine hours

By implementing the clustered re-sampling of daily sunshine hours-years and by using daily sunshine hours from neighbouring locations as a substitute for those locations that did not have measurements, most statistical properties of the observational data have stayed intact. This methodology causes

statistical discrepancies between connecting years, but interannual autocorrelation remains the same. The method proves to be warranted when seeing that the extrapolated results are in very close resemblance with the observational record (appendix, E7), considering the 1496 added months of data. The result was found eligible for use within the WREVAP model.

3.2.1.4 WREVAP output

After systematic bias correction, WREVAP shows to be capable to simulate the trend observed within both the yearly and seasonal cycle (appendix, E8a, b).

When comparing the WREVAP results from model runs with all necessary input available and those runs which used modified daily sunshine hours, the estimates are similar. For both locations that used sunshine hours from nearby stations and for those whom resampled years of daily sunshine hours for its own location (Nakhon Ratchasima and Chaiyaphum), the RSME is within the same range, being an average yearly RMSE of 103 mm (6%) and monthly RMSE of 5 mm (4%) compared to an average yearly RMSE of 116 mm (7%) and monthly RMSE of 7 mm (5%) (table 2a, b).

Location	Yearly RMSE	Monthly RMSE
Khon Kaen	68	6
Loei	96	4
Nakhon Phanom	87	3
Roi Et	94	5
Sakon Nakhon	101	4
Sisaket	163	4
Surin	84	5
Ubon Ratchathani	134	8

Table 2a: Showing RMSE for WREVAP performance having all data input

Location	Yearly RMSE	Monthly RMSE
Kalasin	139	8
Buriram	84	6
Mahasarakham	234	7
Mukdahan	138	4
Nakhon Ratchasima	87	6
chaiyaphum	93	6
Udon thani	91	7
Nong Khai	124	7
Nong bua lamphu	52	12
***Not extended with WREVAP: Buriram, Kalasin, Nong Bua Lamphu, Sisaket		

Table 2b: Showing RMSE for WREVAP performance having neighbouring sunshine data

The one outlier, Mahasarakham (appendix, E9), can be traced back to an anomaly within the observed data. Otherwise, results are comparable to those of the WREVAP model having all data available, justifying the use of daily sunshine hours from neighbouring stations and the resampling of sunshine hours-years.

The seasonal cycle for potential-evaporation was also hardly affected by implementing WREVAP results (appendix, E10), increasing the confidence in model accuracy.

3.2.2 Observational record

Subsequent to the synthetic record is the observational record. The temporal variability (annual and seasonal) reflected by the observational record and how the observational record relates to the synthetic record is discussed below.

In accordance with Limsakul et al. (2019), the yearly average for minimum, maximum and average temperature all show an increase in temperature. The tasmin, with $2.7 \cdot 10^{-2}$ degrees Celsius per year, rises more quickly than the tasmax and tas, with $1.2 \cdot 10^{-2}$ and $5.7 \cdot 10^{-3}$ degrees Celsius per year, respectively. Compared to the synthetic record, the average rise in temperature is continued in the observational record with a similar rate (appendix, E11). Coinciding with this increase in temperature is an increase in precipitation ($8.8 \cdot 10^{-1}$ mm per year) and a decrease in pan-evaporation (2.7 mm per year) (appendix E12a).
This decrease in pan-evaporation is in agreement with the decrease suggested by the synthetic record. Where the historical record shows a reduction in pan-evaporation of 2.9 mm yearly, the observational record shows a 2.7 mm yearly decline in pan-evaporation (appendix, E13).

The seasonal cycle clearly reflects the change in seasons. The dry season is characterised by higher average minimum, maximum and average temperatures, very low quantities of precipitation and an increase in potential evaporation when the rains start to return in March. On the other hand, the rainy season reflects decreasing temperatures and potential evaporation and, of course, an increase in the amount of precipitation (appendix E12b).

Meanwhile, average sunshine hours and relative humidity show quite a strong oscillation. Years with relatively high values for daily sunshine hours seem to correspond with years that have relatively low values for relative humidity (appendix E14a).
The possible correlation between the average number of sunshine hours and the relative humidity is also illustrated within the seasonal cycle. There is a clear decrease in relative humidity during the dry season when the amount of daily sunshine hours is at its peak and a clear increase in relative humidity during the rainy season when the amount of daily sunshine hours is at its lowest (appendix E14b).
However, when comparing the relative humidity in the synthetic record with the observational record on an annual basis for all stations (appendix, E15), there is a tenfold decrease of the variables' rate of change in the observational record, which is rather unexpected for a relatively stable parameter such as relative humidity.

3.2.3 Regional Climate Models

To evaluate RCM quality, historical and future RCM performance for the variable precipitation were evaluated on a yearly basis with the use of the RMSE. The results are summarized (table 3).
The three RCMs and their ensemble were ranked according to their overall performance. The best performing model is then compared to the historical record to evaluate the relative change in the meteorological variables for the 21st century.

As for the historical performance, the IPSL, IMP and Ensemble model perform better than the GFDL, showing a similar deviation with a RMSE around 16/17%. The same holds for the future RCP4.5 scenario.
However, when comparing the future RCP8.5 scenario's, the smallest RMSE corresponds to both the IMP (14%) and the Ensemble (12%) models, suggesting that the RCP8.5 scenario most accurately represents the observational record for the period 2006-2017.

In view of the RMSE as a representation of the average bias throughout the research area, the ensemble model is considered the most accurate overall, followed by the IMP, IPSL and GFDL models, in that order.

Scenario	Historic performance 1970-2005				Control period RCP4.5, 2006-2017				Control period RCP8.5, 2006-2017			
RCM	**GFDL**	**IPSL**	**IMP**	**ENS**	**GFDL**	**IPSL**	**IMP**	**ENS**	**GFDL**	**IPSL**	**IMP**	**ENS**
RMSE	362	256	239	249	362	256	239	249	251	310	215	186
% RMSE	24	17	16	17	24	17	16	17	17	21	14	12

Table 3: RMSE calculations for evaluating historical and future RCM performance.

Putting together the now complete meteorological time-series for the meteorological variables: pr, et, tas, tasmin and tasmax, the changes with respect to the observational record become visible (figure 7).

Whereas the WREVAP modelling results were all in agreement with the direction of change captured within the measurements, the same is not true for all variables projected by the RCMs' ensemble.

Minimum, maximum and average temperatures are all showing an increase in temperature, with the RCP8.5 scenario being an exaggerated version of the RCP4.5 scenario. Compared to the average linear increase in degrees Celsius computed from the observed minimum, maximum and average temperature, temperature rise changes with 61%, 122%, 281% and 167%, 346%, 765% for the RCP4.5 and RCP8.5 scenario, respectively. However, overall, minimum temperature still rises more quickly, followed by maximum temperature and average temperature.

In contrast, both precipitation and evaporation show a clear break in their direction of change were the transition is made from the observational record to the RCM records. Keeping in mind that precipitation is a highly variable parameter, both the RCP4.5 and RCP8.5 show an average decline of 1.14 mm and 3.24 mm per year respectively, compared to an increase of $8.8 \cdot 10^{-1}$ mm per year for the historic period.

Although less variable than precipitation, evaporation for both the RCP4.5 and RCP8.5 scenarios shows an increase of 0.69 and 1.44 mm per year compared to a decrease for the historic period of 2.87 mm per year.

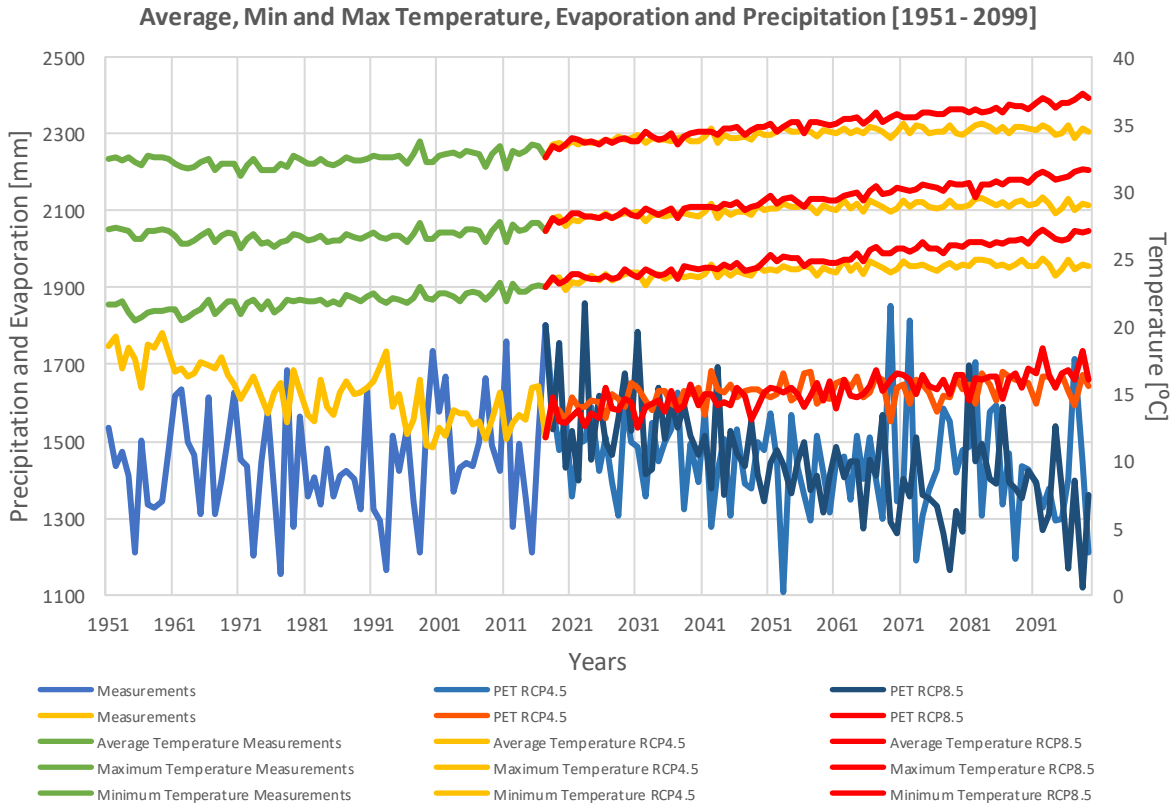

Figure 7: Meteorological time-series for average, minimum and maximum temperature, precipitation and evaporation, all stations' averages, showing the ensemble's RCP4.5 and RCP8.5 scenarios.

Regarding relative humidity and daily sunshine hours, variability decreases with the implementation of the RCM results. Relative humidity decreases slightly over time as daily sunshine hours increases a little for RCP4.5, while relative humidity decreases more quickly, and daily sunshine hours stay more stable for RCP8.5. When comparing these results to those of the historical record, both variables become far less variable (appendix, E16).

3.2.4 Meteorological data analysis

To further analyse how the RCM-records compare to their ensemble and to the observational record on an annual basis, PDFs and CNDs for precipitation and evaporation are presented in this section. Furthermore, the interannual variability for both variables is studied by investigating changes in the seasonal cycle throughout the observational record and the RCMs.

Starting the analysis by looking in more detail to the precipitation results of each RCM, both the IPSL and the GFDL model output suggest less precipitation, while the MPI model output suggest more precipitation. The variability of the MPI and GFDL models are similar to that of the observational data, in contrast with the more variable GFDL. The ensemble shows less variability due to the averaging of the RCM results, as outliers are filtered out, effectively removing extreme values. Also, the ensemble model, combining the output of the three RCMs, shows less precipitation for the period 2018 – 2099 compared to the historical period 1951- 2017 (figure 8).
There are no major differences between the RCP4.5 and RCP8.5 runs, nor are there any patterns visible between the different models' RCP scenarios. Overall, there is no clear consensus between the three RCM models on their trajectory relative to that of the measurements. The same conclusions can be derived from the cumulative normal distribution (appendix, F1).

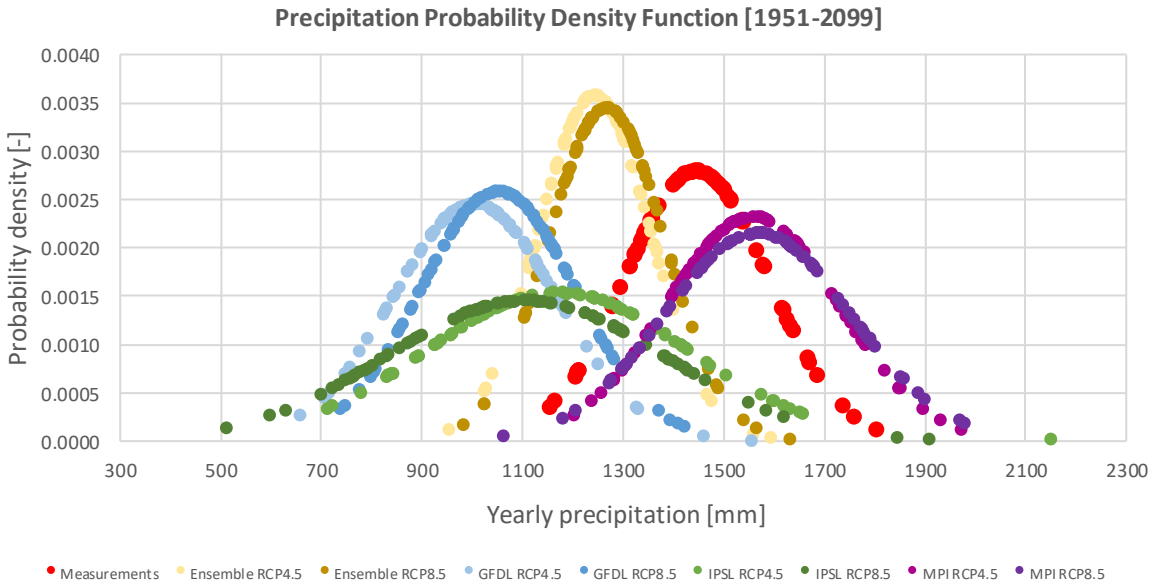

Figure 8: The PDF for the yearly averages of the combined AWSs' precipitation measurements [1951 – 2017] compared to the yearly averages of the three RCMs and their ensemble for both RCP4.5 and RCP8.5 scenarios [2018-2099].

In contrast with the results for precipitation, the probability density function for evaporation shows more concurring results (figure 9). All models show a higher average annual evaporation. Also, variability stays realtively unchanged for the MPI and GFDL model and are comparable to that of pan-evaporation measurements. The IPSL model suggests a less variable result, which is affecting the variability of the ensemble model to be less than that of the observational data. Finally, all RCP8.5 runs give a higher average evaporation than their RCP4.5 counterpart. The same conclusions can be derived from the cumulative normal distribution (appendix, F2).

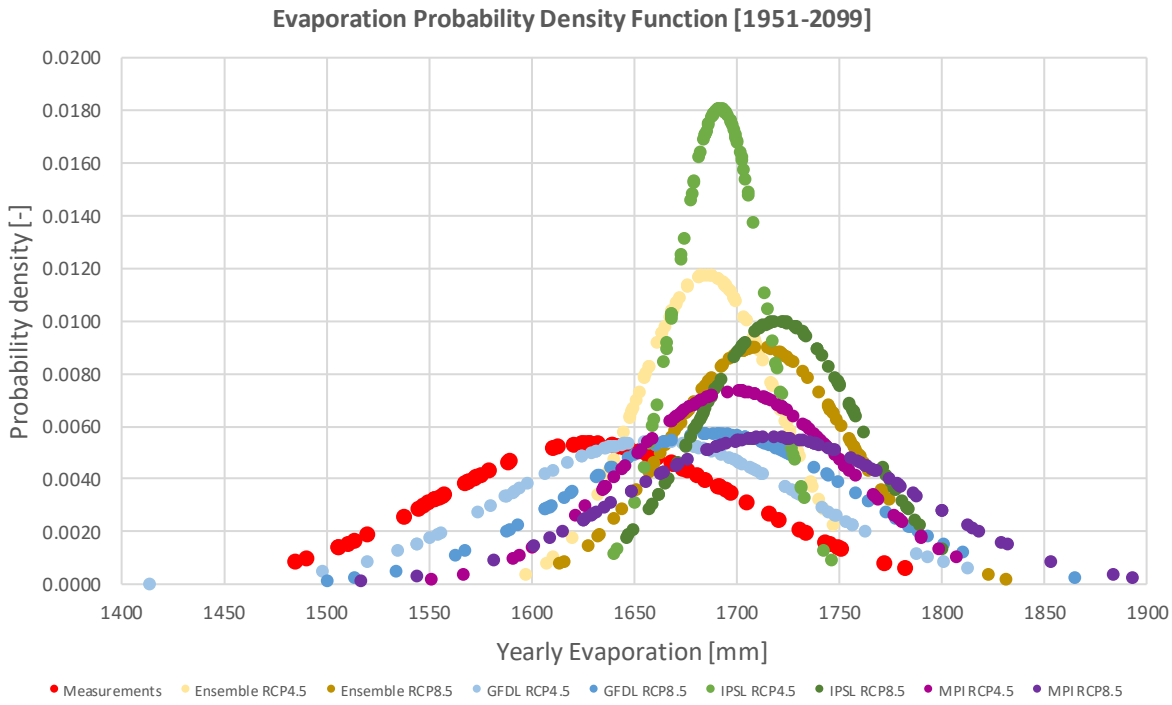

Figure 9: The PDF for the yearly averages of the combined AWSs' evaporation measurements [1951 – 2017] compared to the yearly averages of the three RCMs and their ensemble for both RCP4.5 and RCP8.5 scenarios [2018-2099].

Having considered annual changes, seasonal changes will now be discussed. A frequency analysis of rain-events coupled with a seasonal precipitation distribution shows a shift in the seasonal cylce. It suggests an earlier rainy season, were the number of locations with hardly any precipitation increase during the dry season and the number of locations experiencing more intense rainfall events increases during the rainy season (figure 10).

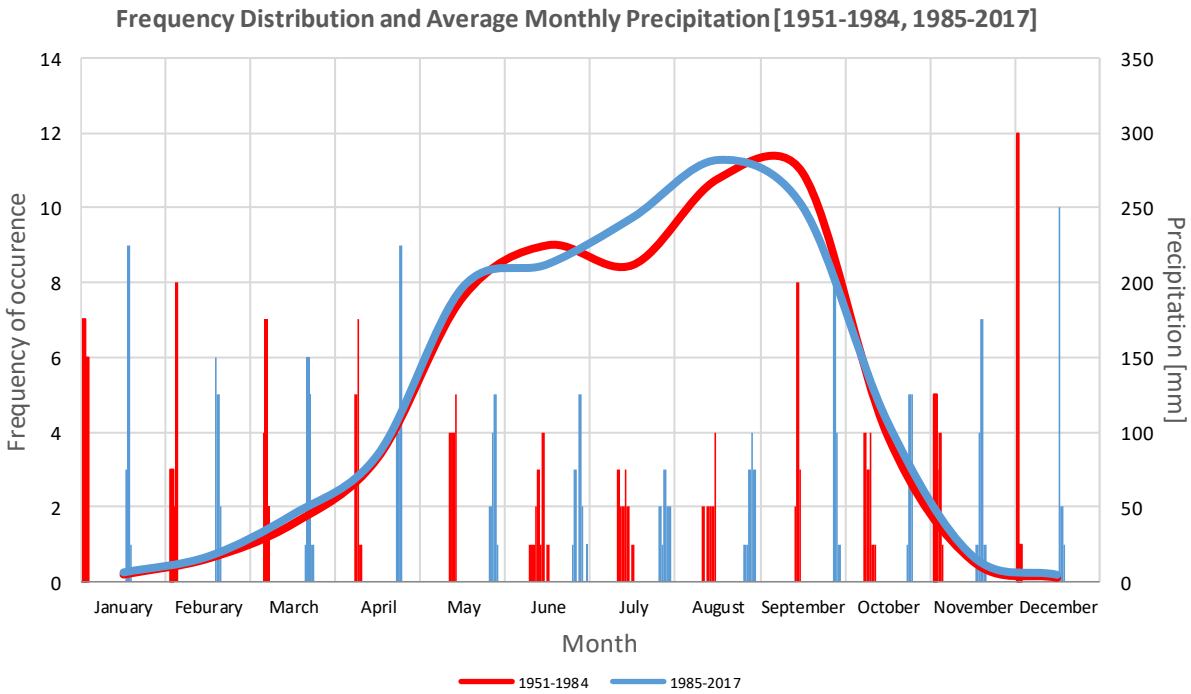

Figure 10: Seasonal precipitation distribution (all stations' averages) and precipitation frequency analysis describing the number of locations experiencing monthly average precipitation values of a certain magnitude. From left to right, monthly histogram binning structure: 0, 5, 10, 15, 25, 35, 45, 60, 80, 100, 125, 150, 175, 200, 250. 300, 350, 500 mm.

To investigate the possibility of confirming and extending the frequency analysis with the results from the RCMs, the RCMs' output is also set-out on a interannual basis. Looking at the average monthly precipitation for the (non-bias corrected) historic RCM runs, it becomes clear that there is a large variation between, not only the magnitude, but also the seasonal distribution predicted by the RCMs. None of the three RCM models are able to recreate the same seasonal pattern suggested by the measurements (figure 11).
According to the observational data, there is a sharp increase in the amount of precipitation at the beginning of the rainy season in April, which attenuates in May, only to increases steadily until it reaches a peak in precipiation around the beginning of September. However, all RCM models propose, with various magnitude, both a peak precipitation at the beginnig and at the end of the rainy season, with declining values in between.
Although not capturing the seasonal cycle very accurately, the ensemble model does show a similar order of magnitude to that of the measurements.

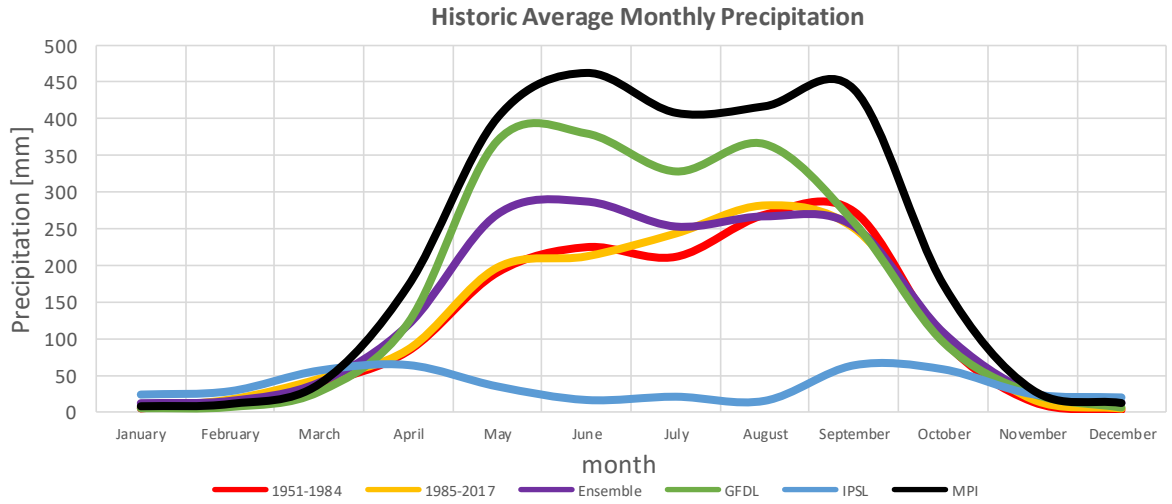

Figure 11: Seasonal historic RCM output [1970-2005] compared to observational records (red/orange lines) [1951-2017] for the averages of all AWSs combined.

Comparing the historical RCM output with its future output, it becomes evident that a similar shift in the distribution of seasonal precipitation, as observed in the analysis of the observational data, cannot be supported by the RCMs' output (appendix, F3a, b, c, d).
The GFDL and IPSL model suggest almost no change in the seasonal cycle. While the GFDL model also suggests no change in magnitude, the IPSL does so relatively slightly. Only the MPI model illustrates a clear shift of the seasonal precipitation, suggesting a delayed rainy season. This shift is also reflected by the ensemble model and is in contradiction with the results from the observational record. Furthermore, no changes are apparent between the RCP4.5 and RCP8.5 scenarios.
Regarding the above, the ability to predict the seasonal variation of precipitation, aided by the three RCMs used, would be questionable at least.

Doubting the usefullness of the RCM precipitation outputs for modelling seasonal variabillity, the seasonal cycle for potential evaporation was also investigated.
No records, other than the pan-evaporation measurements, were available to compare the seasonal cycle of the actual evapotranspiration with. However, the WREVAP model calculations also contained values for actual evapotranspiration and was subsequentually used to compare with the results from the RCMs. In figure 12, the the seasonal cycle for actual evaporation for the observational record was compared to the seasonal cycle proposed by the historical RCM output. All RCM models show similar seasonal patterns and, in general, precede the WREVAP output with one month during dry season. No shift within the cycles' pattern can be observed when comparing the historical RCM run to the RCP4.5 and RCP8.5 scenario's other than an increase in magnitude (appendix, F4a, b, c, d).

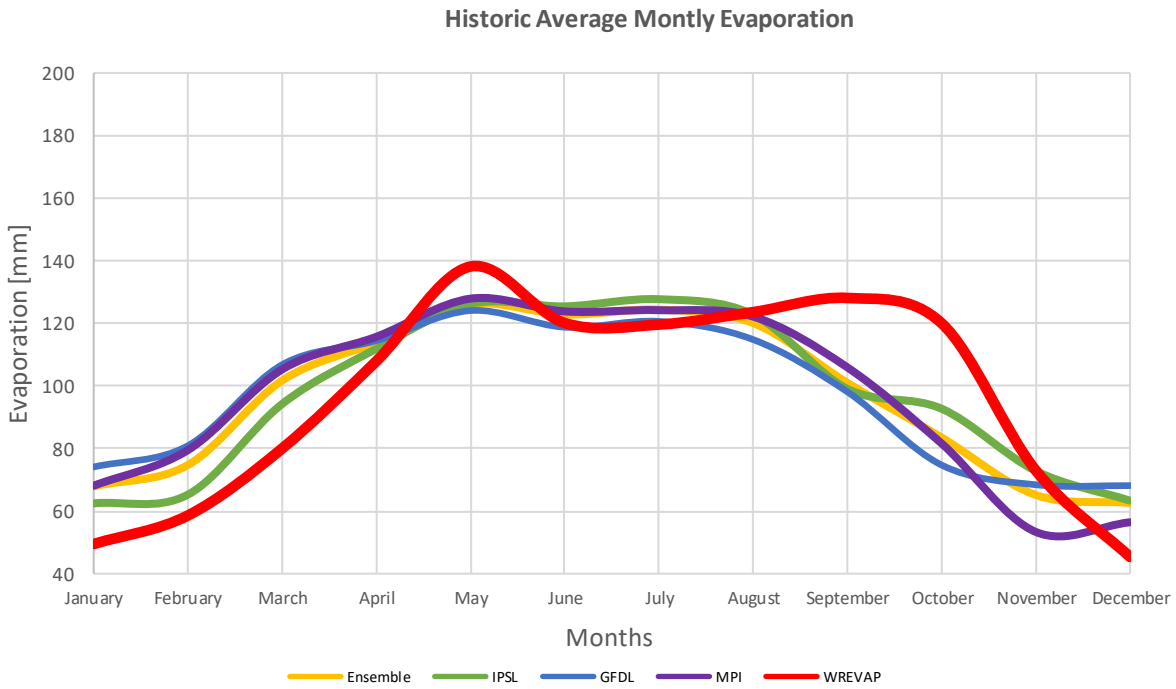

Figure 12: WREVAP E_{act} [1990-2005] compared to E_{act} derived from the historic RCM runs [1990-2005] for the averages of all AWSs combined

Concluding the meteorological time-series analysis, results are unsuitable for predicting seasonal precipitation. The seasonal cycle for actual evaporation might be accurate, but other than the WREVAP actual evaporation output, there is no other way currently at hand to verify the results. Therefore, the meteorological time-series cannot be used to make reliable calculations within a hydrological model on a seasonal basis. However, on an annual basis, these seasonal fluctuations are irrelevant. Therefore, modelling efforts are concentrated on the differences between annual averages only.
Concerning the direction of change, the best performing RCM model (the ensemble model), on average, shows a decreasing precipitation and increasing evaporation. Although lacking consensus, when considering only the three RCMs used, it is thus expected that there will be less water available to replenish groundwater losses throughout the 21st century.

3.3 Steady-state hydrological model

3.3.1 Meteorological model input

The meteorological time-series for the variables precipitation and evaporation were used to derive a climate change driven recharge, which was used as an input for the groundwater model. The recharge results proposed by the ensemble model, for individual AWSs, are grouped per watershed for both the RCP4.5 and RCP8.5 scenarios (figure 13a, b). As proposed earlier, recharge decreases from 2018 onwards, which is in contrast with the observational record.
Comparing each watershed to the average for the entire research area, it becomes clear that the Mekong watershed is the wettest and the Chi basin is the driest on average. RCP8.5 once again shows an exaggeration of the RCP4.5 scenario.

How this ensemble model holds up compared to the individual RCM models is illustrated in the PDF and CND for both RCP scenarios in appendix G1a, b. Recharge is depicted to decrease for the GFDL and IPSL model, which is in accordance with the ensemble model, while for the MPI model recharge increases slightly. This corresponds with the conclusions drawn from the meteorological timeseries-analysis for both precipitation and evaporation.

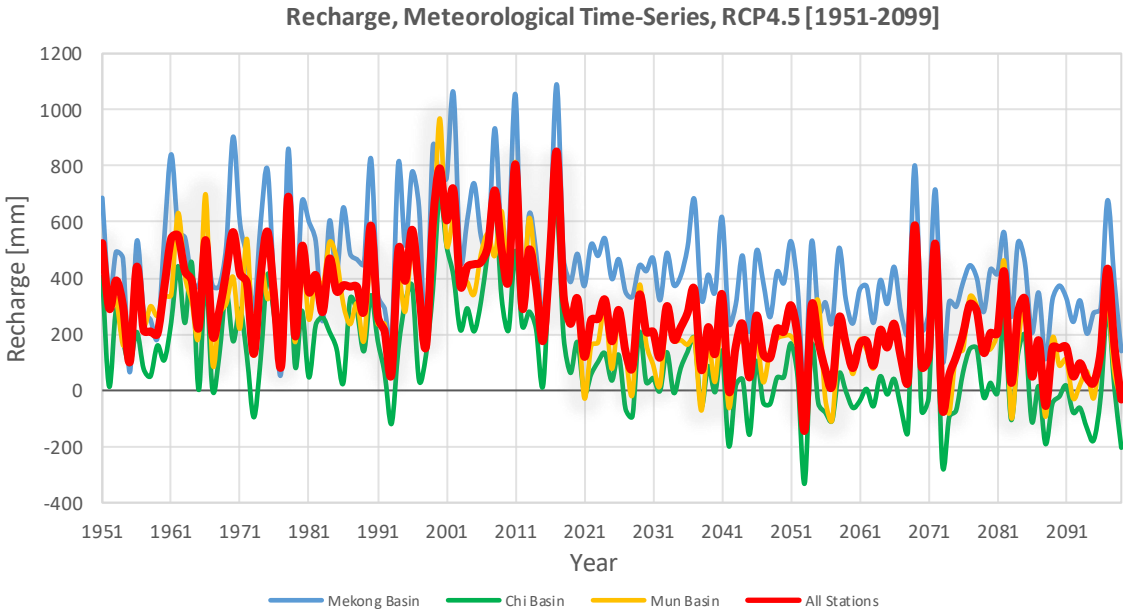

Figure 13a: Recharge, meteorological time series, RCP4.5, individual watersheds compared to the research area's average.

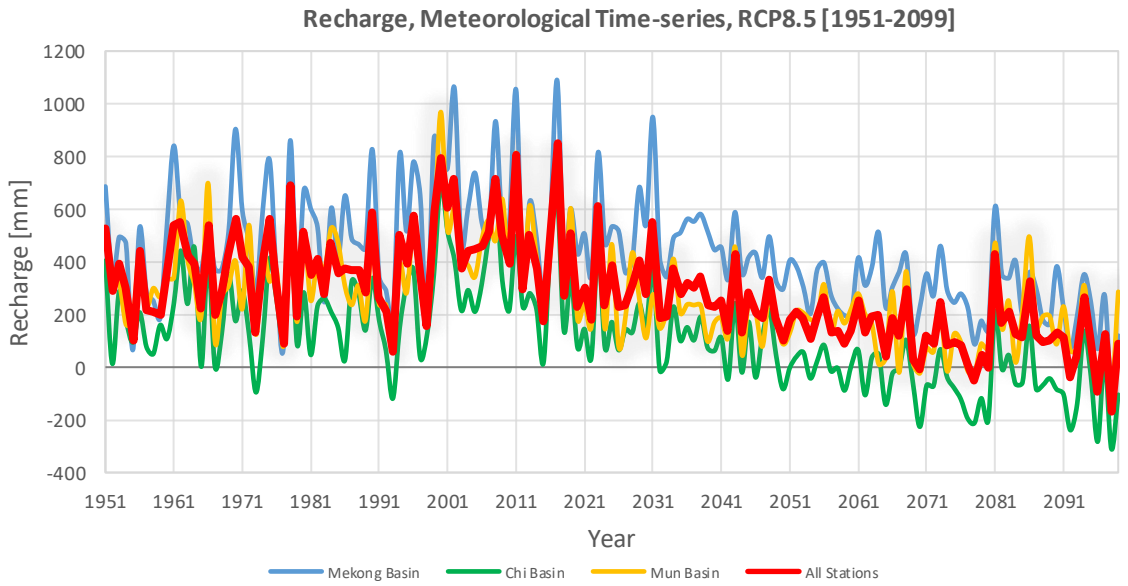

Figure 13b: Recharge, meteorological time series, RCP8.5, individual watersheds compared to the research area's average.

The interpolated recharge results for the entire research area, 1951-2001, are presented in figure 14. The periods 2002 – 2050 and 2051 – 2099 for both the RCP4.5 and RCP8.5 scenarios are available in appendix G2a, b, c, d. The average recharge values used, per AWS, for the interpolation are presented in appendix G3.

The interpolated results provide a clear picture of the recharge's spatial distribution, showing a decrease in recharge from a general east/northeast to west/southwest orientation. This again illustrates that the Mekong watershed is, relatively speaking, the wettest and the Chi watershed the driest.
When compared to the spatial distribution of recharge for 2002-2050 and 2051 – 209, the recharge distribution remains relatively unchanged for both RCP scenarios. However, an overall decrease in the total volume of recharge is evident from the change in magnitude visible in the legend.

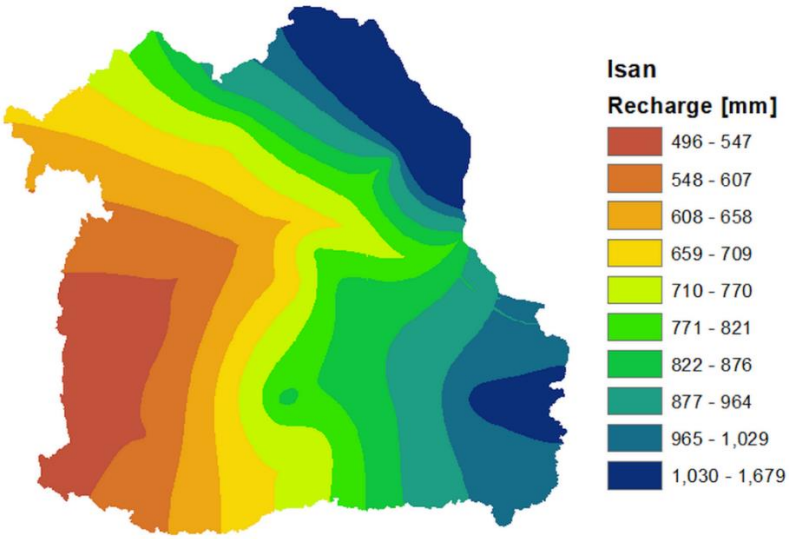

Figure 14: Historic average recharge distribution (1951-2001), Isan, Thailand.

3.3.2 Groundwater model validation

The interpolated hydraulic head, derived from the pumping wells provided by the DGR and now referred to as the "measured head", follows the contours of the DEM as would be expected. Flaws in the interpolation method become evident whenever the hydraulic head exceeds the DEM (appendix, H1).

The measured head, when compared to the historic model run, shows a similar distribution (appendix, H2a, b). The ability of the model to follow the fluctuations of the groundwater is confirmed when analysing cross-sections of the research area. Local trends are, although less so for extreme values, predicted by the model. However, a general underestimation of the hydraulic head is observed (appendix, H3).

The calculated difference between measured and modelled hydraulic head shows, for the most part, a relatively even distribution across the research area (appendix, H4a, b, c). When compensated for the changes in terrain elevation, the modelled SWL is less variable over short distances, providing a smoother image than is depicted by the measurements. Compared to the SWL of the interpolated observations, the historic model run shows strongly deviating values mostly along the edges of the research area fringed by the Mekong river and in the mountainous province of Loei (figure 15).

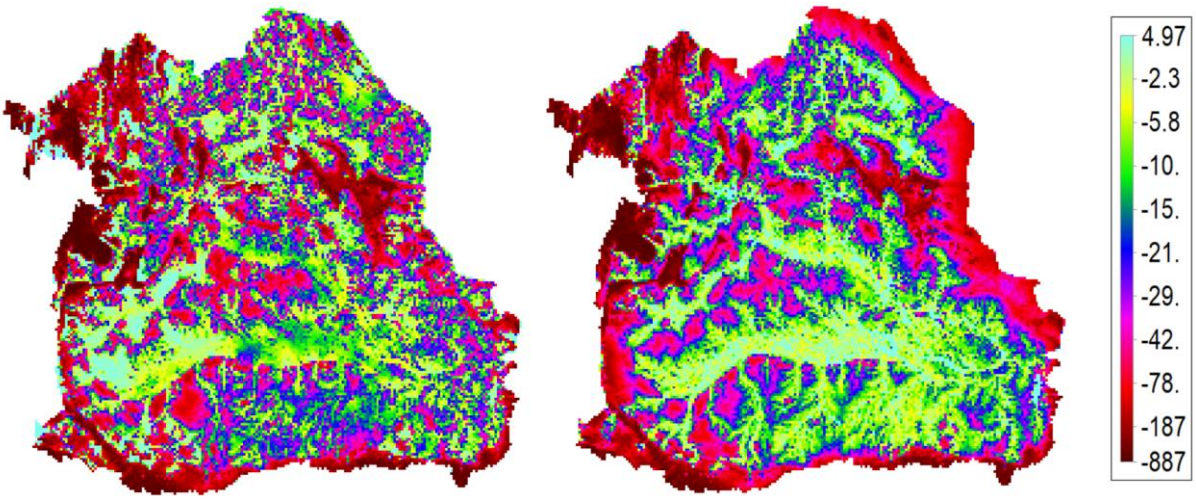

Figure 15: SWL (= HEADS – DEM), in meters, according to the observations (left) and historic model run (right) in 2001.

Statistical analysis of both the measured head and the historic model output, shows a mean value of similar magnitude, but larger standard deviation for the historic model run (table 4). With a RMSE of 39.22 m (18.28%), the model performance is not optimal. However, the RMSE and standard deviation are greatly influenced by the unrealistic drop in head along the north-east of the research area where Isan touches the Mekong river (appendix, H5). This unlikely decline in head is thought to be a error within the model, where it is unable to simulate realistic values due to indiscrepancies between the boundry conditions of the aquifer dataset and DEM used to run the model.

Areas where the difference between the measured head and the historic model run are more than the average deviation are illustrated in figure 16. The areas highlighted all have values that are below that of the observations.

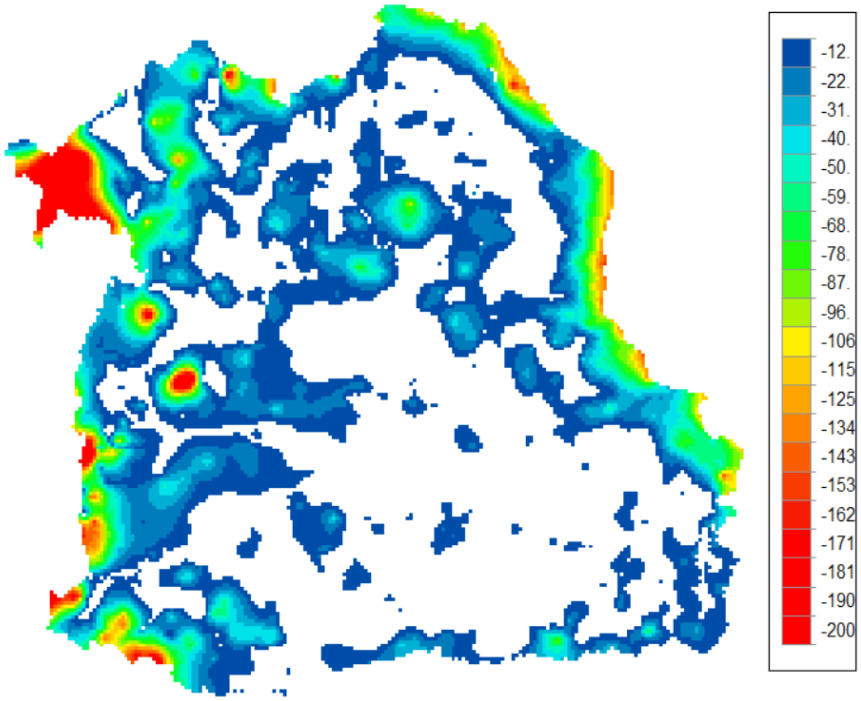

Figure 16: Areas (modelled) with a more than average deviation from the measured SWL, in meters.

	Measured head [m]	Historic model run [m]	Difference [m]
Mean	48.16	46.26	-12.72
Standard deviation	159.58	228.04	37.66

Table 4: Statistics for the difference between measured hydraulic head and the historical model run.

3.3.2 Climate change scenarios

After model performance assessment, differences between the modelled historic period and both future RCP4.5 and RCP8.5 scenarios were assessed spatially to locate those areas that would be most affected by climate change.

Average recharge values for RCP4.5, 2002-2050, suggest an increase in hydraulic head for the Mekong watershed and a decrease for the Mun and Chi watershed (appendix, H6a). Average recharge values for RCP4.5, 2051-2099, suggest a decline in hydraulic head throughout almost the entire research area (appendix, H6b). The more than average difference between both time periods illustrates the areas where the change in head is largest (figure 17a).

The RCP8.5 scenario provides a drier alternative, in which for the period 2002-2050 a decline in the hydraulic head for the entire research area is already visible (appendix, H7a) and is only intensified for the period 2051-2099 (appendix, H7b).

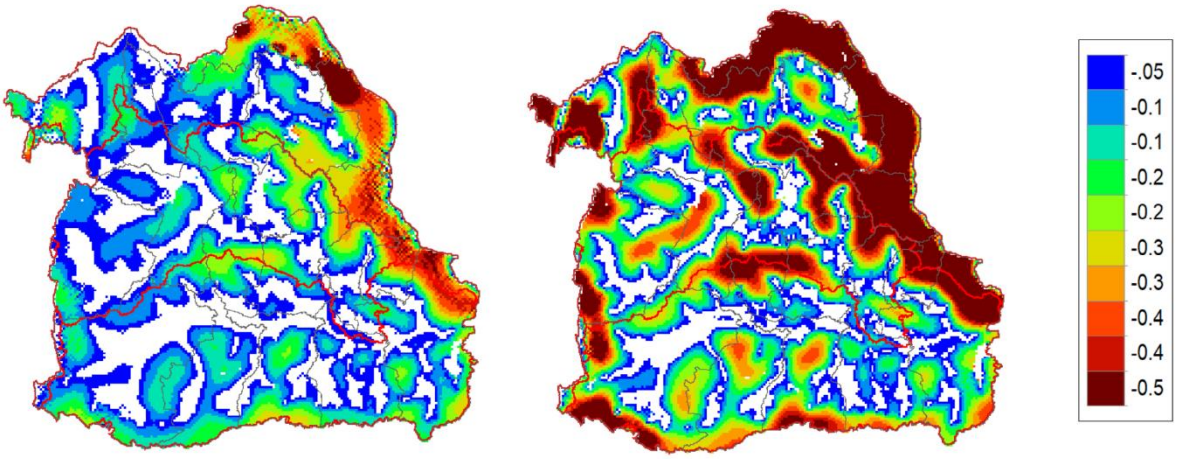

Figure 17a, b: The more than average difference between the historic model run and the ensemble model runs: RCP4.5 2050 (a, left) and RCP4.5 2100 (b, right), in meters.

Overall, the changes suggested by the RCP8.5 scenario portray a more intense version of the RCP4.5 scenario (figure 17b). Both suggest a drop of hydraulic head at the end of the 21st century, with a decrease in head first experienced in the Chi and Mun watershed.
According to the model, the most significant changes are expected to occur around the edges of the recharge area, while locations that are impacted the least correspond to locations in the vicinity of the rivers.
However, considering the incapability of the model to simulate the hydraulic head along the Mekong fringed border, it is uncertain whether these changes are due to an edge effect or that they can be contributed to climate change.

As a control, a derivation of Hooghoudt's formula (Hooghoudt, 1934) for unconfined aquifers was used to test the model's ability to predict the relative change in hydraulic head between the historic and future model scenarios (equation 2).

$$h^2(x) - h_0^2 = -\frac{N}{K}(x^2 - xL) + \frac{(h_L^2 - h_0^2)}{L}x \qquad \textit{(eq. 2)}$$

With "h(x)" being the hydraulic head at location x of the cross-section in meters. When calculated for all possible locations x, h(x) represents the potentiometric surface. "h(0)" is the hydraulic head of river one, at x equals 0 in meters and "h(l)" is the hydraulic head of river two, at x equals L in meters. "L" is the length of the cross-section, the distance between river one and two, in meters. "N" is the amount of recharge in meters and "K" is the hydraulic conductivity in meters per day. Finally, "x" is a chosen point location along length L in meters. The full derivation of Hooghoudt's formula is available in the appendix (H8).
The results from implementing Hooghoudt's empirical equation on a random cross-section in the research area between two river tributaries of equal elevation were compared to the differences in hydraulic head computed by the groundwater model. The cross-section used is presented in appendix H9a and b and its derived input for Hooghoudt's equation is made available in appendix H9c. The results are summarized in table 5.

Historic head (2001) according to interpolation of the observational data = 181.24 for x = 9000 m				
	RCP4.5, 2050	**RCP4.5, 2099**	**RCP8.5, 2050**	**RCP8.5, 2099**
Head difference Hooghoudt	305.86	307.43	273.28	319.82
Head difference iMOD model	0	-0.08	0.02	-0.13

Table 5: Hooghoudt's formula results compared to modelling output, in meters

Modelled results resemble the suggested interpolated value for hydraulic head derived from the observed SWL in 2001, with only a drop-in head of 13 cm for the most intense scenario (RCP8.5, 2051 - 2099).
Calculations using Hooghoudt's formula suggests unrealistically high groundwater levels, exceeding the DEM. Besides this impossibility, groundwater levels are rising throughout the 21st century, which is in contrast with expectations, referring to a decrease in recharge according to the meteorological time-series and the modelled hydraulic head.

Concluding the modelled climate change scenarios results, besides an increase in groundwater levels in the Mekong watershed for the first half of the 21st century, all modelled scenarios suggest a decrease in hydraulic head, whereas the RCP8.5 scenario presents a more intensified version of the RCP4.5 scenario.
Especially along the Mekong fringed border towards the east/northeast of the research area, but also along the edges of the research area, model results are questionable. In contrast to the relatively large drop in hydraulic head are the only small deviations near the rivers, which were assumed to have a constant head throughout the years.
To verify model accuracy, the Hooghoudt's equation was implemented. However, the unrealistic results suggest that the empirical formula is not suitable to calculate changes in hydraulic head within the research area.

3.3.3 Pumping Scenarios

Two pumping scenarios were fed to the hydrological model. Using the historic model run as a basis, the first scenario applied pumping at current capacity and the second implemented pumping at double capacity (figure 18).

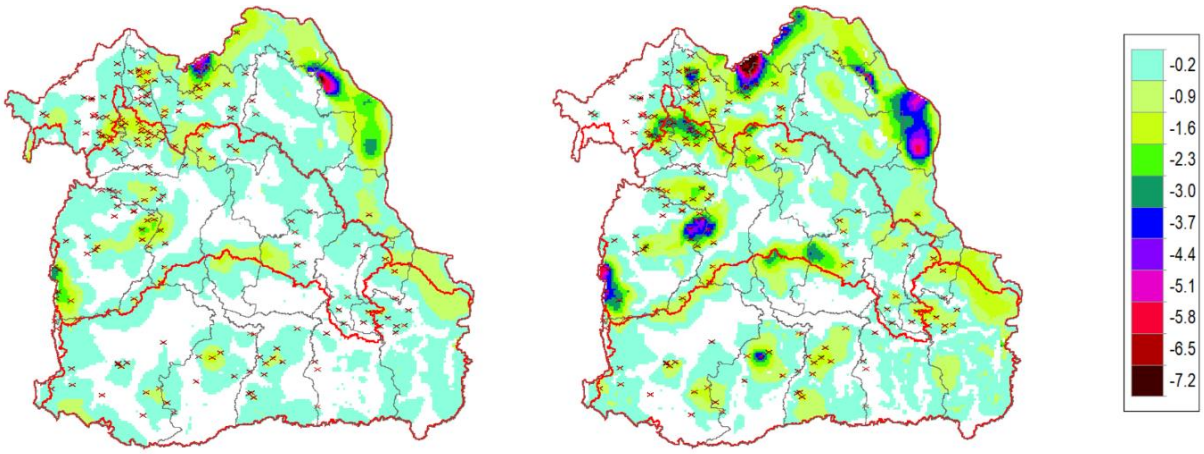

Figure 18: Pumping wells with more than twice the median capacity relative to the more than average difference between the historic model run without pumping and the historic model run with pumping at 100% (left) and 200% (right), in meters.

It needs to be mentioned that an increase in pumping with 200% effects individual pumps with varying magnitude relative towards each other. Pumping wells already running at high capacity were increased with an extra volume that, in some cases, was much larger relative to pumps that are running at low capacity. For example, a pumping well pumping 3 m^3/h was set to 6 m^3/h, while a pumping well which was pumping at 36 m^3/h was set to pump up 72 m^3/h of water. This implies a much bigger drawdown at location's were high capacity pumping stations are located.
Nevertheless, figure 17 shows that not all locations with a more than average deviation from a no pumping scenario have a high capacity pumping station present. While this is the case mostly in the south, southwest, west and northwest, both the centre and Mekong fringed border of the research area show a relatively big decline in SWL due to pumping.

Overall, in order, the watersheds most effected by pumping activities relative to each other are the Mekong, Chi and Mun watershed. On a provincial level, putting together a top seven, the biggest changes are expected for the provinces: Nakhon Phanom, Nong Khai, Chaiyaphum, Nong Bua Lamphu, Roi Et, Mahasarakham and Buriram.

3.3.4 Groundwater fluctuations

So far, the effects of climate change on groundwater fluctuations and the impact of groundwater pumping have been considered separately, but in reality they coincide.
Because of the model's consistent underestimation of the hydraulic head, the addition of pumping at the capacity registered for the historic model run for the year 2001 did not result in a better prediction of the absolute difference. However, on a relative basis, climate change results and pumping impact were combined to get a comprehensive view on the model's expected groundwater fluctuations for the 21st century, using the RCP8.5 and pumping at 200% scenarios for the biggest possible shift to occur (figure 19).

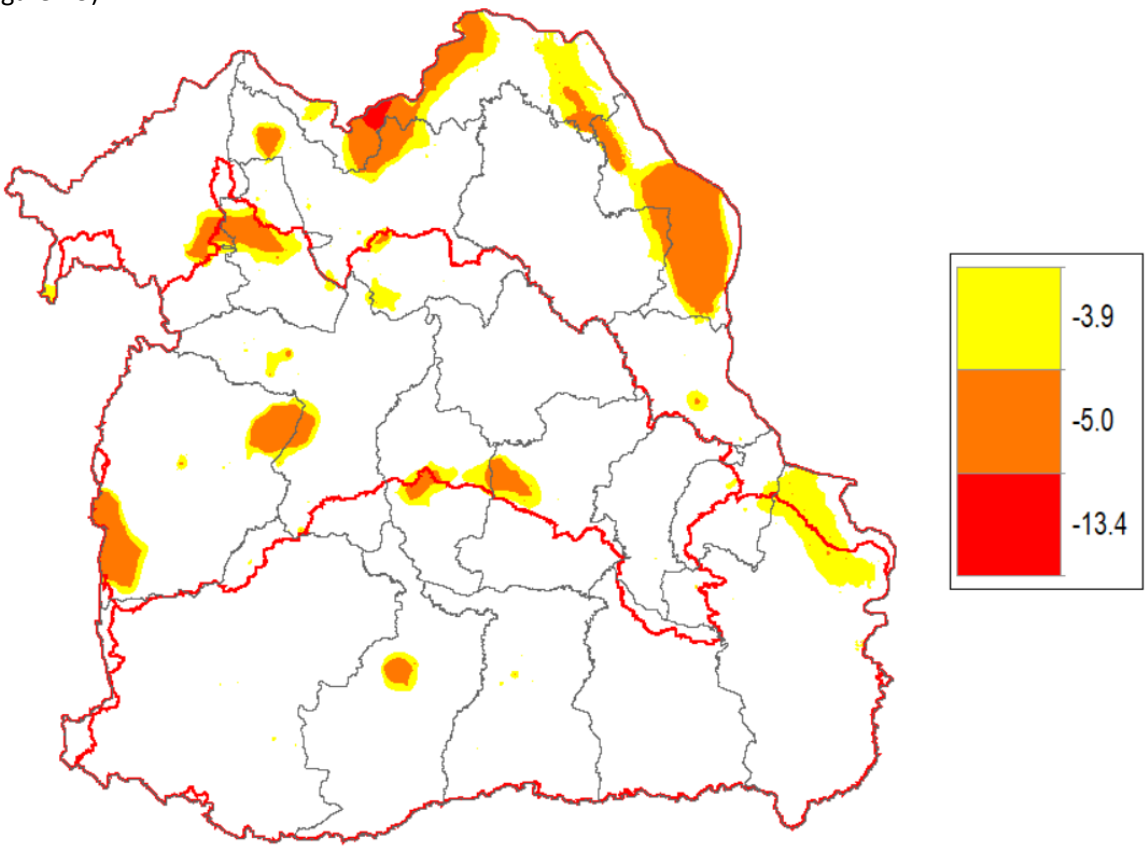

Figure 19: Abstract of the most effected areas according to the combined impact of pumping at double capacity and climate change scenario RCP8.5. The numbers, in meters, -3.9, -5.0 and -13.4 represent the 10, 5 and 1 percentile, respectively. A more detailed and extensive overview of these results is presented in appendix I.

The combined effect of the pumping of groundwater and reduction in recharge due to climate change results in the biggest drop in hydraulic head in the provinces: Nong Khai, Nakhon Phanom, Chaiyaphum, Nong Bua Lamphu, Roi Et, Mahasarakham and Buriram.
However, taking into consideration the model performance when recreating the historic SWL, the results along the Mekong fringed border and the edges of the research area should be interpreted with care. Also, those area's experiencing heavy drawdown, but that overlap with pumping wells with a high capacity are not to be taken as fact. When leaving both areas out of the analysis, the most remarkable changes in hydraulic head are found in the Chi watershed and include for the most part the provinces of Chaiyaphum Mahasarakham, Roi Et and Nong Bua Lamphu.
A more detailed and extensive overview of these results is provided in A0-format for management purposes and can be found in appendix I.

4. Discussion

As earlier work is not available to use as a comparison for the findings in this thesis, this discussion will give insight in the interpretation of the results and provides an overview of the potential improvements that could be made during future research.

4.1 Meteorological time-series

Seventeen AWSs were available for the determination of the magnitude and change of the meteorological variables. Considering the size of the research area (approximately 1.67×10^5 km^2), more measurement locations are needed to capture meteorological variability on a resolution comparable to that of the RCMs. Therefore, especially in areas where more variability can be expected, e.g. mountainous regions, interpolated values should be interpreted with more care.
Nevertheless, considering the overall flatness of the research area and the well-spaced distribution of the used AWSs, the data does provide a general distribution of the inter-provincial meteorological variation. To increase the operational resolution, the integration of daily rain-gauge data provided by APHRODITE (NCAR, 2017) can be considered to better the estimates of the highly variable precipitation distribution.

Besides the number of AWSs, the length of the historic record relative to that of the RCM records must also be taken into consideration.
With the creation of the synthetic record, the observational evaporation record was extended with 39 years, making it possible to calculate recharge for a historical period of 67 years. By doing so, the confidence in the historical record to serve as a representative reference for the RCM records (83 years) was increased considerably. Although average values for precipitation and temperature were similar to those found in literature (Floch & Molle, 2008; Marks, 2011), it can be argued that the synthetic record's accuracy might be less than desired. Therefore, its reconstruction regarding the individual variables (pr, et, tas, sh and rh) is discussed in greater detail below.

The tas reconstruction provided exceptionally well results, with an average deviation within 1% of the observed values. While the results for sh were good, they were not as accurate. However, its use was limited to the addition of 5 years prior to the observations. Therefore, its influence on the alteration of the observational record is negligible.

The results for the relative humidity extrapolation were less than desirable, compared to the satisfying average temperature and daily sunshine synthetic records.
When computing the relative humidity, both the revised MTCLIM and FAO method suggested by Emanuele Eccel (Eccel, 2012) were adopted as well for the computation of the saturation vapour pressure (e_s). However, results were not more favourable than those calculated by the standard formula for saturation vapour pressure, having a R^2 of 0.4, 0.11 and 0.4 for the FAO, MTCLIM and e_s calculation methods, respectively (appendix J1). Furthermore, the improved methodology recommended by Eccel, 2012 was not applicable due to the lack of certain parameters (e.g. extra-atmospheric radiation).
When verifying the assumption $T_{min} = T_{dew}$, by rewriting the formula for the calculation of the saturated vapour pressure for T_{min}, the calculated dew point temperatures did not match with the minimum (night time) temperatures. Only in 14% of all cases, dew point temperature was reached. Therefore, it must be concluded that the assumption $T_{min} = T_{dew}$ during night time is incorrect and the empirical formula for calculating saturation vapour pressure is not a viable method for computing relative humidity in Isan.
Due to the need for the relative humidity parameter in the WREVAP model and for lack of a better method it was implemented regardless. Unequivocally, its use is defensible when considering the acceptable WREVAP results.

Building upon the historical time series, the RCMs' precipitation outputs were lacking consensus for the direction of change in respect to the measurements. The ensemble model's credibility, and therefore the recharge calculations as well, would benefit from the inclusion of more than the three RCMs used, which could lead to a better consensus concerning the direction of change regarding precipitation. Unfortunately, other RCMs were not yet available during the time of writing. More climate models (that can be implemented) are currently being processed by the RU-CORE department and will be available at the end of 2019, provided by the Ramkhamhaeng University (RU-CORE, 2019).

In contrast to the results for precipitation, the RCM evaporation forecasts were coherent regarding the direction of change, showing an increase in the total amount of evaporation. Interestingly, the full time-series shows a decreasing trend throughout the extended pan-evaporation records, which is carried through by the measurement data for pan-evaporation. However, this trend is interrupted when the transition to the delta change extrapolated time-series occurs.
The extension of the potential evaporation time-series was realised using the delta change method for the actual evaporation variable supplied by the RCMs. Thus, the time-series shows a decreasing trend for potential evaporation derived from the measurements and an increasing trend for actual evaporation projections.
Considering the location of the research area and its topography, these results are in line with the pan-paradox theory (Brutsaert & Parlange, 1998; Liu, B. et al., 2009), which provides a possible explanation for this discontinuity.
Instead of using a pan-coefficient or a crop-coefficient to calculate actual-evaporation, a reduction factor was applied to convert the potential evaporation, which corresponded well with the values proposed by Fornés & Pirarai (2014). However, this method does not apply for water limited situations during dry season, leading to an overestimation of the total amount of evaporation during this period. Although the use of a reduction factor is an unsuitable method for modelling the seasonal cycle, it does not interfere on an annual basis for a steady state model.
Furthermore, the reduction factor was calculated for each individual watershed, because of the availability of potential runoff values in literature which were divided in the same way. The consequence of using this method is a sharp contrast in the amount of evaporation taking place between the different watersheds. However, it also resulted in a more evenly distributed recharge, because of the increased evaporation for those areas that received more precipitation. A result that would be expected for basins with similar characteristics in close proximity to each other.

4.2 Model input

The recharge, closely resembling the distribution pattern also described by Mongkolsawat et al. (2009), was used to simulate a changing climate and was calculated with the use of the meteorological time-series as (P + I) - E = R. This is an over-simplification, because fluxes like overland flow and soil moisture are being ignored. Also, values for irrigation emanate from the need to compensate negative recharge values and were assumed to be uniform across the research area. These simplifications overlook local variations in the topography and irrigation intensity, which could influence the recharge distribution. However, large parts of the research area, mostly the agricultural areas, have a consistent topography and therefore are likely to have little variation in e.g. overland flow characteristics.
Irrigation on the other hand, due to the lack of a national water distribution network, could very well have wildly variable intensities. Nevertheless, by implementing the different climate scenarios, the ability to identify areas that are most sensitive to a relative change in recharge is thereby not impeded.

The recharge was combined with the topography, simulated within the model using the DEM provided by the DGR. The DEM's inaccuracies resulted in a diversion of the river flow path compared to its flow path according to aerial photography. It was deemed unpractical and unnecessary to manually reroute the river system for a preliminary evaluation of the entire research area. However, one major difference was corrected (figure 5), leading to a redistribution of the surface area appointed to the Chi and Mun watershed.

The total surface area of each individual watershed after the correction was compared to the values suggested by Sanyu Consultants Inc. (2010). Relative surface areas of the different watersheds are now 96 %, 105% and 99% of the suggested values for the Mun, Chi and Mekong watersheds respectively. The implication resulting from the discrepancy in the relative size of the watersheds were minor inaccuracies in the values attributed to the watersheds when suggested values from literature are adopted. To further enhance flow accumulation patterns extracted from the DEM, and possibly reduce the differences with values for the relative surface areas of the three watersheds found in literature, manual rerouting of the river system can be expanded upon.

Furthermore, part of the Mekong and Chi watersheds extended over the administrative boundaries of the research area and had to be omitted. However, in reality, these areas would be contributing to the water balance of the Mekong and Chi watershed. The percentage of the total area cut relative to the watersheds is 0.6% relative to the research area (appendix J2). Although it concerns only a relatively small percentage of the watersheds, it leads to an underestimation of the total amount of precipitation that would have contributed to the watersheds overall recharge.
In contrast to the areas that extended over the administrative boundaries were the parts of Isan that did not belong to any of the three watersheds (1.1% of the entire research area, appendix J2). There, the modelled result, mostly along the south and southwest edge of the Mun watershed, compared to the observational hydraulic head, shows a more than average deviation.

A steady-state modelling method was opted to simulate groundwater fluctuations instead of a more desirable transient modelling method to reduce computational demands. Another reason for choosing a steady-state modelling method lies in the limitations of the ensemble model. The ensemble model was constructed using the average values from three RCMs. The variability of the ensemble was minimalized in comparison to the individual RCMs. This implies that for the ensemble, outliers are removed making the PDF for the period 2018-2100 much narrower than for the historical record. Therefore, the ensemble model would not be suitable for transient modelling. However, the three time-steps used to capture a change in recharge throughout the 21st century all use a single averaged value. The use of these averages' disregards variability throughout the years within each time-step. Thus, the ensemble model, for the methodology used, does not obscure model results for a multi-year period.

4.3 Model results

Concerning the model results, the trends in hydraulic head throughout the research area are, although less so for extreme values, replicated by the groundwater model. Model performance shows a general underestimation of the hydraulic head, rendering it currently unfit to express a realistic absolute change. However, this does not affect the model's capability to express the relative change between the periods 1951-2001, 2002-2050 and 2051 until 2100. It is possible that the systematic underestimation is caused by either insufficient irrigation or an overestimation of the horizontal permeability.
Irrigation values were set to counter negative recharge values. However, due to a lack of information concerning irrigation volumes and the spatial distribution thereof, the influence of the irrigation component could be underestimated. In comparison to the 440 mm average yearly irrigation used to supplement recharge values, literature suggestions, for irrigation of paddy rice fields in other areas under similar circumstances, provide low estimations of 550 mm during wet seasons and high estimations of over 1500 mm during dry seasons (Henry et al., 2016; Mandal et al., 2019; Materu et al., 2018). To compensate for the structural underestimation of the model's groundwater head, information on irrigation volumes, available upon request at the RID, could be used to enhance recharge calculations. Ideally, this information should be spatially defined to be able to model distributional differences.
Additionally, the horizontal permeability and transmissivity could benefit from a better connection between the information collected by the pumping wells and their corresponding aquifer. Due to the

lack of aquifer-ID's, concessions had to be made when coupling the pumping wells to their specific aquifer. This could have led to improper drainage, with current horizontal permeability values possibly draining the groundwater too quickly.
To enhance the accuracy of the hydrological conductivity and transmissivity values, aquifer-ID's are required, which can be provided by the DGR. With them, it would also be possible to group wells within the same aquifer together and construct a 3-D image of the aquifers' positions. The construction of a 3-D aquifer map would make a multi-layered hydrological groundwater model possible, better representing aquifer characteristics.

When interpreting the groundwater model's performance compared to the 2001 observations, it must not be forgotten that the strongly deviating values along the Mekong river play a substantial role in the establishment of the 18% RMSE. In contrast, all relatively flat areas, especially those along the rivers, show a less than average deviation from the suggested observational interpolation. Therefore, the inclusion of the Mekong river as a constant head boundary along the north-eastern border would prevent the extreme decline of hydraulic head near the edges of the research area fringed by the Mekong and thus, increase model performance.
Because of the river's absence within the DEM, the Mekong as a constant head boundary was not yet implemented. It is advised to expand upon the DGR's DEM to encompass the first neighbouring watersheds around the research area, not only to be able to include the Mekong as a constant head boundary, but also to resolve the discrepancies between watershed and administrative boundaries mentioned earlier.
If no extension of the DEM is available at the DGR for the areas outside of Thailand's borders, use can be made of e.g. the SRTM-DEM (USGS, 2015), which uses the same resolution. Otherwise, it would be recommended to convert the outer rim of the DEM into an artificial river, using aerial photography as a reference, e.g. Bing maps (Bing maps, 2019).

Furthermore, the assumption of the river being a constant head boundary is an oversimplification. According to Toda et al. (2004), the average Mun-Chi river discharge in the rainy-season is 3.65 times higher than during the dry-season (appendix, J3). This indicates that substantial fluctuations in the rivers head most certainly occur.
Also, a cell flow accumulation value of 200,000 was derived visually to encompass most of the research area. However, optimization has not yet taken place. Therefore, areas mostly fed by smaller tributaries might not be accounted for, leading to an underestimation of the amount of water flowing through a specific area and an overestimation of the decline in hydraulic head away from the riparian areas.
To further improve upon simulating the river's influence, optimization of the flow-accumulation raster could be performed by using the methodology described by Taroton et al. (1991) to derive an appropriate threshold value for stream network delineation.

When combining the impact of climate change with the expected pumping activity, the relative effect on the decline of the groundwater level from pumping is much bigger. While already a large number of wells (2396) were used to simulate the impact of groundwater extraction, their impact might be an underestimation. Considering that in 2008, throughout Thailand, an estimated 1,405,401 dug wells and 738,406 groundwater wells already existed, and that their numbers were rapidly increasing, more wells are likely to be present within the research area (Fornés & Pirarai, 2014; Sanyu Consultants Inc., 2010). Their location and annual yield could be incorporated in the model to get a more accurate representation of the effect of groundwater extraction on the lowering of the groundwater table. However, obtaining an accurate number and location of all wells in the region has proven to be very difficult, because low capacity wells are often constructed illegally and are therefore unregistered. Nevertheless, during data reconnaissance it was established that provincial departments might be able to provide more information on the matter.

Besides the possible model enhancements suggested above, extra analysis, outside of the scope of this research, could benefit the mapping of sensitive areas as well.
If the model's results would be compared with the location of irrigation projects (currently unknown), it is possible to cross reference which areas could either experience a more extreme decline in hydraulic head where groundwater extraction is the main source of irrigation waters or a lessened decline in hydraulic head, when receiving irrigation waters from the redirection of surface waters.
Also, the consequences of the lowering of the water table for the propagation of salt water intrusion could be investigated. Because of the importance of fresh groundwater for the livelihood of the region, salt water intrusion would render groundwater unfit for domestic use and therefore should be closely monitored.
Lastly, it would be advisable to invest in modelling efforts that describe the interannual groundwater fluctuations. Groundwater extraction is expected to be the most intense during the dry season, which will most certainly cause groundwater fluctuations to be more variable on a seasonal basis than on the modelled annual basis. In turn, this could also have consequences for the groundwater availability and salt water intrusion.

5. Conclusion

Several studies have investigated Isan's drought sensitivity and underlined the regional consequences. With the anticipated climate change induced rise in evaporation and more intense, less frequent rainfall, the already limited water resources are unable to regenerate under the increasing water demand. Therefore, it was expected that an increasing groundwater dependency for domestic and agricultural purposes would lead to a decline in groundwater head, especially during dry season and away from riparian areas.

The meteorological time-series constructed to investigate the change in recharge throughout the 21st century corresponds with the expected seasonal fluctuations for the historic period only. The historic record suggests an earlier peak precipitation in the rainy season, were the number of locations with hardly any precipitation increase during the dry season and the number of locations experiencing more intense rainfall events increases during the rainy season. This corresponds with expectations found in literature. However, the RCM records were not suitable for either verifying or expanding upon this analysis, rendering the possibility of making reliable calculations within a hydrological model on a seasonal basis forfeit.

On an annual basis, results are inconclusive on the direction of change regarding rh and sh. However, a rise in temperature is observed similar to that which is described in literature for all RCMs, whereas RCP8.5 shows an exaggeration of RCP4.5.
There is no consensus on either the change in direction or variability of the precipitation according to the RCMs used. In contrast, actual evaporation, although with varying variability, is increasing for all RCMs and their scenarios. The reduction in the total amount of precipitation for the RCM ensemble model, combined with a suggested increase in the amount of actual evaporation, results in less recharge available to replenish groundwater. Showing a decrease in recharge from a general east/northeast to west/southwest orientation, the RCP8.5, although with an overall smaller magnitude, suggests a similar recharge distribution as the RCP4.5, with the Chi watershed receiving the least recharge, followed by the Mun and Mekong watersheds.

The change in recharge throughout the 21st century is reflected by the groundwater model results. Showing only an increase in hydraulic head in the Mekong watershed for the period 2002-2050 for the RCP4.5, a decrease in the hydraulic head is predicted for all other scenario's and time periods for the entire research area, whereas the RCP8.5 provides a drier alternative relative to the RCP4.5 scenario. Although, the largest changes are expected to be along the Mekong fringed border and the edges of

the research area, these are likely to be related to model shortcomings. Relatively large declines that are believed to be accurate are in general distributed the furthest from riparian areas.
Regarding groundwater extraction, the largest impact of the modelled increase in pumping activity, due to higher water demands in the future, is found in Nakhon Phanom, Nong Khai, Chaiyaphum, Nong Bua Lamphu, Roi Et, Mahasarakham and Buriram. However, considering the methodology used, the most interesting changes occur in Mahasarakham crossing the border into Roi Et and in Nakhon Phanom, because of their change being unrelated to high intensity pumping wells.

Combining the modelled changes in hydraulic head predicted by the RCP scenarios and pumping scenarios, pumping showed to have greater consequences for the lowering of the groundwater table than climate change, locally. On the other hand, climate change causes a more evenly spread decline of the groundwater head over the entire north-east of Thailand, which is minimal only in the proximity of rivers. Therefore, areas most notable for their decline in hydraulic head at the end of the 21st century are located the furthest from riparian areas and coincide with location most effected by groundwater extraction. Taking into consideration the model's uncertainties mentioned in the discussion, these areas are, besides Buriram, all situated in the Chi watershed and include for the most part the provinces of Chaiyaphum Mahasarakham, Roi Et and Nong Bua Lamphu. A graphical representation of the locations where groundwater is most affected is given in appendix I.

To conclude, the line of reasoning in the paragraph below, based on both literature suggestions and this reports' research results, leads to a recommendation regarding the management of groundwater resources in Isan.
It is expected in literature, and confirmed by this study, that less precipitation and higher evaporation rates will reduce the availability of surface waters, resulting in droughts becoming more intense and frequent and the recharge of groundwater becoming less. With the growing practice of dry season irrigation, because of, amongst other things, rural poverty, water shortages will most likely increase, as well as the reliance of the population on groundwater for domestic use, especially during dry season. With an already expected decline of groundwater head defined within this study throughout all of Isan because of climate change, a continued intensification of groundwater extraction could lead to an increase in saltwater intrusion and eventually the unavailability of the groundwater resources. This is especially true for those areas defined within this study to be the most severely affected. Because of its importance for the livelihood of the region during droughts, it is advised not to expand upon groundwater use for irrigational purposes, to be able to keep the resource available for domestic use as a safeguard throughout periods of extended water shortages.

References

Bell, R. W., Seng, V., 2004, Rainfed lowland rice-growing soils of Cambodia, Laos, and North-east Thailand, Water in agriculture, Australian Centre for International Agricultural Research, No. 116, 239p

Bing Maps Aerial ©, 2019, Microsoft Corporation Earthstar Geographics, SIO

Boonlue C., 2005, The present condition on water resources development in the northeast region of Thailand, Proceedings of the International Symposium on Sustainable Development in the Mekong River Basin, Japan Science and Technology Agency

Brutsaert, W., Parlange, M.B., 1998, Hydrologic Cycle Explains the Evaporation Paradox, Nature, 396, 30, https://doi.org/10.1038/23845 [accessed: 14 june 2019]

Chitradon, R., Boonya-aroonnet, S., Thanapakpawin, P., 2009, Risk Management of Water Resources in Thailand in the Face of Climate Change, Sasin journal of management

Cruz F. T., Narisma G. T., Dado J. B., Singhruck P., Tangang F., Linarka U. A., Wati T., Juneng L., Phan-Van T., Ngo-Duc T., Santisirisomboon J., Gunawan D., Aldrian E., 2017, Sensitivity of temperature to physical parameterization schemes of RegCM4 over the CORDEX-Southeast Asia region, International Journal of Climatology, 37, 5139-5153, doi:10.1002/joc.5151

Eccel, E, 2012, Estimating air humidity from temperature and precipitation measures for modelling applications, *Meteorol. Appl.* 19, 118–128, DOI: 10.1002/met.258, San Michele all'Adige, Italy

Eckstein, D., Hutfils, M. L., Winges, M., 2019, Global Climate Risk Index 2019, Who Suffers Most From Extreme Weather Events?, Weather-related Loss Events in 2017 and 1998 to 2017, Germanwatch, available at: https://germanwatch.org/sites/germanwatch.org/files/Global%20Climate%20Risk%20Index%202019_2.pdf [accessed: 13 June 2019].

FAO, 2016, AQUASTAT Thailand, Food and Agriculture Organization of the United Nations (FAO), available at: http://www.fao.org/nr/water/aquastat/countries_regions/THA/ [accessed: 12 June 2019]

Floch, P., Molle, F., 2008, marshalling water resources: a chronology of irrigation development in the Chi-Mun river basin, northeast Thailand

Fornés, J., Pirarai, k., 2014, Groundwater in Thailand, Journal of Environmental Science and Engineering B3, 304-315, doi: 10.17265/2162-5263/2014.06.003

Fukai, S., Rajatsasereekul, S., Boonjung, H. and Skulkhu, E., 1995, Simulation modelling to quantify the effect of drought for rainfed lowland rice in Northeast Thailand, Fragile Lives in Fragile Ecosystems, Proceedings of the International Rice Research Conference, Los Baños, Philippines, IRRI, 657–674.

Friend, R., Thinphanga, P., 2018, Urban Water Crises under Future Uncertainties: The Case of Institutional and Infrastructure Complexity in Khon Kaen, Thailand, Sustainability 10, 3921, MDPI

Global Administrative Areas (2015). GADM database of Global Administrative Areas, version 2.8, www.gadm.org [accessed: 14 June 2019]

Henry, C. G., Hirsh, S. L., Anders, M. M., Vories, E. D., Reba, M. L., Watkins, K. B., Hardke, J. T., 2016, Annual Irrigation Water Use for Arkansas Rice Production, Journal of Irrigation and Drainage Engineering, Vol. 142, Issue 11, DOI: 10.1061/(ASCE)IR.1943-4774.0001068

Hobbins, M. T., Ramírez, J. A., Brown, T. C., and Claessens, L. H. J. M., 2001, The complementary relationship in estimation of regional evapotranspiration, The Complementary Relationship Areal Evapotranspiration and Advection-Aridity models, Water Resour. Res., 37, 1367–1387

Holbo, H.R., 1981, A dew-point hygrometer for field use, Agricultural Meteorology, 24, 117–130

Hutchinson, M. F., 1988, Calculation of hydrologically sound digital elevation models, Third International Symposium on Spatial Data Handling, Sydney, Australia

Hooghoudt, S. B., 1934, Bijdrage tot de kennis van enige natuurkundige grootheden van de grond, Verslagen Landbouwkundig Onderzoek, No. 40 B, pp 215-345

Hutchinson, M. F., Xu, T., Stein, J. A., 2011, Recent Progress in the ANUDEM Elevation Gridding Procedure, Geomorphometry, 19-22, Redlands, California, USA, http://geomorphometry.org/HutchinsonXu2011 [accessed: 14 June 2019]

Jenson, S. K., Domingue, J. O., 1988, Extracting Topographic Structure from Digital Elevation Data for Geographic Information System Analysis, Photogrammetric Engineering and Remote Sensing, 54 (11), 1593-1600

Juneng L., Tangang F., Chung J. X., Ngai S. T., Tay T. W., Narisma G., Cruz F., Phan-Van T., Ngo-Duc T., Santisirisomboon J., Singhruck P., Gunawan D., Aldrian E., 2016, Sensitivity of the Southeast Asia Rainfall Simulations to Cumulus and Air-Sea Flux Parameterizations in RegCM4, Climate Research, 69, 59-77, doi: 10.3354/cr01386

Kemtong, T., Angskul, T., 2019, Seven provinces declared drought disaster zones, National News Bureau of Thailand (NNT), available at: http://nbtworld.prd.go.th/en/news/detail/TCATG190510105006723 [accessed: 12 June 2019]

KKU-Ford, 1982, An Agroecosystem Analysis of Northeast Thailand, KKU-Ford Cropping System Project, Faculty of Agriculture, Khon Kaen University

Krittasudthacheewa, C., Polpanich, O., Bush, A., Srikuta, P., Kemp-Benedict, E., Inmuong, Y., Inmuong, U., Featherston, P., Eagleton, G., Naruchaikusol, S., Pravalprukskul, P., Krawanchid, D., 2012, Final Report for the Northeast Thailand Futures: A Local Study of the Exploring Mekong Region Futures Project, Commonwealth Scientific and Industrial Research Organisation

Lightfoot, R. P., 1981, Problems of Resettlement in the Development of River Basins in Thailand, River Basin Planning: Theory and Practice, Interscience Publications, Great Britain

Limpinuntana, V., 2001, Physical Factors as related to agricultural potential and limitations in the northeast Thailand, Natural Resources Management Issues in the Korat Basin of Northeast Thailand, International Rice Research Institute, Los Banos, Philippines

Limsakul, A., Kachenchart, B., Singhruck, P., Saramul, S., Santisirisomboon, J., Apipattanvis, S., 2019, Updated Basis Knowledge of Climate Change Summarized from the First part of Thailand's Second Assessment Report on Climate Change, Applied Environmental Research

Liu, B., Ma, Z., Xu, J., Xiao, Z., 2009, Comparison of pan evaporation and actual evaporation estimated by land surface model in Xinjiang from 1960 – 2005, Journal of Geographical Sciences, Volume 19, Issue 4, pp 502-512, https://doi.org/10.1007/s11442-009-0502-5 [accessed: 14 June 2019]

Mandal, K.G., Thakur, A., Ambast, S.K., 2019, Current rice farming, water resources and micro-irrigation, Current Science, 116, 568-576, DOI: 10.18520/cs/v116/i4/568-576

Marks, D., 2011, Climate Change and Thailand: Impact and Response, contemporary Southeast Asia Vol. 33, No. 2, pp 229 -58, DOI: 10.1355/cs33-2d

Materu, S. T., Shukla, S., Sishodia, R. P., Tarimo, A., Tumbo, S. D., 2018, Water Use and Rice Productivity for Irrigation Management Alternatives in Tanzania, Water, DOI: 10.3390/w10081018

McMahon, T. A., Peel, M. C., Lowe, L., Srikanthan, R., and McVicar, T. R., 2013, Estimating actual, potential, reference crop and pan evaporation using standard meteorological data: a pragmatic synthesis, Hydrol. Earth Syst. Sci., 17, 1331-1363, https://doi.org/10.5194/hess-17-1331-2013 [accessed: 13 June 2019]

Molle, F., 2003, Development Trajectories of River Basins: A Conceptual Framework, Research Report No 72, Colombo: IWMI, http://www.iwmi.cgiar.org/pubs/pub072/Report72.pdf [accessed: 13 June 2019]

Mongkolsawat, C., Thirangoon, P., Suwanweramtorn, R., Karladee, N., Paiboonsank, S., Champathet, P., 2009, An evaluation of drought risk area in Northeast Thailand using remotely sensed data and GIS, Faculty of Agriculture, Khon Kaen University, Thailand

Morton, F. I., 1983, Operational estimates of areal evapotranspiration and their significance to the science and practice of hydrology, J. Hydrol., 66, 1–76

Morton, F. I., Richard, F., and Fogarasi, S., 1985, Operational estimates of areal evapotranspiration and lake evaporation – Program WREVAP, NHRI Paper 24, Inland Waters Directorate, Environment Canada, Ottawa

NCAR, 2017, "The Climate Data Guide: APHRODITE: Asian Precipitation - Highly-Resolved Observational Data Integration Towards Evaluation of Water Resources, National Center for Atmospheric Research Staff, https://climatedataguide.ucar.edu/climate-data/aphrodite-asian-precipitation-highly-resolved-observational-data-integration-towards [accessed: 20 June 2019]

NEDECO, 1988, Perspectives for Mekong development: Indicative plan for the development of land, water and related resources of the Lower Mekong Basin, Electrowatt Engineering Services Ltd. and Asian Engineering Consultants Corp. Ltd. For the Interm Committee for Coordination of Investigations of the Lower Mekong Basin

Ngo-Duc T., Tangang F. T., Santisirisomboon J., Cruz F., Trinh-Tuan L., Nguyen-Xuan T., Phan-Van T., Juneng L., Narisma G., Singhruck P., Gunawan D., Aldrian E., 2017, Performance evaluation of RegCM4 in simulating extreme rainfall and temperature indices over the CORDEX-Southeast Asia Region, International Journal of Climatology, 37, 1634-1647, doi: 10.1002/joc.4803

Palanisami, K., Apinantara, A., 1984, Performance Evaluation and Investment Priorities in Irrigation Systems of Northeast Thailand, Faculty of Agriculture, Khon Kaen University, Khon Kaen, Thailand

Patamatamkul, S., 2001, Water Resources Development and Management in the Korat Basin, Northeast Thailand, Natural Resource Management Issues in the Korat Basin of Northeast Thailand, International Rice Research Institute, Los Banos, Philippines

Pholkern, K., Saraphirom, P., Srisuk., 2018, Potential impact of climate change on groundwater resources in the Central Huai Luang Basin, Northeast Thailand, Science of the Total Environment, 633, 1518-1535

Planchon, O., Darboux, F., 2002, A fast, simple and versatile algorithm to fill the depressions of digital elevation models, Catena 46 (2), 159-176

Prapertchob, P., 2001, Human Resources and the Economy of the Northeast Region of Thailand, Natural Resource Management Issues in the Korat Basin of Northeast Thailand, International Rice Research Institute, Los Banos, Philippines

RU-CORE, 2019, Ramkhamhaeng University Center of Regional Climate Change and Renewable Energy, Ramkhamhaeng University, Bangkok, Thailand, http://www.rucore.ru.ac.th/SARCCIS [accessed: 14 June 2019]

Sanyu Consultants Inc., 2010, Survey on Basic Data/Information Collection and Confirmation on Water Resource Management in Northeast Region of Thailand Final Report, Japan International Cooperation Agency

SEACLID-CORDEX, 2019, Southeast Regional Climate Downscaling - Coordinated Regional Climate Downscaling Experiment, http://www.ukm.edu.my/seaclid-cordex/ [accessed: 14 June 2019]

Sethaputra, S., Thanopanuwat, S., Kumpa, L., Pattanee, S., 2001, Thailand's water vision: A case study, Vision to Action: A synthesis of experiences in Southeast Asia, Food and Agricultural Organization/Economic and Social Commission for Asia-Pacific

Srisuk, K., 1997, Conceptual groundwater model for saline water and saline soils in the Chi-Mun basin, northeast Thailand, International Symposium on Hydrology and Water Resources for Research and Development in Southeast Asia and the Pacific, Nong Khai, Thailand

Szilagyi, J., 2001, Modeled areal evaporation trends over the conterminous United States, J. Irrig. Drain. E. ASCE, 127, 196–200

Tangang, F., Supari, S., Chung, J., Cruz, F., Salimun, E., Ngai, S., . . . Hein-Griggs, D., 2018, Future changes in annual precipitation extremes over Southeast Asia under global warming of 2°C, APN Science Bulletin, 8 (1), doi:10.30852/sb.2018.436

Taroton, D. G., Bras, R. L., Rodriguez-Iturbe, I., 1991, On the Extraction of Channel Networks from Digital Elevation Data, Hydrological Processes 5, 81-100

Thailand Country Report, 2009, Department of Disaster Prevention and Mitigation (DDPM), Ministry of Interior, Thailand, Asian Disaster Reduction Center

Thailand Country Report, 2016, Department of Disaster Prevention and Mitigation (DDPM), Ministry of Interior, Thailand, Asian Disaster Reduction Center

Toda, O., Tanji, H., Somura, H., Higuchi, K., Yoshida, K., 2004, Evaluation of tributaries contribution in the Mekong river basin during rainy and dry season

USGS, 2015, Shuttle Radar Topography Mission, void-filled SRTM v3.0, Global Land Cover Facility, University of Maryland, College Park, Maryland

Vermeulen, P.T.M, L.M.T. Burgering, F.J. Roelofsen and B. Minnema, J. Verkaik, 2018, *iMOD user manual* version 4.2.1, Deltares, The Netherlands, http://oss.deltares.nl/web/iMOD [accessed: 13 June 2019]

Wongsomsak, S., 1986, Salinization in Northeast Thailand, Southeast Asian Studies, Vol. 24, No. 2, Kyoto University, Japan

WMO, 1979, World Meteorological Organization, Technical Regulations, Vol. I, No. 49, I-Ap-C-3, Geneva, Switzerland

Worldometers.info, 2019, Thailand Population (2019), Worldometers [online], available at: https://www.worldometers.info/world-population/thailand-population/ [accessed: 12 June 2019]

Appendices

Table of contents

Overview of all graphs and figures presented in the appendices with their (abbreviated) description.

Appendix A: Provinces and TDS

A1: The 19 provinces that constitute Isan.

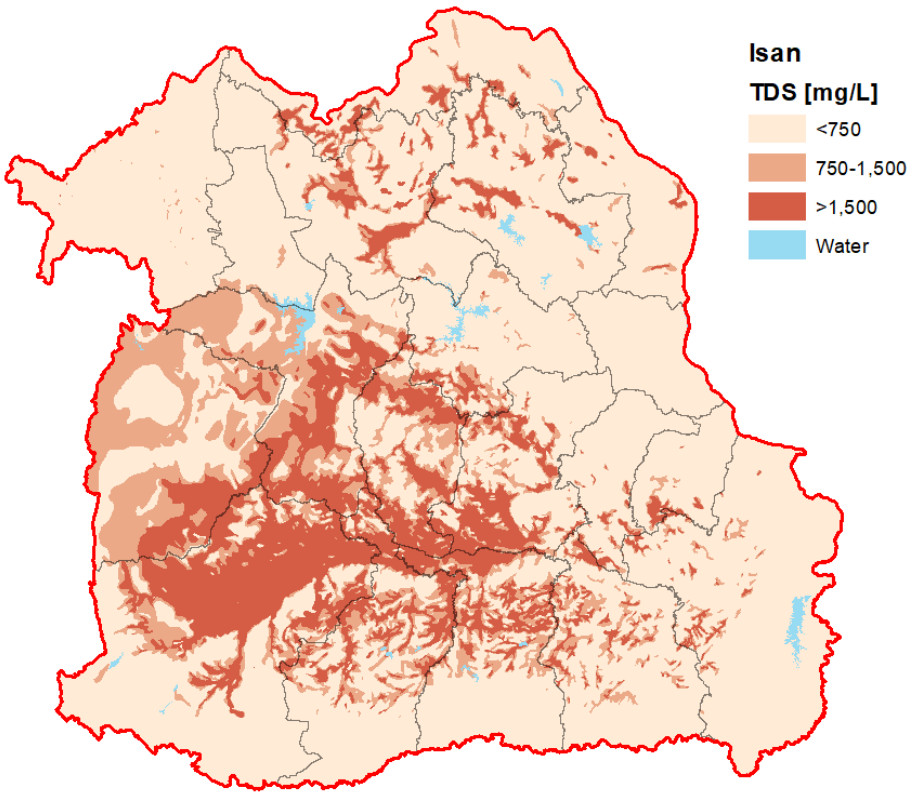

A2: The distribution of the total dissolved solids (TDS) concentration throughout the research area (data provided by the DGR).

Appendix B: Observational and synthetic record

Thai Meteorological Department (TMD)																
Data overview	Khon Kaen	Mukdahan	Mahasarakham	Kalasin	Roi et	Ubon Ratchathani	Nakhon Ratchasima	Surin	Buriram	Sisaket	Nong Khai	Nong Bua Lamphu	Nakhon Phanom	Sakon Nakhon	Loei	Udon Thani	Chaiyaphum
Max daily temp (°C)	1951-2017	1953-2017	1970-2017	1996-2017	1953-2017	1951-2017	1951-2017	1951-2017	2001-2017	1984-2017	1968-2018	2013-2018	1953-2018	1951-2018	1955-2018	1951-2018	1957-2018
Min daily temp (°C)	1951-2017	1953-2017	1970-2017	1996-2017	1953-2017	1951-2017	1951-2017	1951-2017	2001-2017	1984-2017	1968-2018	2013-2018	1953-2018	1951-2018	1954-2018	1951-2018	1957-2018
Avg daily (dry bulb) temp (°C)	1951-2017	1951-2017	1989-2017	1999-2017	1951-2017	1951-2017	1951-2017	1951-2017	2004-2017	2007-2017	1968-2018	2014-2018	1953-2018	1951-2018	1954-2018	1951-2018	1957-2018
Relative humidity (%)	1981-2017	1981-2017	1987-2017	2000-2017	1981-2017	1981-2017	1981-2017	1981-2017	2004-2017	2007-2017	1981-2018	2011-2018	1981-2018	1981-2018	1981-2018	1981-2018	1981-2018
Rainfall daily (mm)	1951-2017	1951-2017	1970-2017	1996-2017	1951-2017	1951-2017	1951-2017	1951-2017	2001-2017	1984-2017	1965-2018	2013-2018	1953-2018	1951-2018	1954-2018	1951-2018	1957-2018
DailySunshine hours (hrs)	1958-2018	N/A	N/A	N/A	1961-2018	1956-2018	1957-1981	1961-2018	N/A	1984-2018	N/A	N/A	1958-2018	1962-2018	1961-2018	N/A	N/A
Pan evaporation (mm)	1990-2018	1990-2018	1990-2018	1996-2018	1990-2018	1990-2018	1990-2018	1990-2018	2001-2018	1990-2018	1990-2018	2013-2018	1990-2018	1990-2018	1990-2018	1990-2018	1990-2018
WREVAP	1981-2017	1981-2017	1987-2017	2000-2017	1981-2017	1981-2017	1981-2017	1981-2017	2004-2017	2007-2017	1981-2017	2013-2018	1981-2017	1981-2017	1981-2017	1981-2017	1981-2017
WREVAP extended	1951-2017	1953-2017	1970-2017	1996-2017	1953-2017	1951-2017	1951-2017	1951-2017	2001-2017	1984-2017	1968-2018	2013-2018	1953-2018	1951-2018	1955-2018	1951-2018	1957-2018

B1: The length of observations for all TMD AWS associated variables.

TMD AWS locations, Isan					
Province/Location	**Station Code/WMO Index**	**Provided Lat/longitude**	**Adjusted Lat/longitude**	**UTM Zone 48 Coordinates**	**Station elevation in meters**
Khon Kaen	381201/48381	N16.27.40.0 & E102.47.23.0	N16.46.49.5 & E102.78.70.7	N1821660.366 & E263741.794	214
Roi Et	405201/48405	N16.10.12.0 & E103.44.38.0	N16.11.65.8 & E103.77.83.0	N1782218.576 & E369356.818	155
Surin	432201/48432	N14.53.00.0 & E103.30.00.0	N14.87.13.2 & E103.49.72.1	N1644638.613 & E338334.883	164
Nakhon Ratchasima	431201/48431	N14.58.50.9 & E102.50.90.7	N14.92.75.1 & E102.07.42.0	N1652380.938 & E185229.868	248
Mukdahan	383201/48383	N16.32.29.0 & E104.43.44.0	N16.54.59.6 & E104.72.59.4	N1829348.671 & E470759.453	159
Ubon Ratchathani	407501/48407	N15.15.00.0 & E104.52.00.0	N15.24.67.8 & E104.87.05.2	N1685625.941 & E486096.826	138
Buriram	436201/48437	N15.13.32.7 & E103.14.53.1	N15.22.81.7 & E103.24.77.1	N1684319.421 & E311791.641	206
Mahasarakham	387401/48382	N16.14.50.0 & E103.40.50.0	N16.18.48.3 & E103.30.06.7	N1790131.722 & E318331.291	170
Kalasin	388401/48390	N16.19.57.0 & E103.35.18.0	N16.42.44.0 & E103.51.17.4	N1816465.317 & E341094.770	165
Sisaket	409301/48409	N15.00.00.0 & E104.30.00.0	N15.12.03.4 & E104.32.16.1	N1671749.479 & E427107.324	149
Udon Thani	354201/48354	N17.23.00.0 & E102.48.00.0	N17.38.70.5 & E102.77.53.4	N1923745.402 & E263642.508	194
Loei	353201/48353	N17.27.00.0 & E101.44.00.0	N17.44.57.7 & E101.72.69.7	N1931849.005 & E152285.735	285
Sakon Nakhon	356201/48356	N17.90.00.0 & E104.80.00.0	N17.18.84.7 & E104.11.50.4	N1900620.338 & E405894.912	179
Nong Khai	352201/48352	N17.52.10.8 & E102.43.58.9	N17.86.77.4 & E102.74.42.7	N1976997.679 & E260975.151	197
Nakhon Phanom	357201/48357	N17.24.39.0 & E104.46.57.0	N17.38.89.7 & E104.64.45.8	N1922621.382 & E462247.866	199
Nong Bua Lumphu	360201/48360	N17.13.57.0 & E102.25.46.0	N17.20.74.4 & E102.44.60.0	N1904295.238 & E228371.132	247
Chaiyaphum	403201/48403	N15.48.00.0 & E102.20.00.0	N15.80.79.2 & E102.03.30.1	N1749932.818 & E182134,737	203

B2: The suggested and adjusted locations of the TMD AWSs and their elevation in Isan.

Missing values (%)	Average %	SD	>SD + avg no. locations	Total no. Locations
All (7) variables	1.0	3.2	6	111
Max daily temp (°C)	0.6	1.0	3	17
Min daily temp (°C)	0.6	0.9	2	17
Avg daily (dry bulb) temp (°C)	0.1	0.1	3	17
Relative humidity (%)	1.6	6.4	1	17
Rainfall daily (mm)	0.4	1.1	2	17
Daily Sunshine hours (hrs)	4.8	3.8	1	9
Pan evaporation (mm)	1.0	2.8	2	17

B3: Percentage of missing values in TMD observational data per meteorological variable.

Location	Data records	extension	Extended months	Substitute location
Khon Kaen	4-1957 until 12-2017	01-1951 until 04-1957	75	N/A
Mukdahan	4-1957 until 12-2017	01-1953 until 04-1957	51	Nakhon Phanom
Mahasarakham	N/A	Substitute	Full duration	Roi Et
Kalasin	N/A	Substitute	Full duration	Roi et
Roi Et	9-1960 until 12-2017	01-1953 until 9-1960	92	N/A
Ubon Ratchathani	1-1955 until 12-2017	01-1951 until 01-1955	48	N/A
Nakhon Ratchasima	1-1957 until 10-1981	01-1951 until 01-1957 & 11-1981 tot until met 12-2017	506	Nakhon Ratchasima
Surin	9-1960 until 12-2017	01-1951 until 9-1960	116	N/A
Buriram	N/A	Substitute	Full duration	Surin
Sisaket	N/A	Substitute	Full duration	N/A
Nong Bua Lamphu	N/A	Substitute	Full duration	Khon Kaen
Nong Khai	N/A	Substitute	Full duration	Khon Kaen
Chaiyaphum	1-1957 until 10-1981	11-1981 until 12-2017	434	Nakhon Ratchasima
Nakhon Phanom	4-1957 until 12-2017	01-1953 until 04-1957	51	N/A
Sakon Nakhon	4-1961 until 12-2017	01-1951 until 04-1961	123	N/A
Udon Thani	4-1957 until 12-2017	01-1951 until 04-1957	75	Khon Kaen
Loei	9-1960 until 12-2017	01-1955 until 9-1960	68	N/A

B4: A description of the locations used as a substitute for other locations that did not have daily sunshine hours measurements.

Appendix C: RCM records

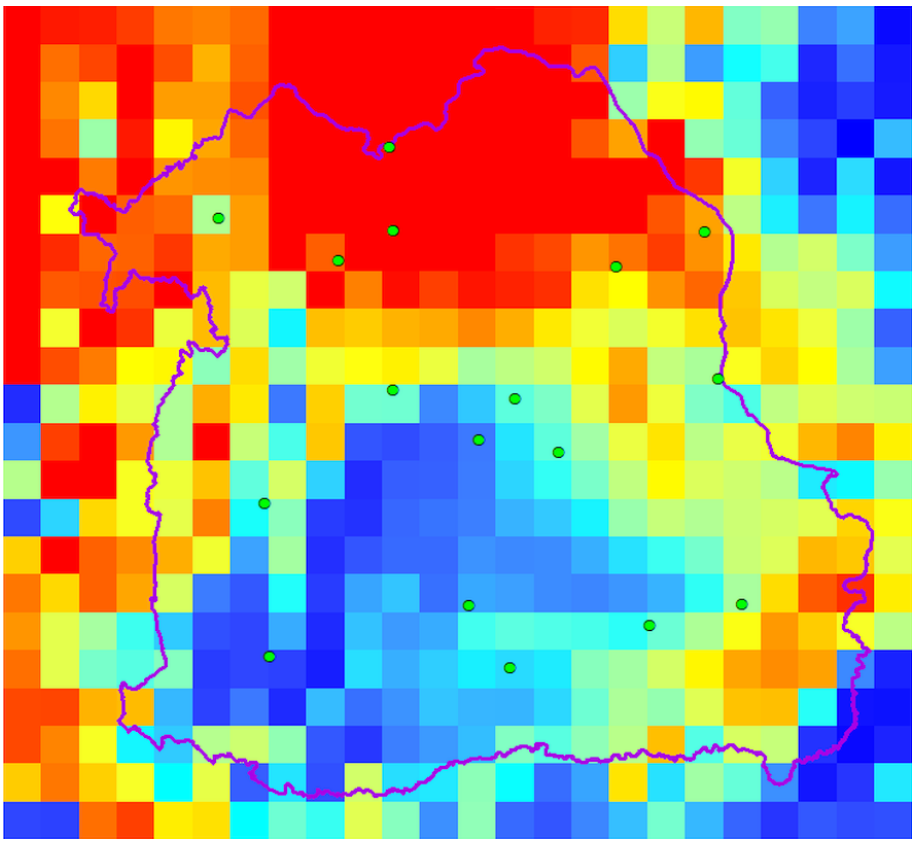

C1a: An example RCM raster in respect to the research area, serving as a spatial illustration to give the relative position of the AWSs (green dots) to the RCM model cells.

Selected RCM cells*		
Cell Number	→	↓
Khon Kaen	11	11
Mukdahan	19	11
Mahasarakham	13	12
Kalasin	14	11
Roi et	15	13
Ubon Ratchathani	20	17
Nakhon Ratchasima	8	18
Surin	14	18
Buriram	13	17
Sisaket	18	17
Nong Khai	11	5
Nong Bua Lamphu	9	8
Nakhon Phanom	19	7
Sakon Nakhon	17	8
Loei	6	7
Udon Thani	11	7
Chaiyaphum	7	14
*starting from the top left towards to bottom right		

C1b: The extracted cell numbers from the RCM raster, representing the individual AWSs.

R_script_netCDF_ climate_data_extraction

```
###working R_script historical GFDL-output###                    #working title

setwd("C:/R_Workdirectory/R_data/Batchtest_in")                  #set the work directory
getwd()                                                          #check work directory
dir()                                                            #check files

library(ncdf4)                                                   #load packages
options(max.print=9999)                                          #printing capabilities

files <- list.files(".", pattern="\\.nc$")                       #group files

###Precipitation & Temperature###
ncname <- files                                                  #name

pr.sum.month.NakhonRatchasima = array()                          #output-type = array
pr.sum.month.Buriram = array()
pr.sum.month.Surin = array()
#Etc.

#the same for other variables

count = 1                                                        #for-loop through dir.
for(ncname in files){
  ncin <- nc_open(ncname)                                        #open netCDF
  pr <- ncvar_get(ncin,"pr")                                     #get variable
  pr <- pr*(60*60*24)                                            #change units
  pr.sum.month.NakhonRatchasima[count] <- sum(pr[8,18,])         #select cell
  pr.sum.month.Buriram [count] <- sum(pr[13,17,])
  etc.
  nc_close(ncin)                                                 #close netCDF
  count = count + 1                                              #count all files
}                                                                #close loop

#the same for other variables

###Evaporation###Relative Humidity###Sunshine Hours###           #same as for pr

###Create dataframes###
pr.sum.month.df <- data.frame(pr.sum.month.NakhonRatchasima,     #group var. output
                              pr.sum.month.Buriram,
                              etc.)

#the same for other variables

setwd("C:/R_Workdirectory/R_data/batchtest_out")                 #change output dir.

###group output all variables per cell####
for(ncname in files){                                            #create loop
sink('all_mean_month.csv')                                       #file name

cat('')                                                          #title
write.csv(pr.sum.month.df, row.names = FALSE)                    #write dataframe to .csv
cat('\n')                                                        #spacing

#the same for other variables

sink()                                                           #close sink
}                                                                #close loop
```

C2: Abstract of the R-code used to extract the climate data from the netCDF-files provided by RU-CORE.

Appendix D: iMOD model input

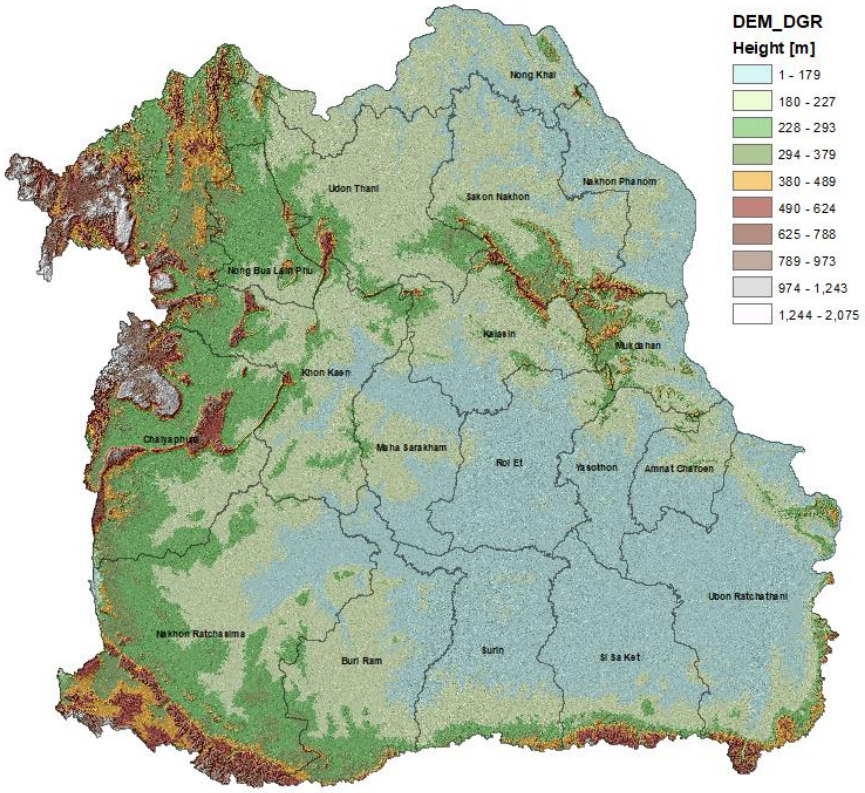

D1: The DEM of the research area provided by the DGR.

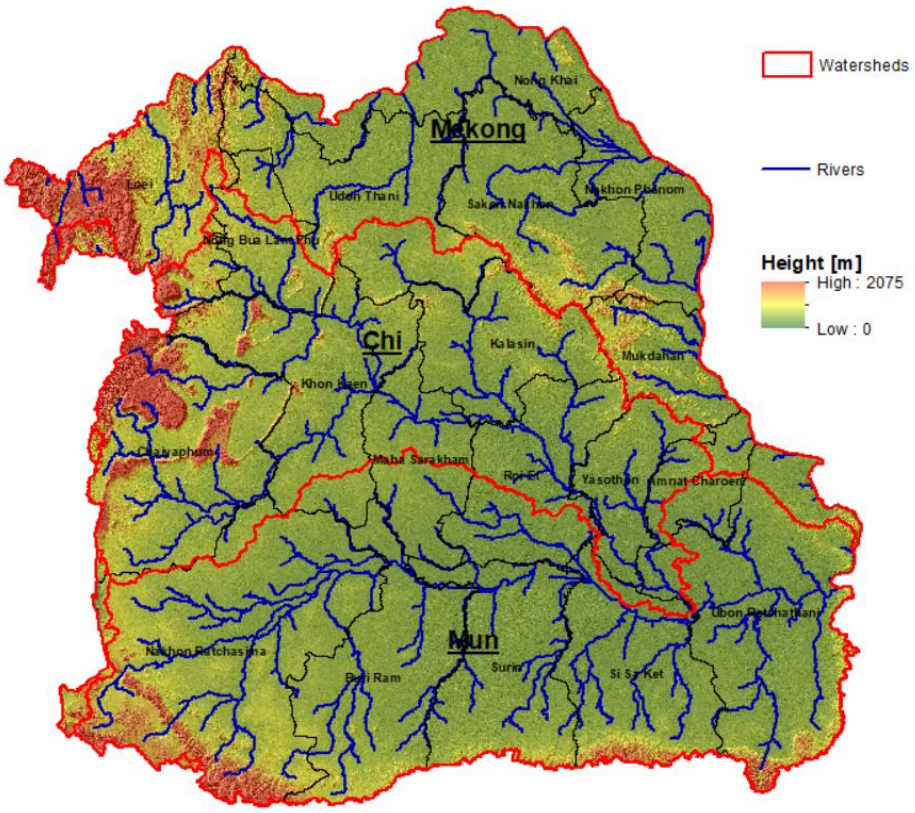

D2: The final river flow path, relative to the Mun, Chi and Mekong watersheds and provinces.

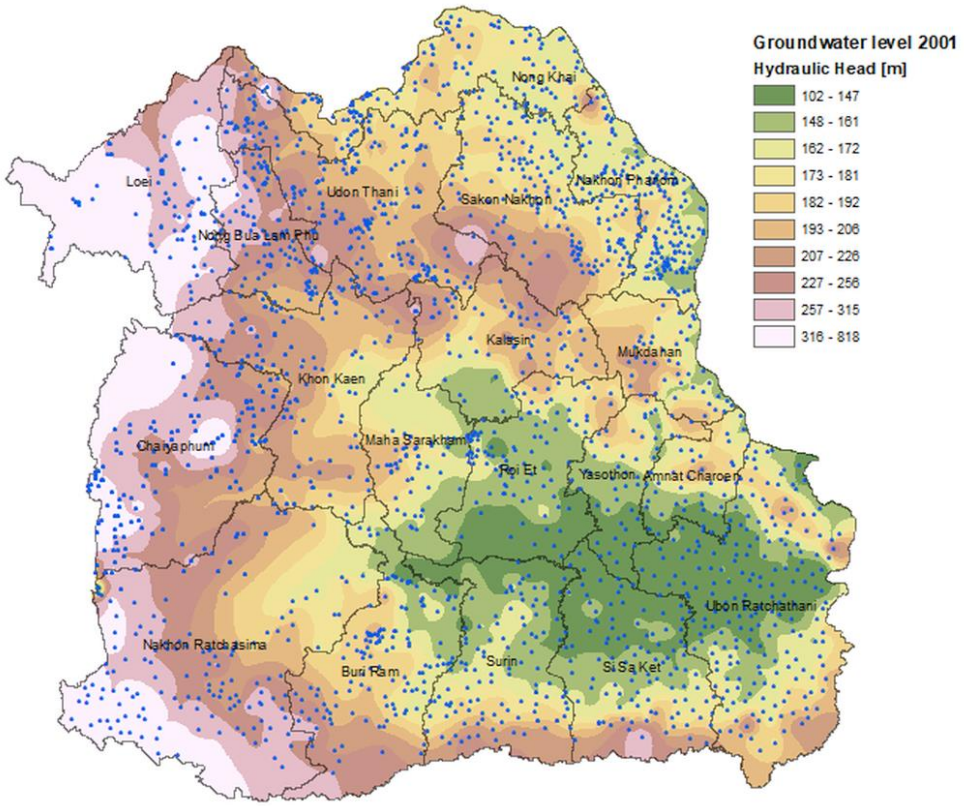

D3: The initial hydraulic head in 2001, including the position of the wells used for the interpolation (blue dots).

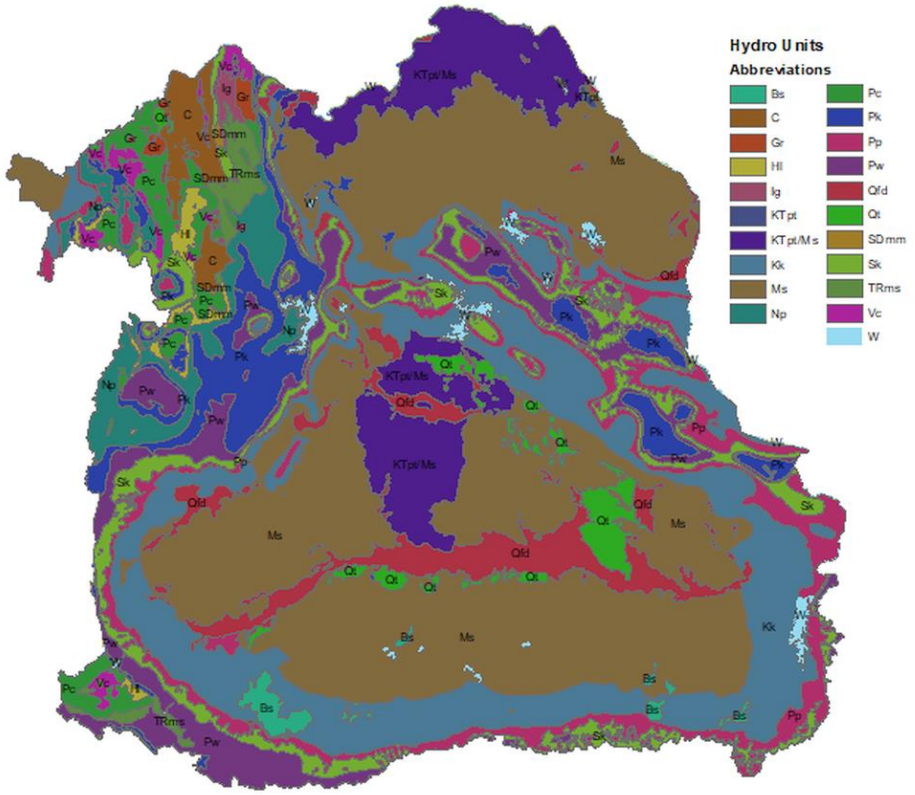

D4: A 2-D map of the main aquifers in Isan. Abbreviations are explained in appendix D7.

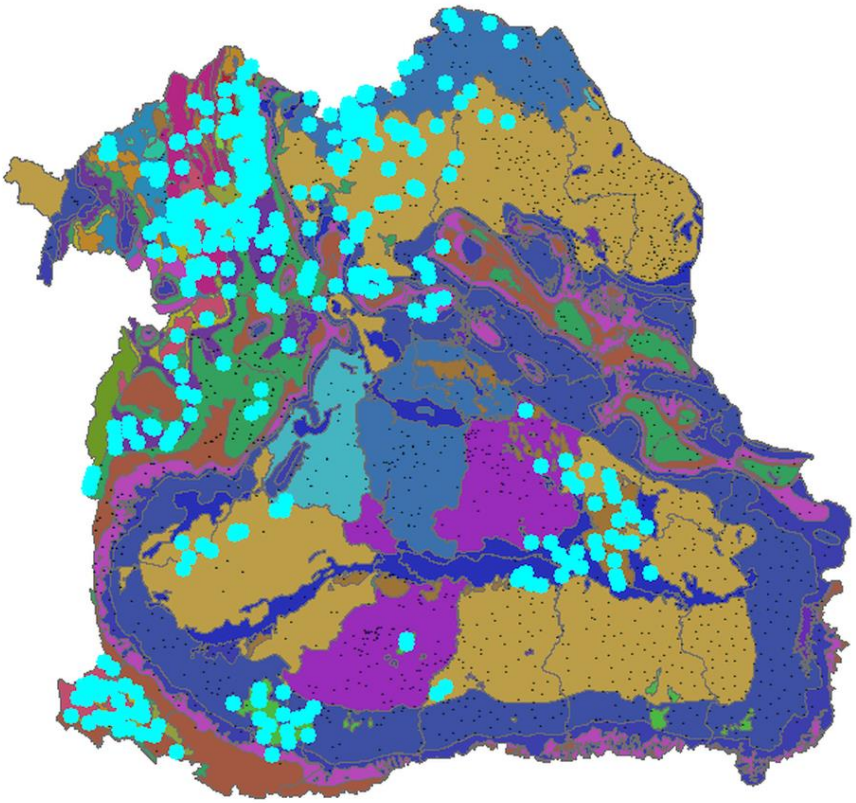

D5: The Wells used (highlighted in cyan-blue) for the calculation of the transmissivity (T) and horizontal permeability (K), using their corresponding hydro-unit.

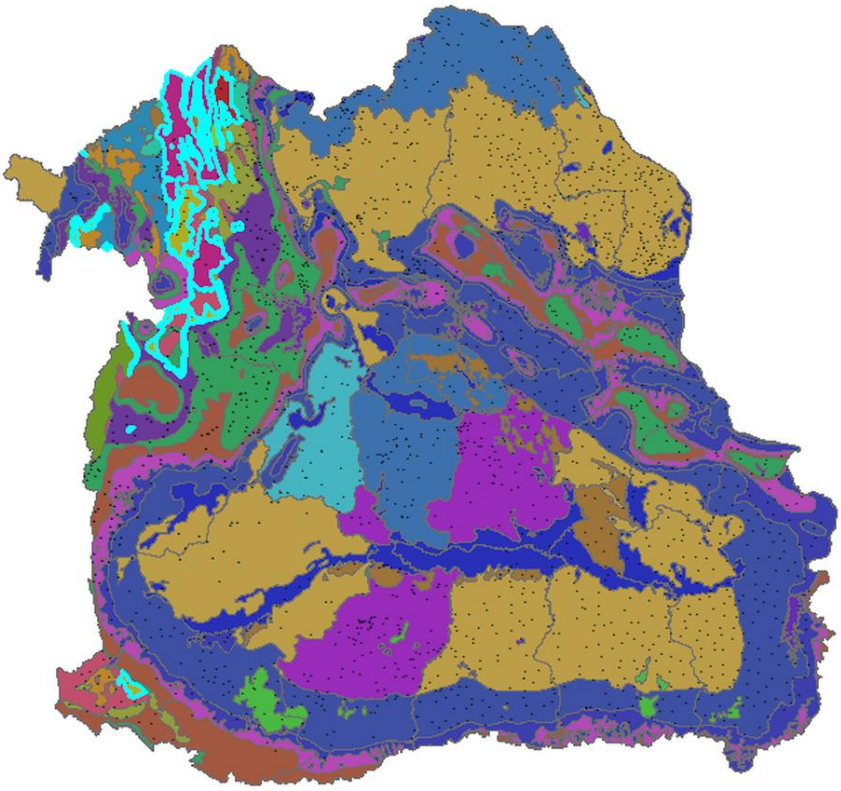

D6: Highlighted are those aquifers whose K and T values were calculated by using wells coinciding with their relative position due to a lack of corresponding hydro-units.

Hydro-units	Wells used	Description
Bs	Bs	Basaltic
C/D	location	Carboneferous & Devonian
Gr	Gr	Granitic
Hl	Location	Hua Hin lat
Ig	location	Igneous
Kk	Kk	Khok Kruat
KTpt	KTpt	Phu thok
KTpt/Ms	KTpt/ms	Phu thok/Maha Sarakham
Ms	Ms	Maha Sarakham
Nd/Np	Np	Namphon
Pc/Pcl	PCcn/PCms	Permian carbonate/Clastic sediment
Pk	Pk	Phu Kradung
Pp	Pp	Phuphan
Pw	Pw	Phra Wihan
Qfd	Qfd	Floodplain deposits
Qt	Qt	Terrace deposits
S/Sk	Sk	Sao Khua
SDmm	SDmm	Silurian-Devonian Metamorphic
TRms	TRhl/TRnp	Triassic Metasedments
Vc	Vc	Volcanic
W	No value	Water body

D7: A table showing which wells and hydro-units were used for the calculation of which aquifer as well as their description.

Results	No. wells	T [m^2/day]	SD T	K [m/day]	SD K
Bs	19	4.31	10.8	0.72	4.7
C/D	14	11.95	7.7	1.79	1.9
Gr	7	12.30	21.6	1.53	3.0
Hl	17	4.50	5.3	0.46	0.6
Ig	1	4.85	0.0	1.21	0.0
Kk	11	5.18	28.4	1.11	4.7
KTpt	21	4.46	8.4	0.34	0.7
KTpt/Ms	26	5.84	26.5	0.94	4.7
Ms	40	7.67	25.1	1.22	4.5
Np/Nd	8	9.48	9.3	1.52	1.4
Pc/Pcl	70	6.63	7.6	0.72	1.3
Pk	13	6.96	21.3	0.95	3.0
Pp	3	3.60	0.6	0.57	0.4
Pw	1	2.86	0.0	0.72	0.0
Qfd	2	13.57	11.3	1.22	0.8
Qt	35	5.72	16.5	0.96	3.4
S/Sk	6	3.81	4.3	0.58	0.6
SDmm	6	8.03	7.7	1.41	1.4
TRms	78	3.75	5.0	0.40	0.7
Vc	43	8.04	6.5	1.01	1.3

D8: The table shows the number of wells involved and their median T and K value, and corresponding standard deviation, used for the calculation of both the T- and K-layer.

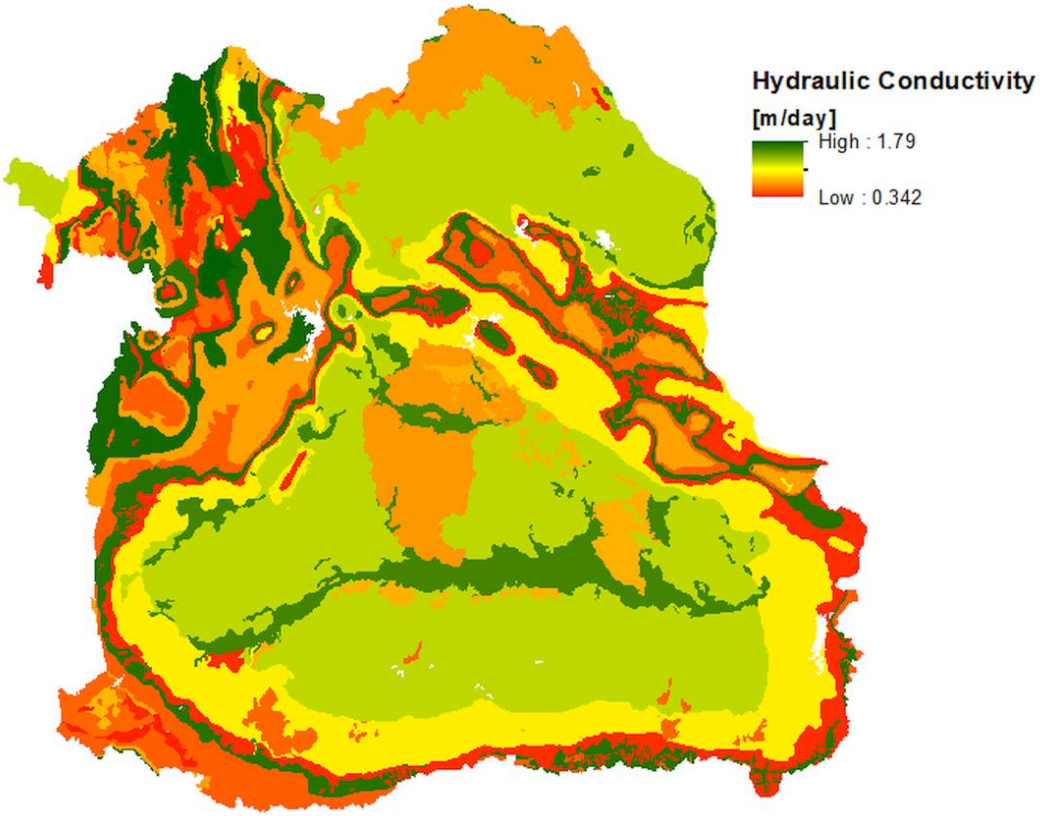

D9: Resulting K-layer for the entire research area (areas in white represent lakes).

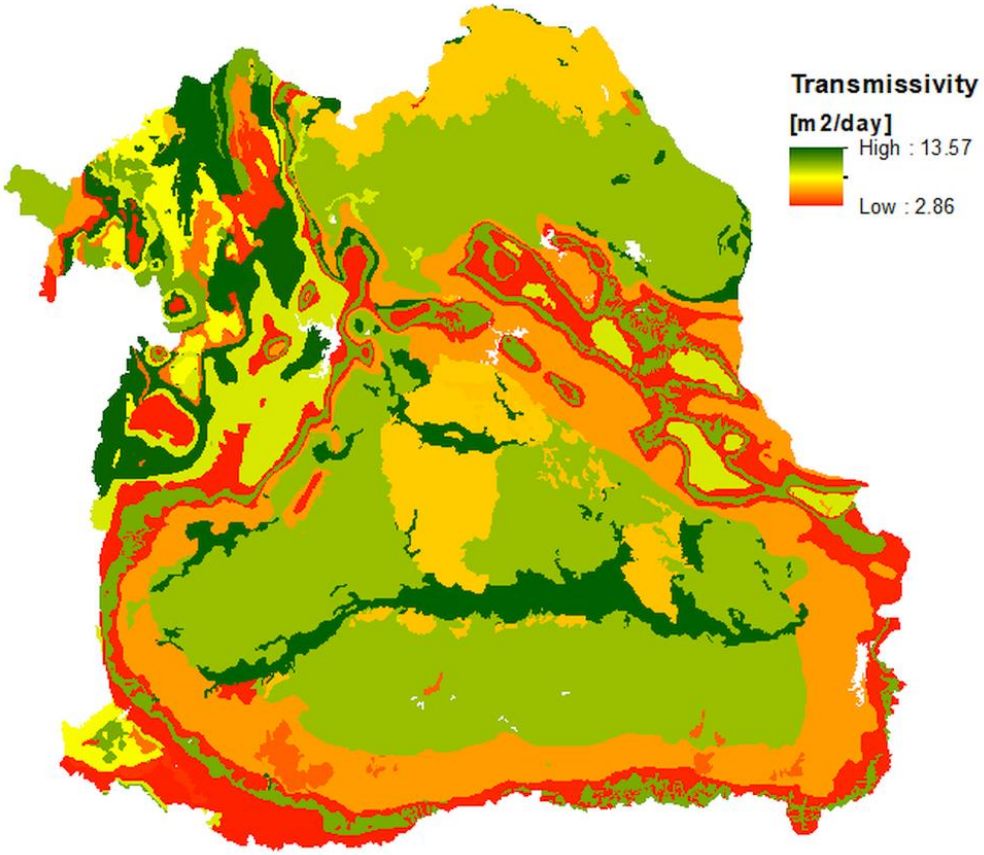

D10: Resulting T-layer for the entire research area (areas in white represent lakes).

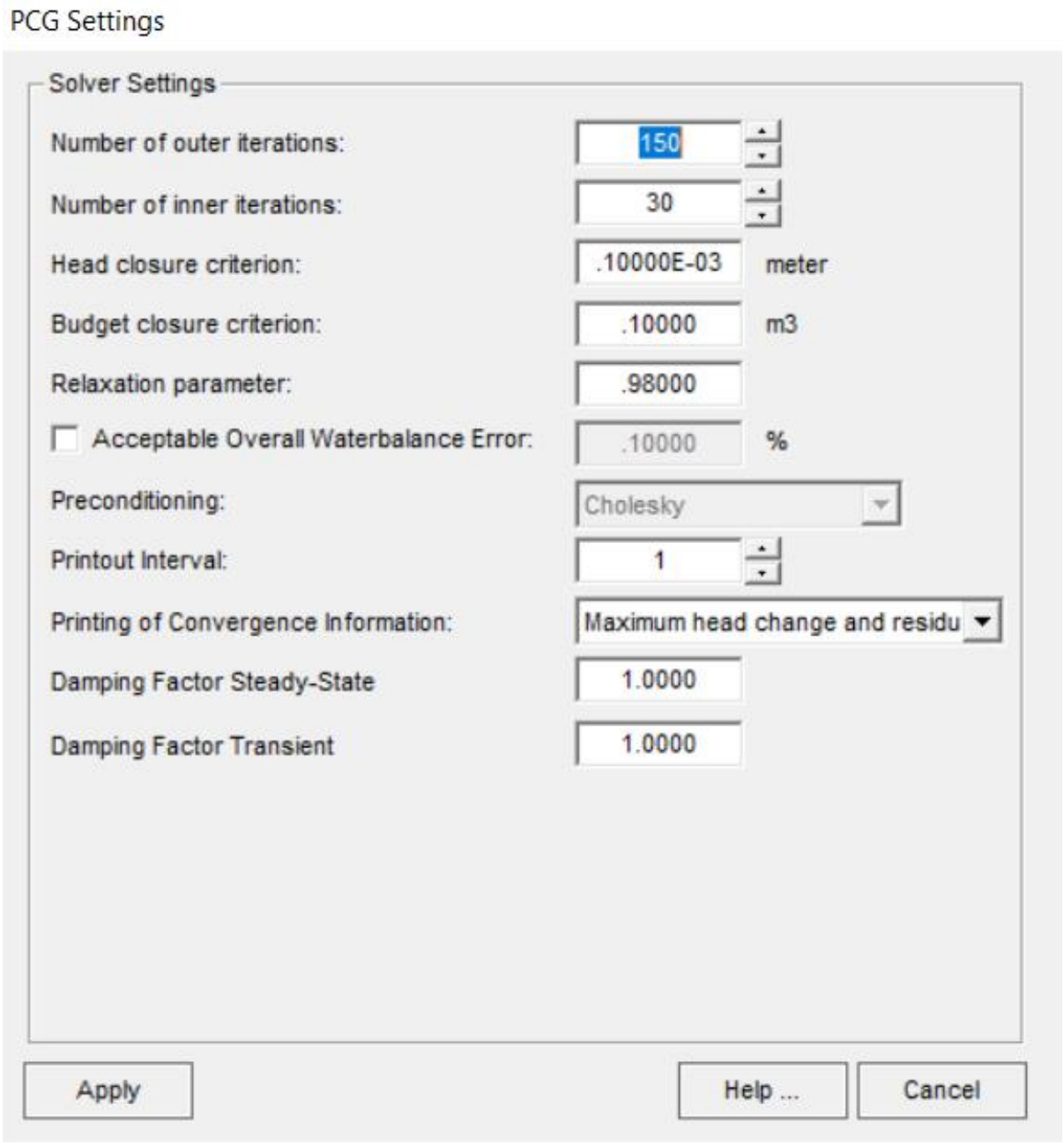

D11: The default settings for the PCG-solver in iMOD.

Appendix E: Results synthetic data reconstruction and observational record

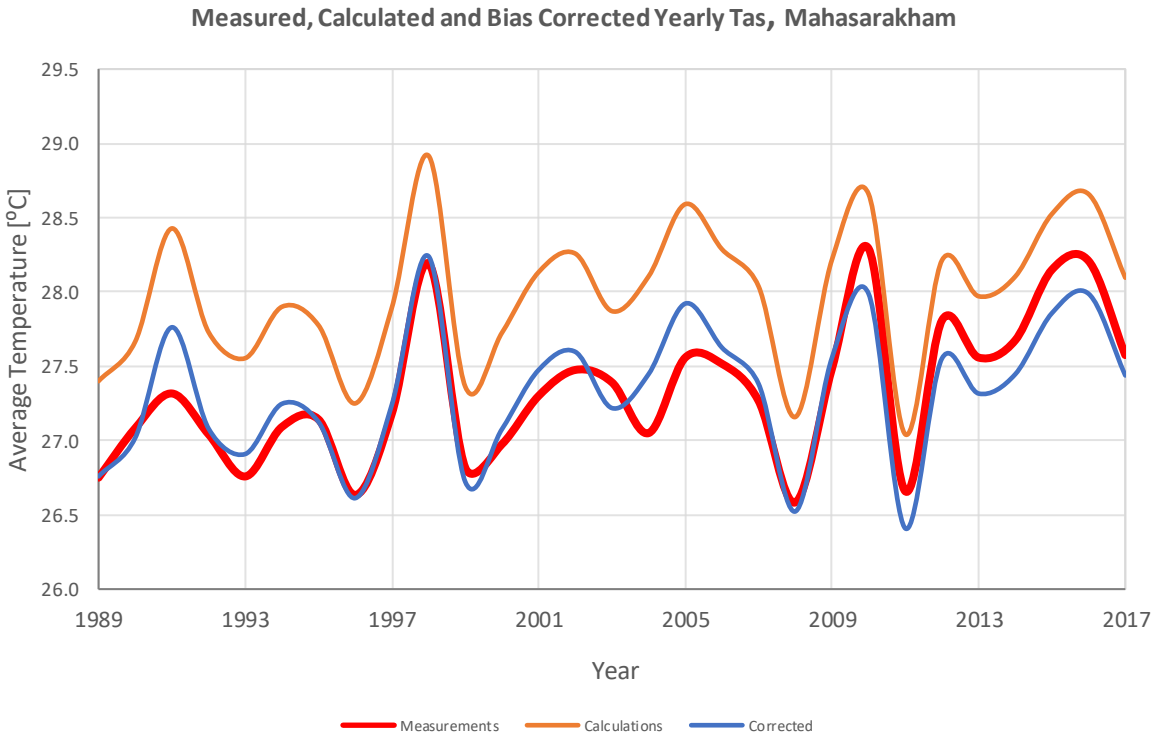

E1a: Comparing the measured (red), modelled (orange) and bias corrected (blue) annual average temperature fluctuations, example site Mahasarakham, [1989-2017].

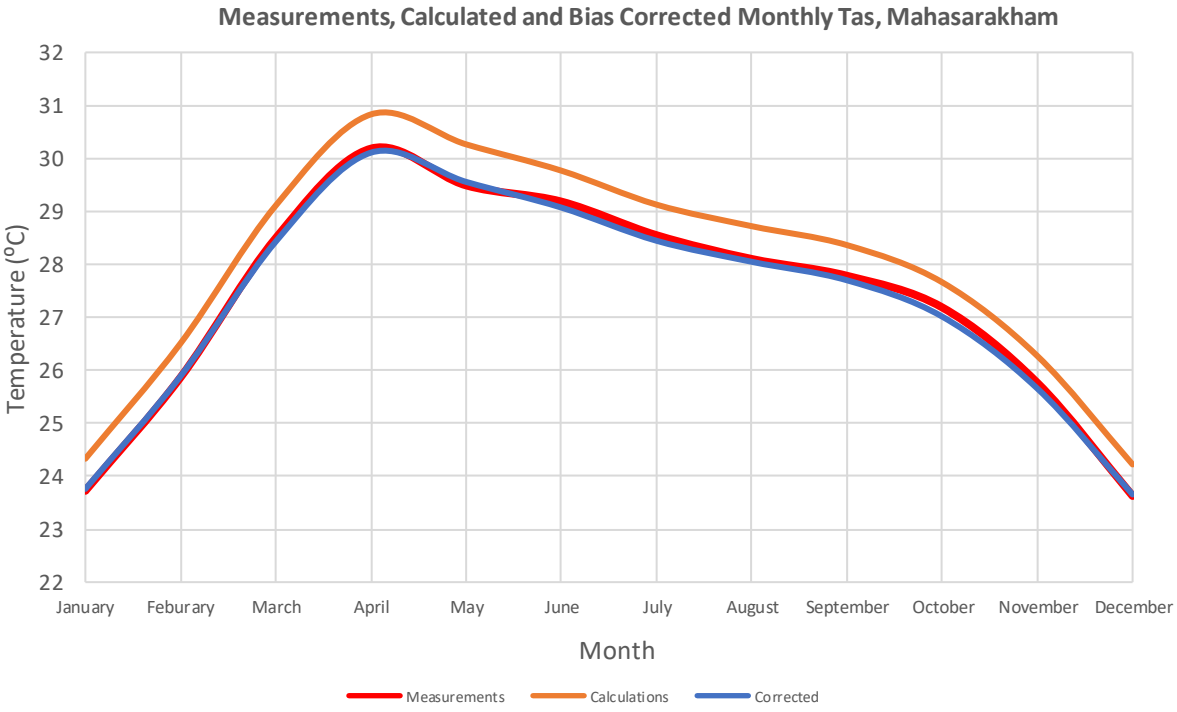

E1b: Comparing the measured (red), modelled (orange) and bias corrected (blue) monthly average temperature fluctuations, example site Mahasarakham, [1989-2017].

Location	Yearly R^2	Yearly RMSE	Monthly R^2	Monthly RMSE
Mahasarakham	0.83	0.20	1.00	0.09
Kalasin	0.14	0.68	1.00	0.26
Buriram	0.88	0.15	0.99	0.17
Sisaket	0.99	0.06	1.00	0.09
Nong Bua Lamphu	0.89	0.08	1.00	0.28

E2: Statistics for all stations that required average temperature modelling.

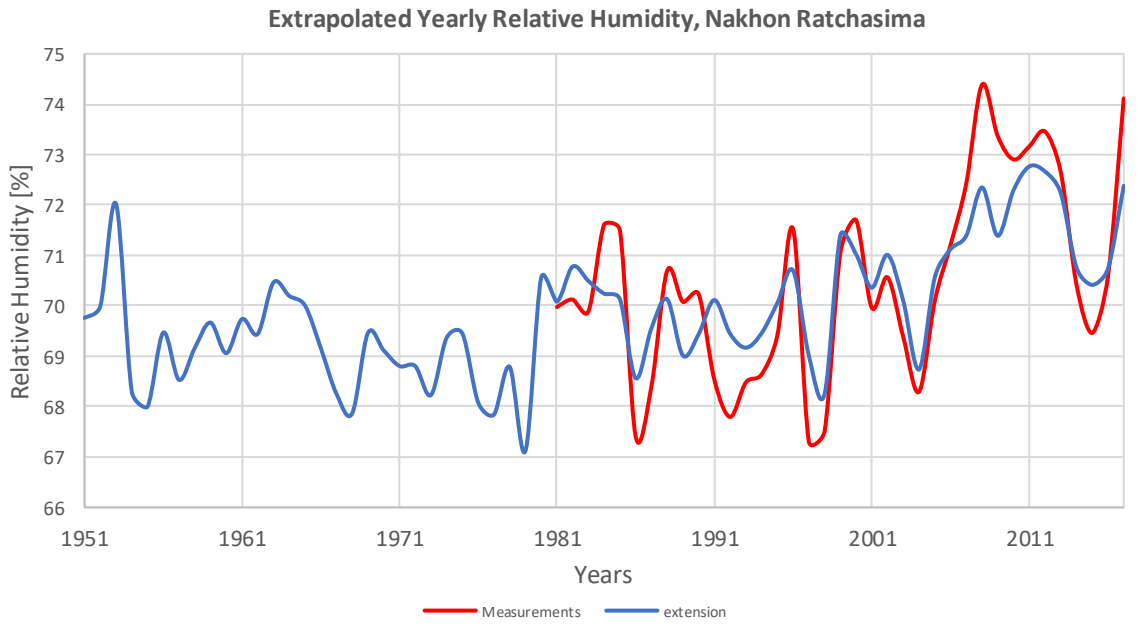

E3: Modelled (blue) versus measured (red) annual average relative humidity, example Nakhon Ratchasima, [1951 – 2017].

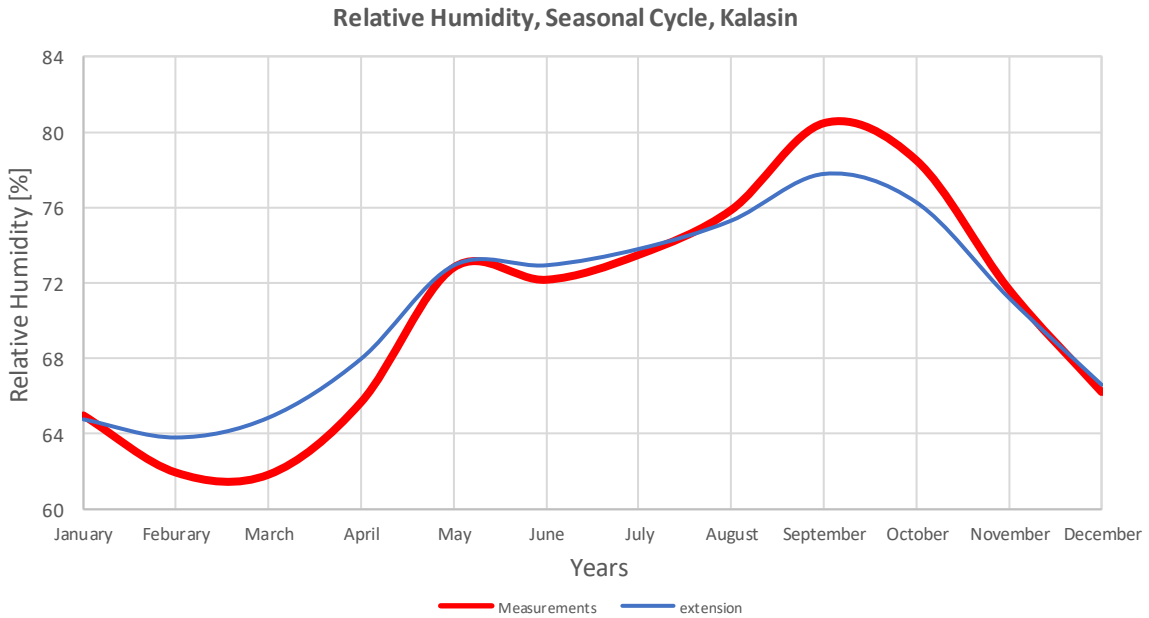

E4: Seasonal cycle for relative humidity, example site Kalasin, relative humidity measurements (red) versus modelling efforts (blue), [2000 – 2017].

Location:	Yearly RMSE	Seasonal Cycle RMSE
Khon Kaen	1.80	3.47
Mukdahan	1.45	3.40
Mahasarakham	2.37	2.84
Kalasin	1.00	1.65
Roi Et	0.93	2.84
Ubon Ratchathani	2.31	2.63
Nakhon Ratchasima	1.00	1.62
Surin	1.27	3.00
Buriram	2.82	3.75
Sisaket	1.30	1.84
Nong Khai	1.71	3.36
Loei	1.17	2.23
Udon Thani	1.97	2.65
Sakon Nakhon	1.17	2.75
Nakhon Phanom	1.76	3.51
Chaiyaphum	1.35	3.86
Nong Bua Lamphu	1.56	3.03

E5: Statistics for modelled average relative humidity compared to observed averages.

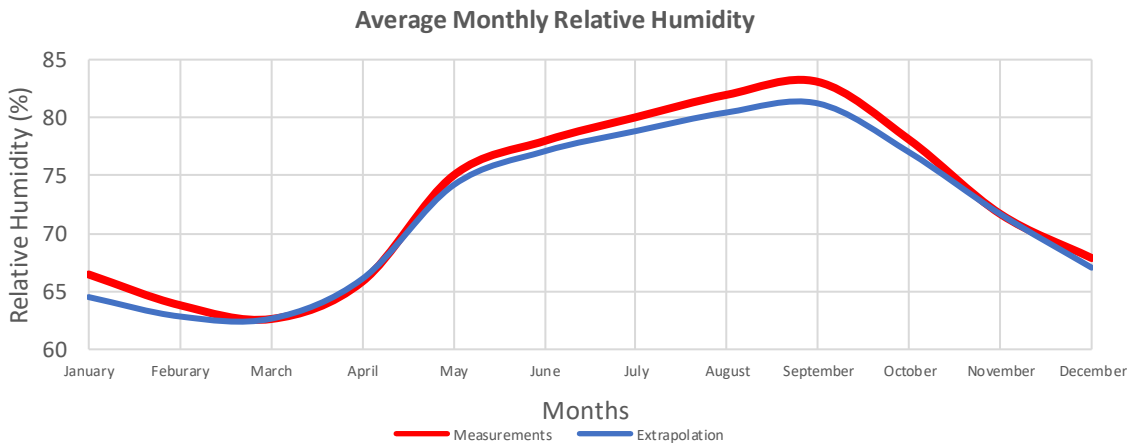

E6: Measurements (red) versus modelling results (blue), Interannual cycle, relative humidity, all stations average, [1951-2017].

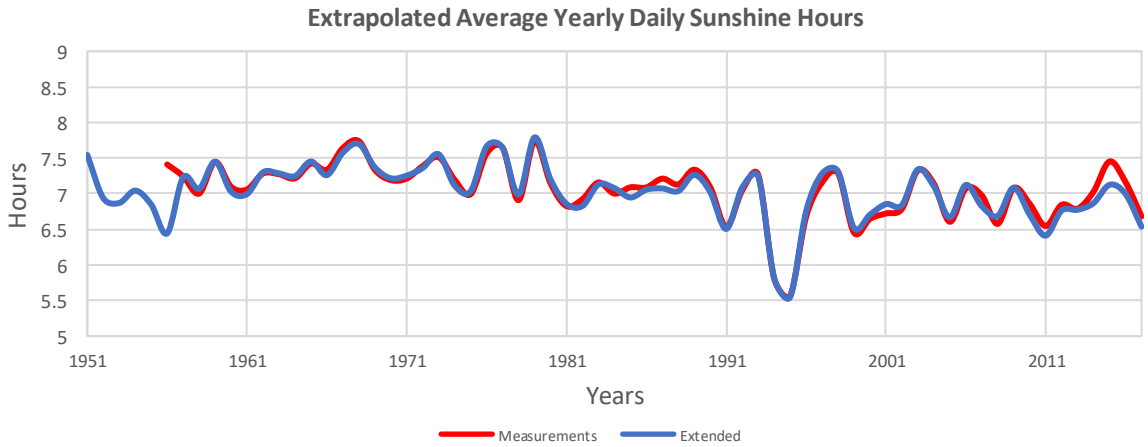

E7: Daily sunshine hours, yearly averages extrapolation, all stations average, measurements (red), modelled (blue), [1956-2018].

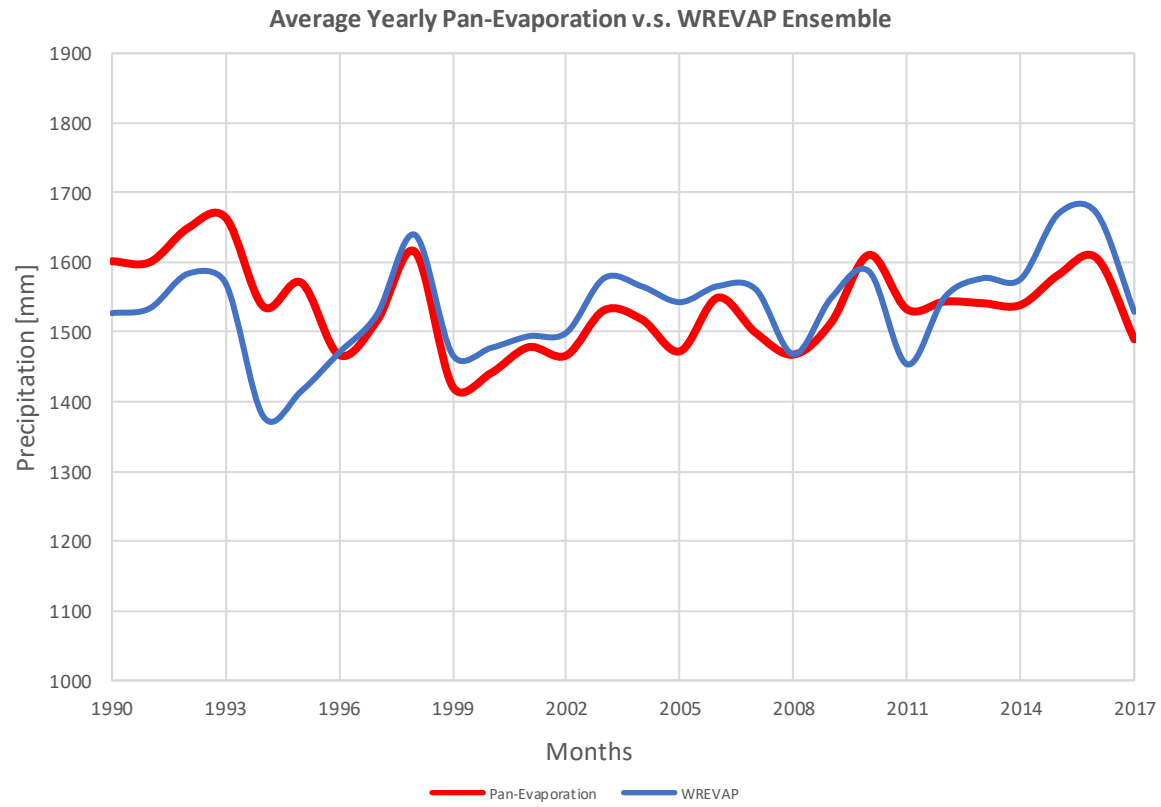

E8a: Annual results, WREVAP model (blue) compared to pan-evaporation measurements (red), all stations average, [1990-2017].

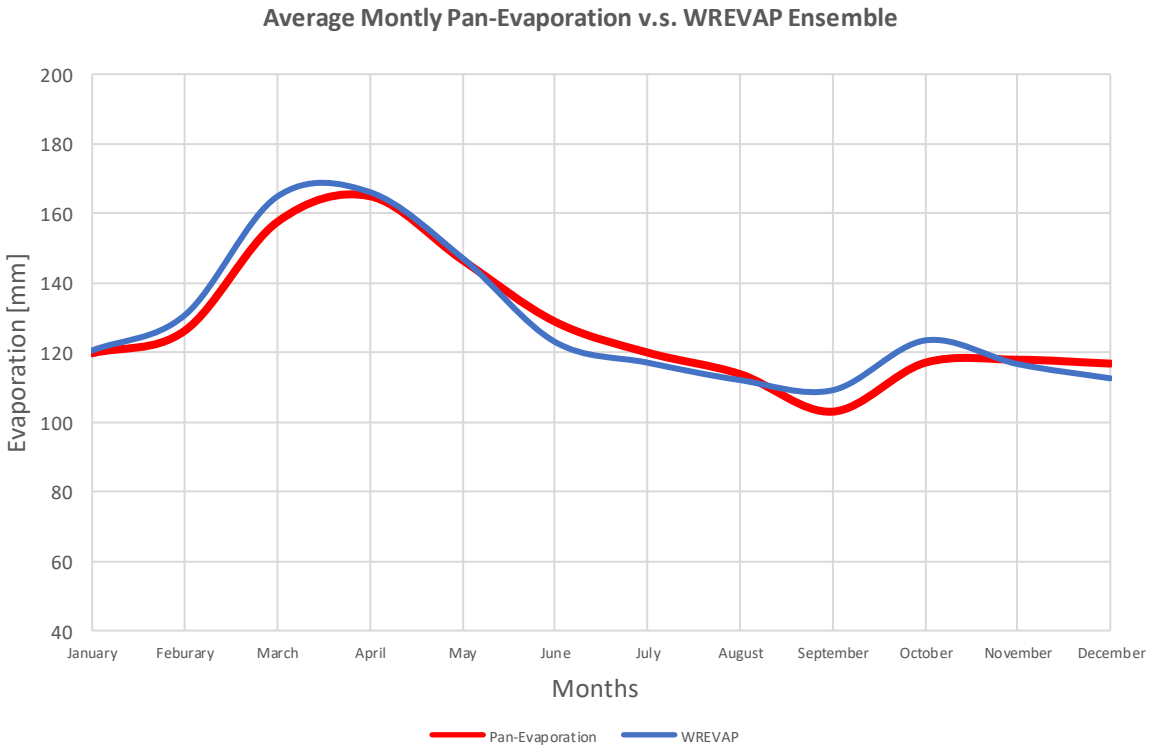

E8b: Seasonal results, WREVAP model (blue) compared to pan-evaporation measurements (red), all stations average, [1990-2017].

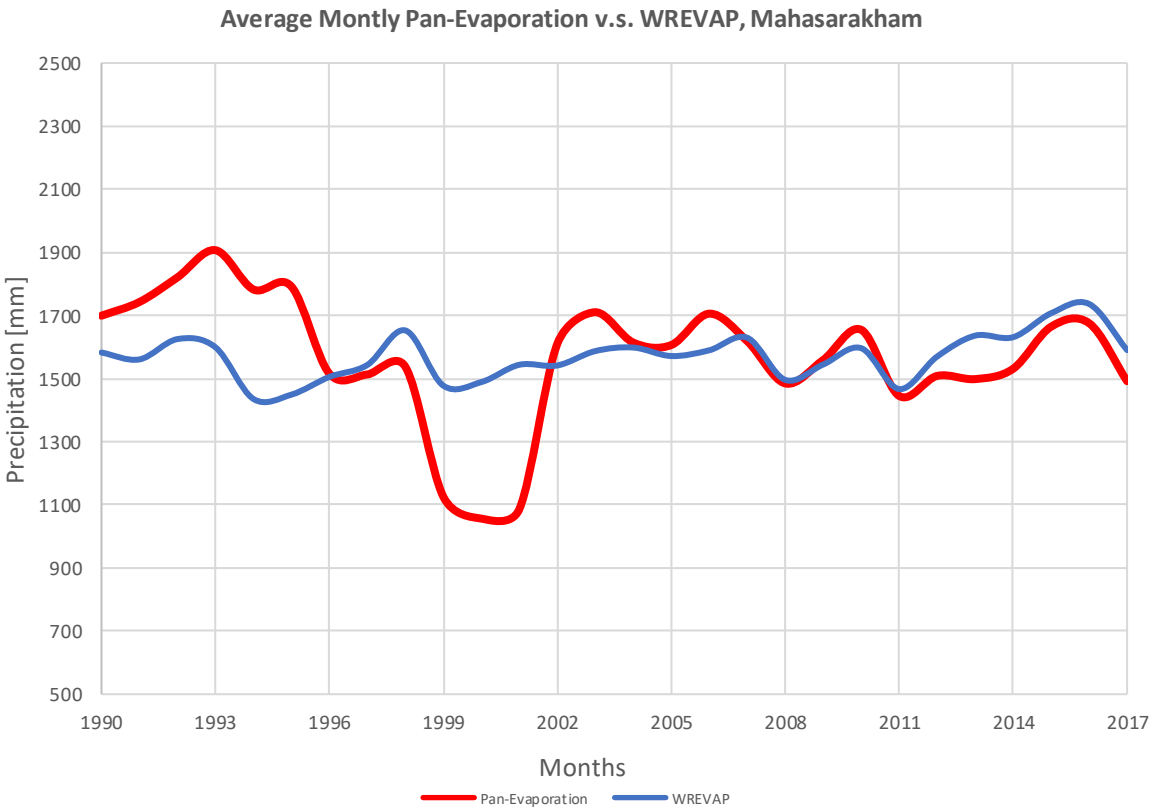

E9: Annual results, WREVAP model (blue) compared to pan-evaporation measurements (red), Mahasarakham, outlier example, [1990-2017].

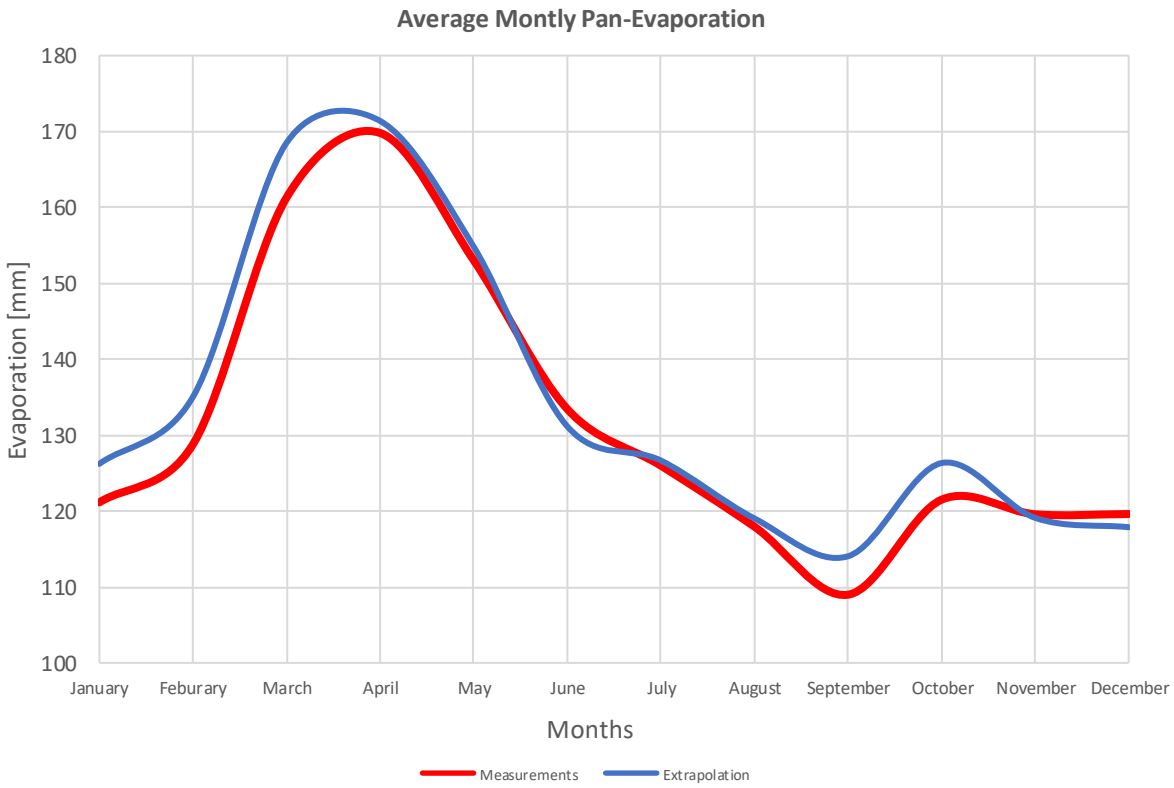

E10: Extrapolated monthly pan-evaporation results, measurements (red) versus extrapolated results (blue), all station average, [1951-2017].

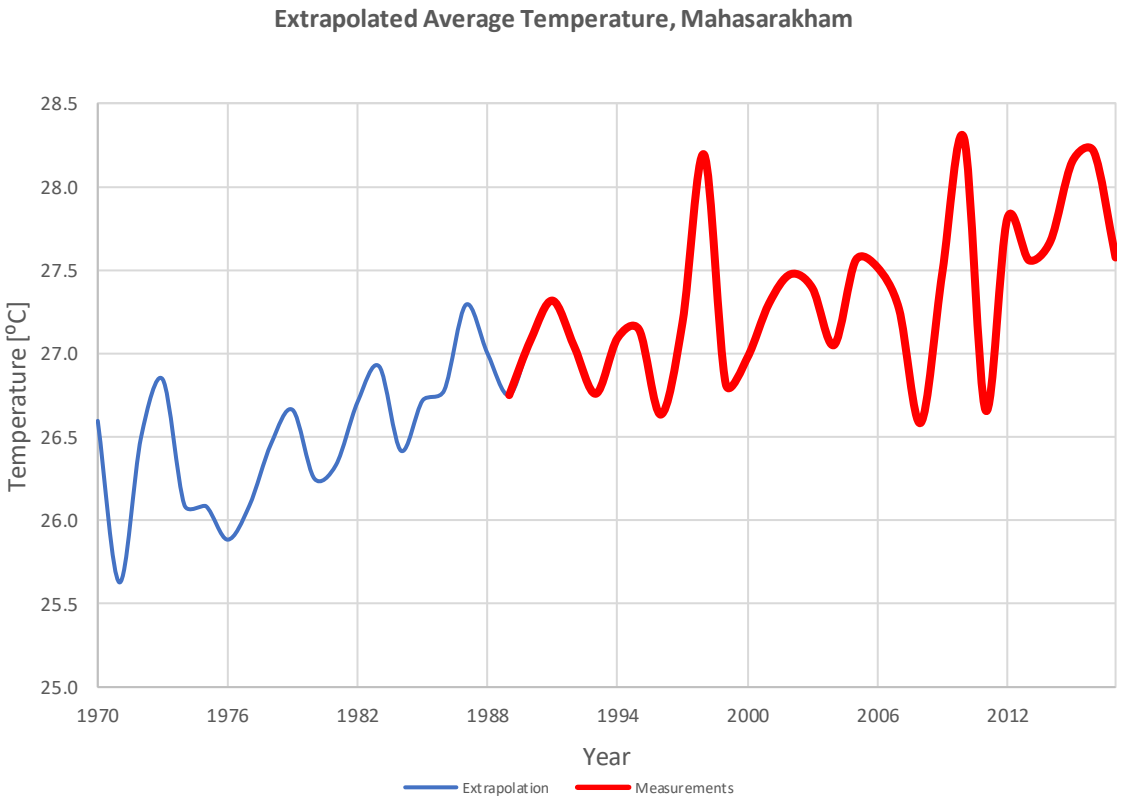

E11: Extrapolated annual average temperature, measured (red) and modelled (blue), example site Mahasarakham, [1989-2017].

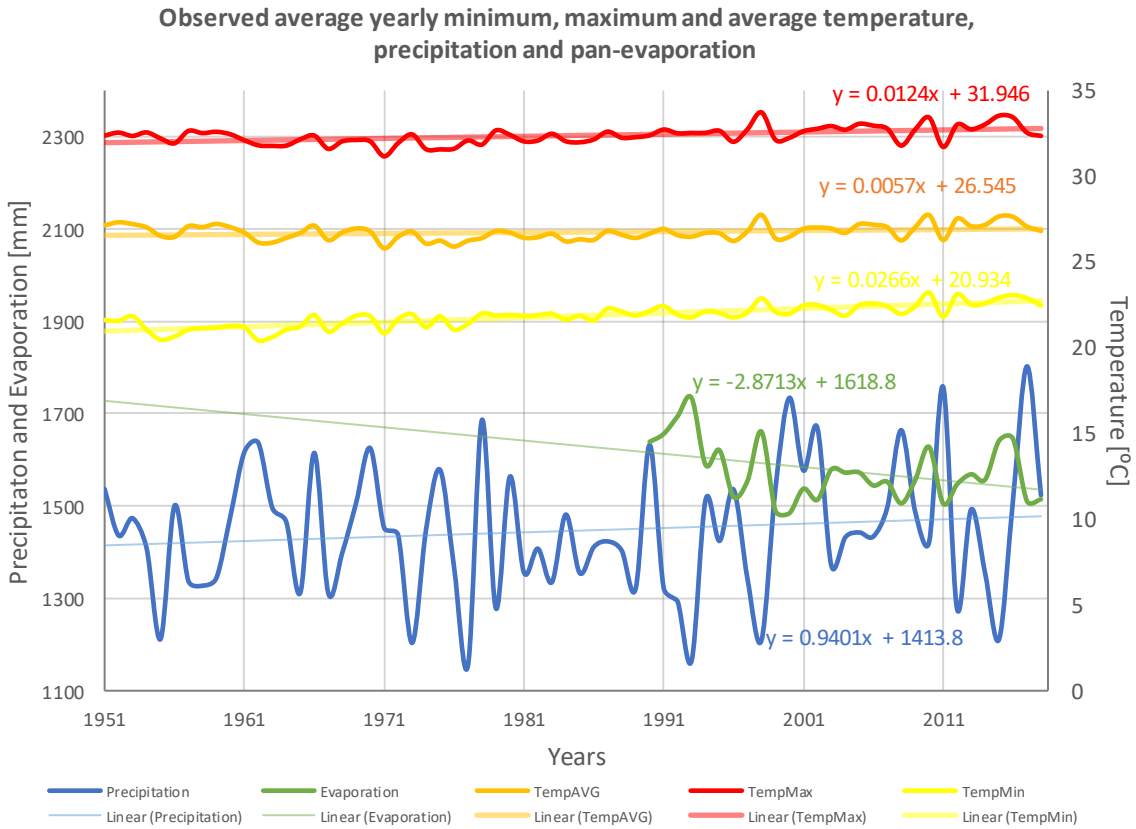

E12a: The observed yearly minimum, maximum and average temperature, precipitation and pan-evaporation, all station averages, [1951-2017].

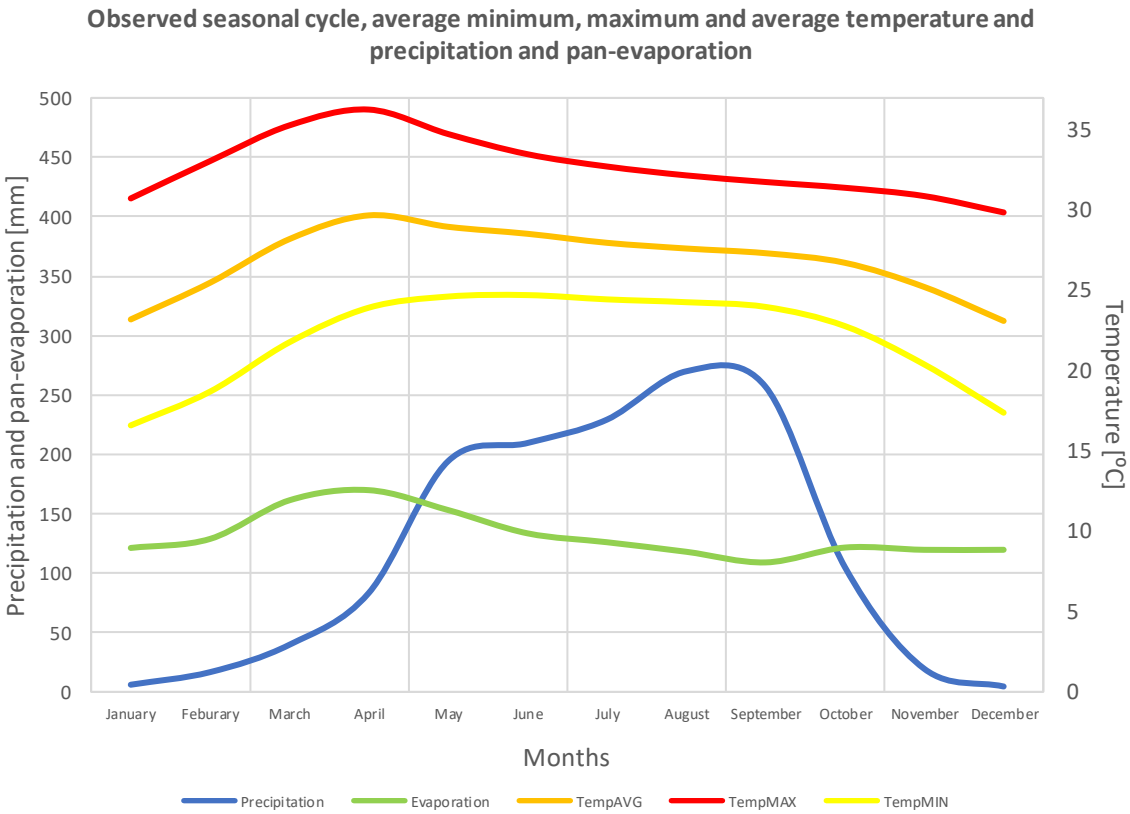

E12b: Observed monthly tas, tasmin and tasmax, pr [1951-2017] and et [1990-2017], all stations average.

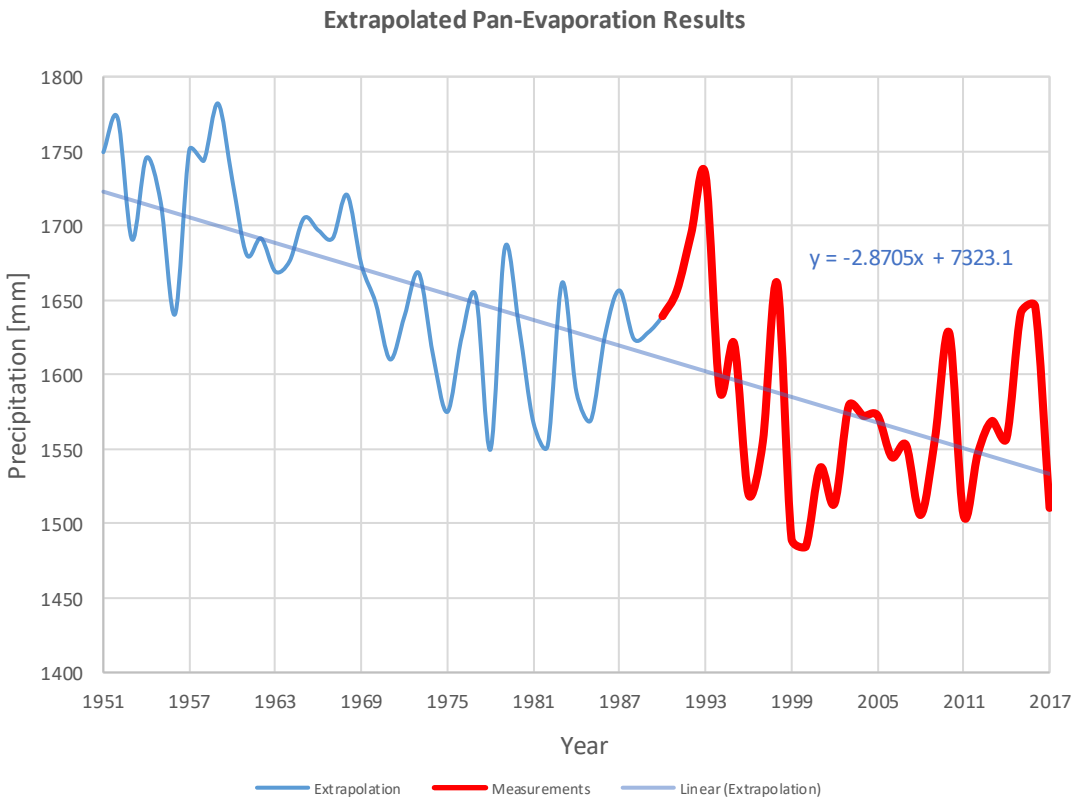

E13: Extrapolated yearly pan-evaporation results, all station average, [1951-2017].

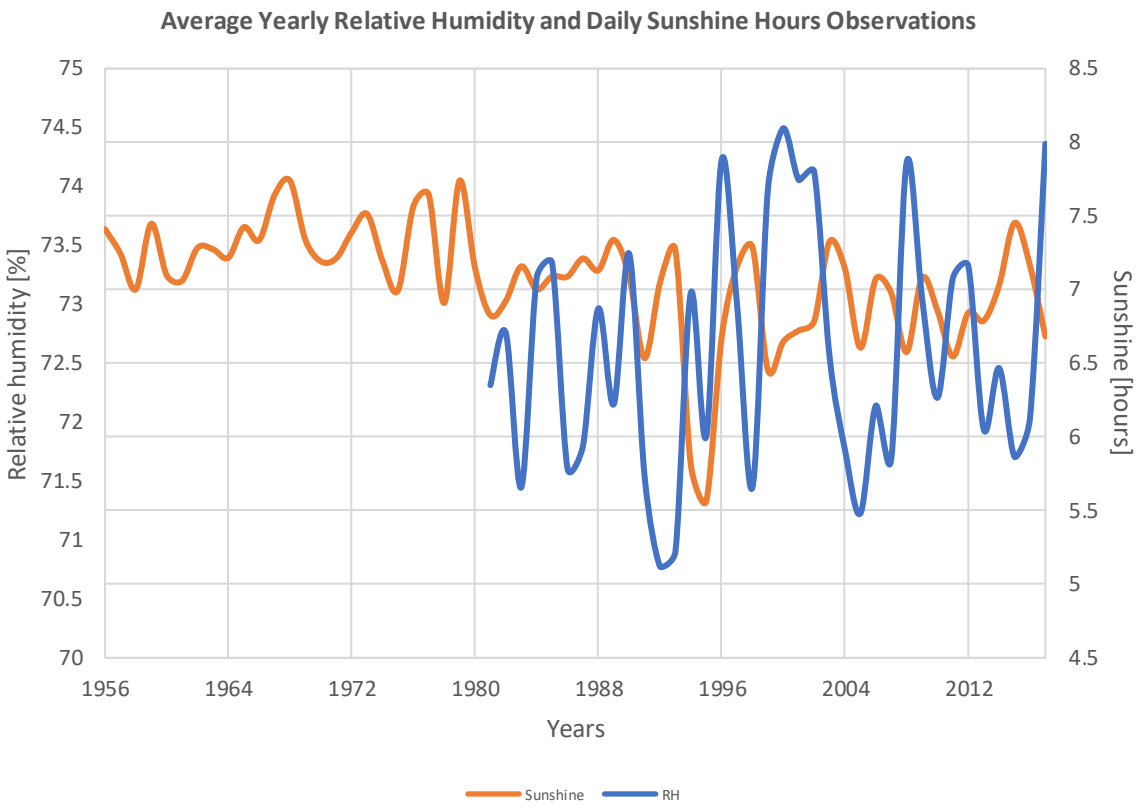

E14a: Yearly relative humidity [1981-2017] and daily sunshine hours [1956-2017] observations.

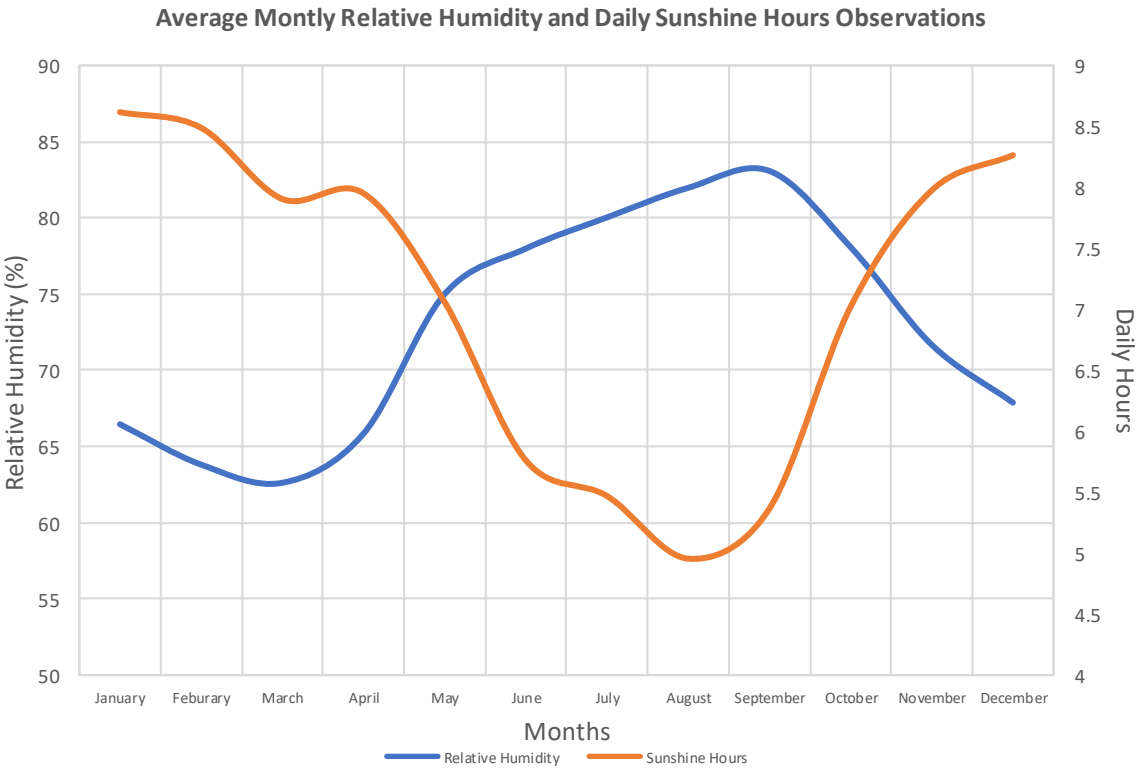

E14b: Monthly relative humidity [1981-2017] and daily sunshine hours [1956-2017] observations.

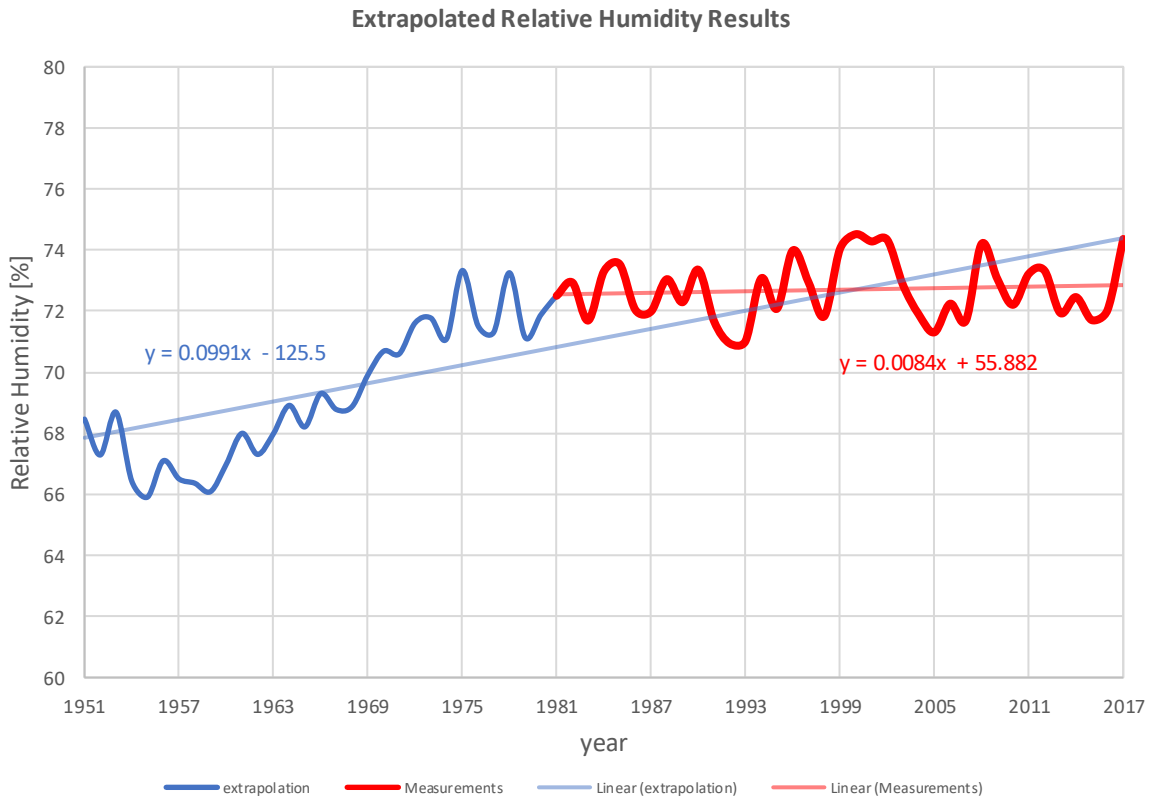

E15: Extrapolated yearly relative humidity, all stations average, [1951-2017].

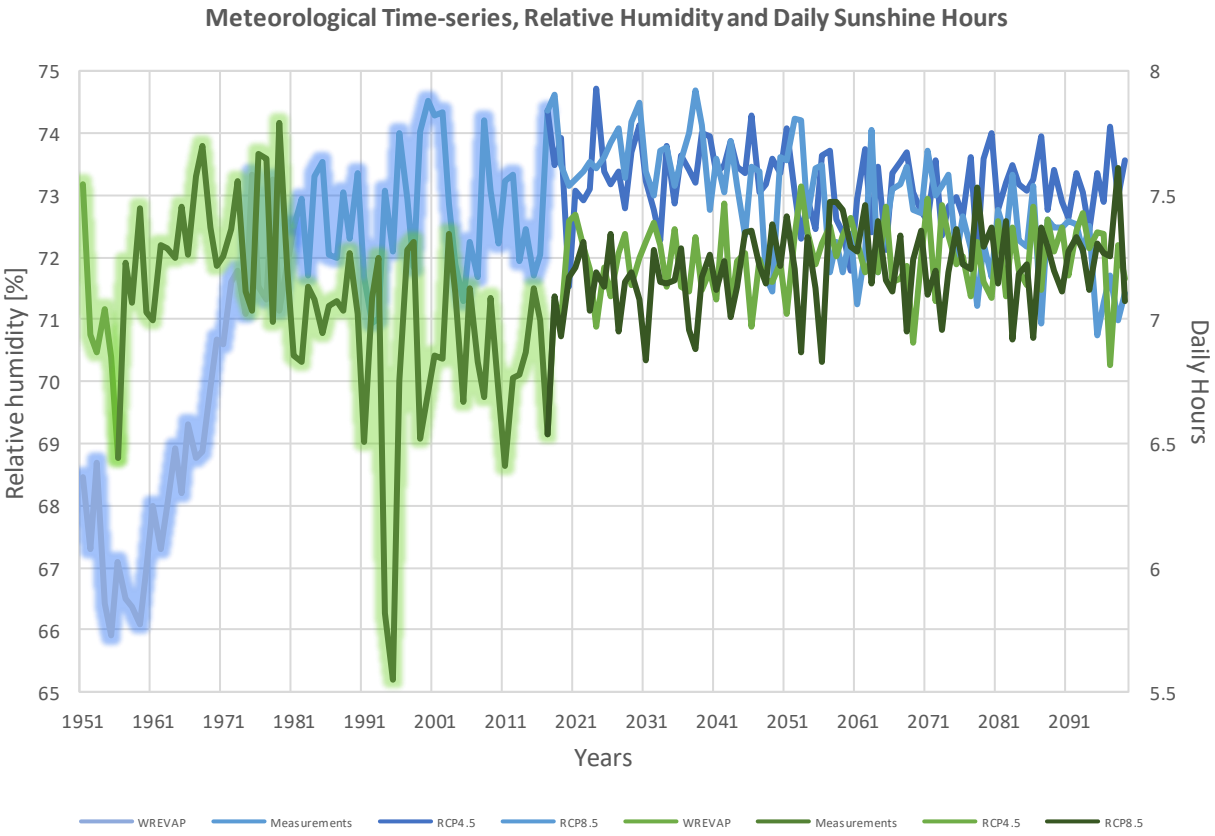

E16: Complete time-series, relative humidity and daily sunshine hours, all stations averages, ensemble model RCP4.5 and RCP8.5, [1951-2099].

Appendix F: Meteorological time-series analysis

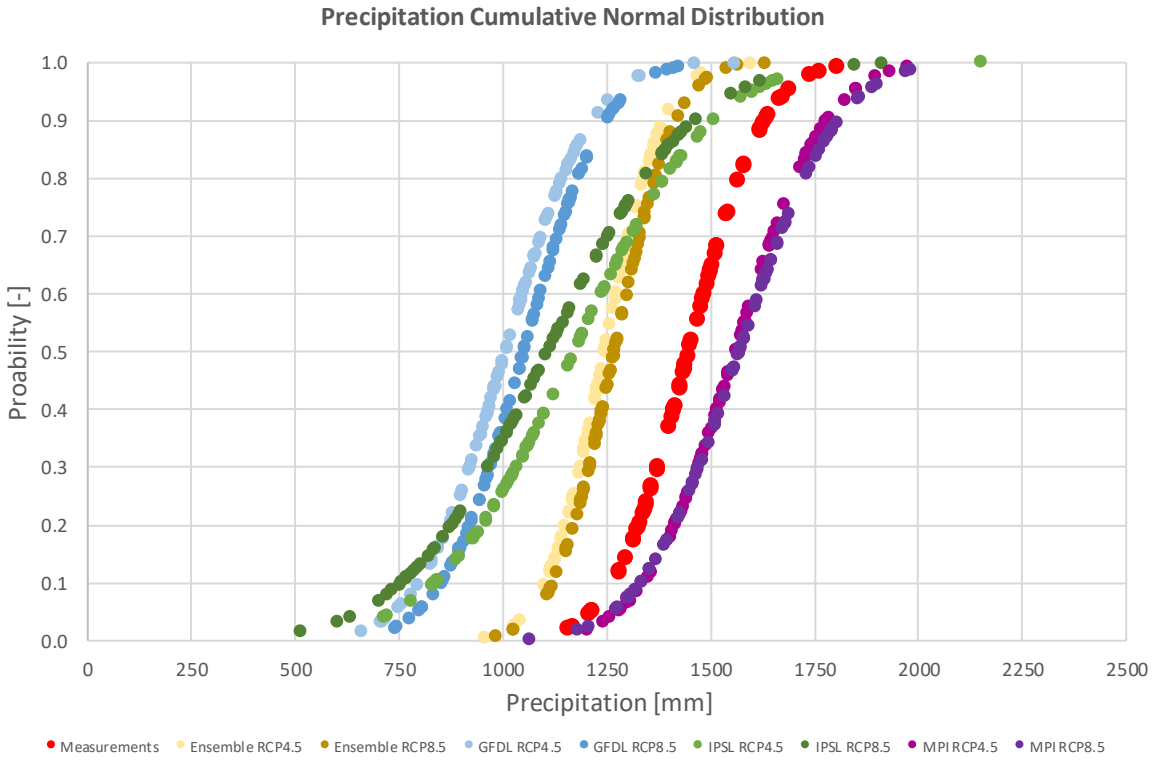

F1: Cumulative normal distribution, precipitation, all climate models, RCP4.5 and RCP8.5 [2017-2099], versus observations, [1951-2017].

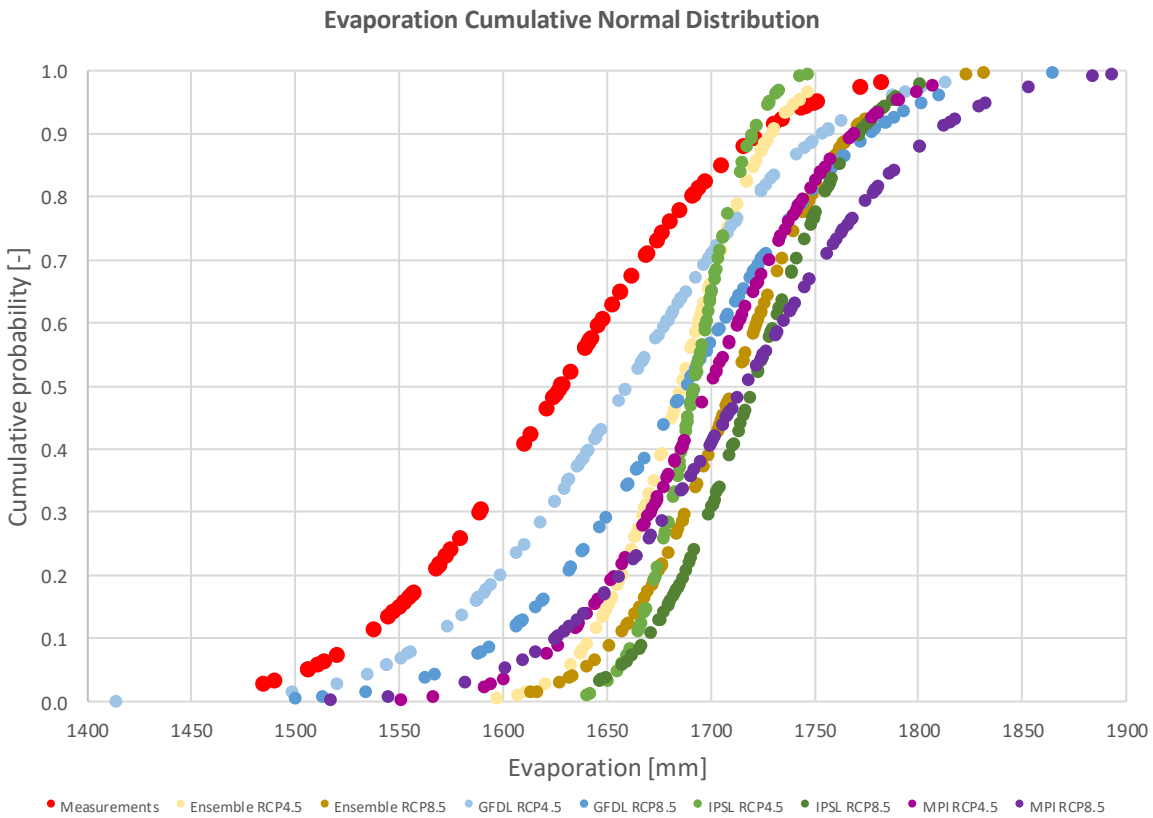

F2: Cumulative normal distribution, evaporation , all climate models, RCP4.5 and RCP8.5 [2017-2099], versus observations, [1951-2017].

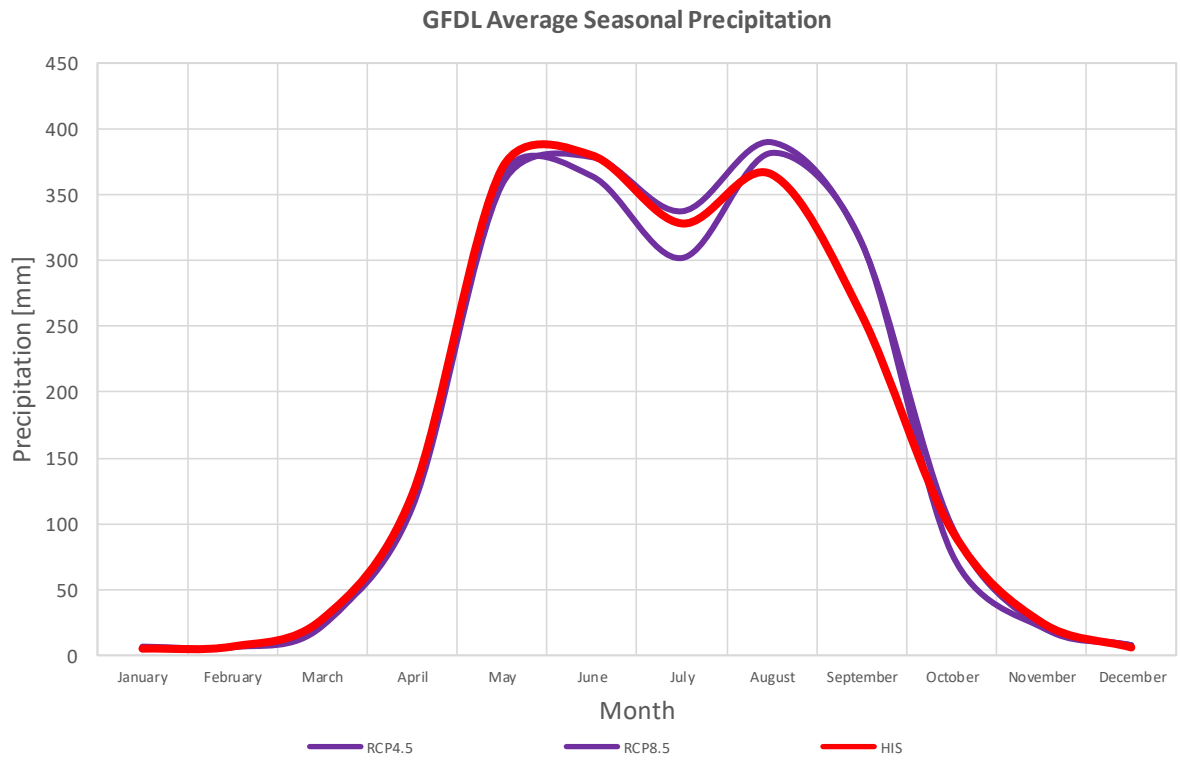

F3a: RCM GFDL, seasonal precipitation cycle, historical [1970-2005] versus future [2006-2099] output, all stations average.

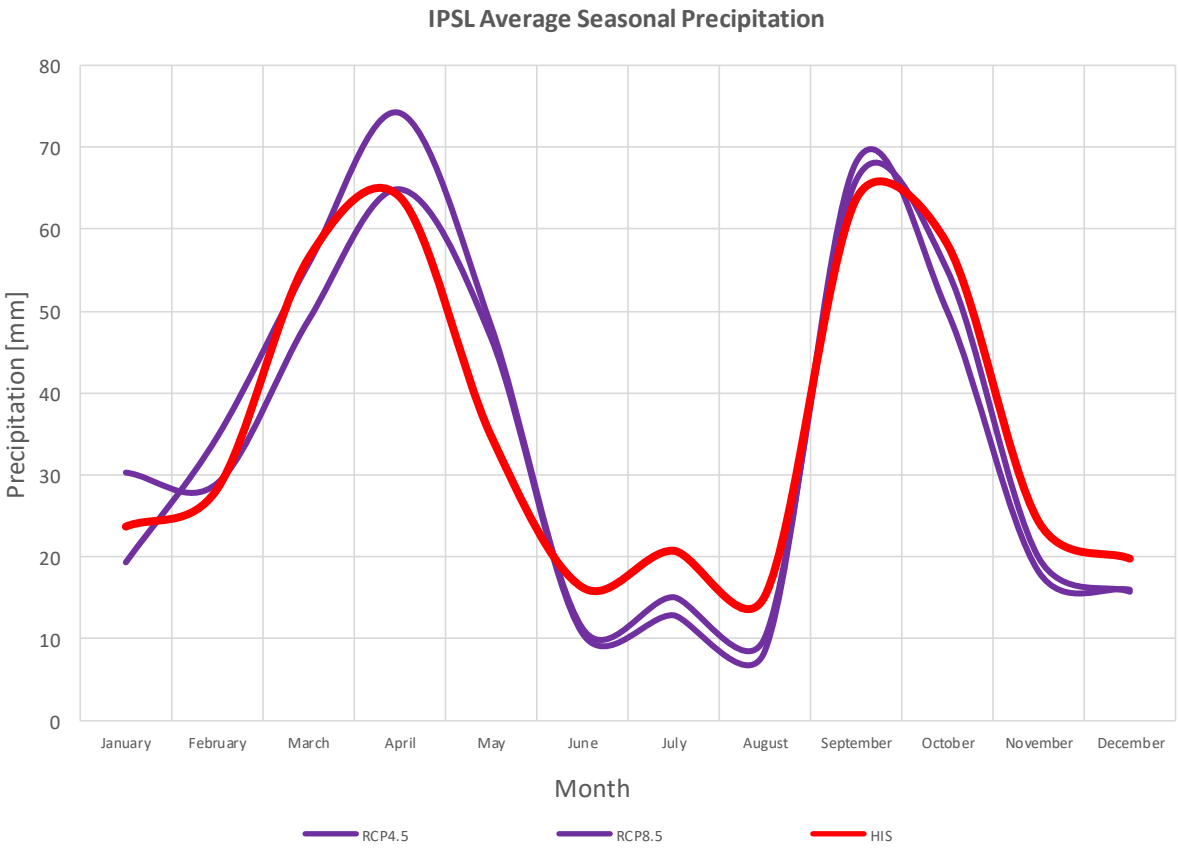

F3b: RCM IPSL, seasonal precipitation cycle, historical [1970-2005] versus future [2006-2099] output, all stations average.

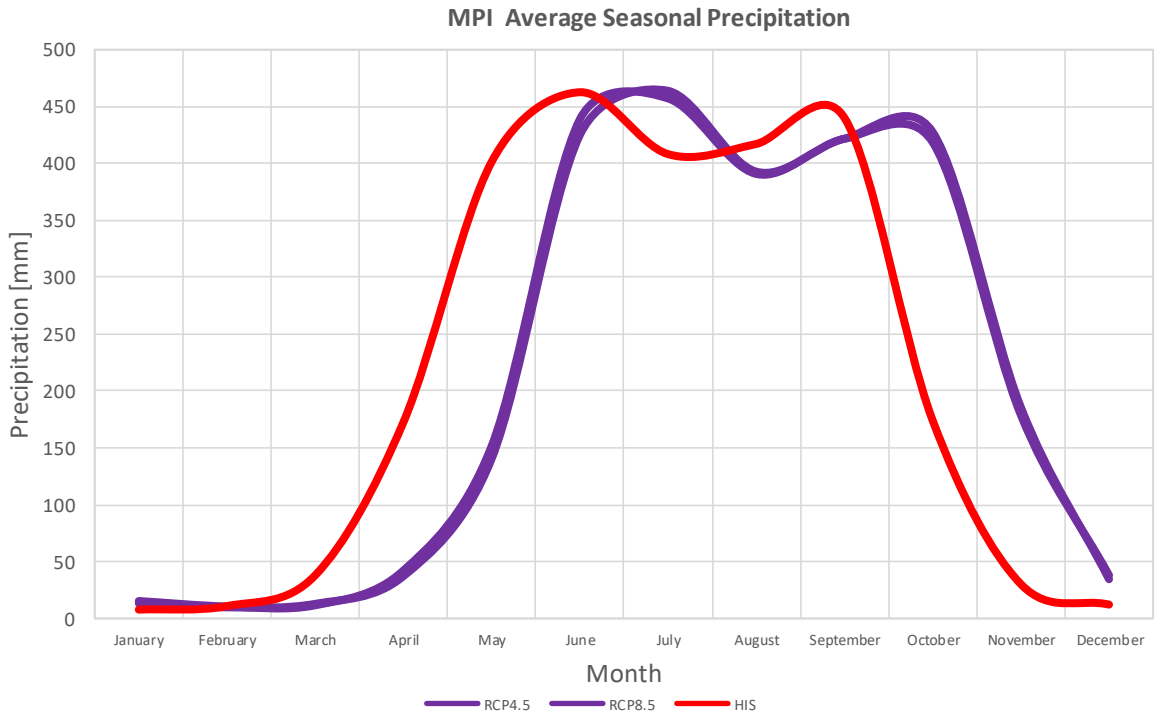

F3c: RCM MPI, seasonal precipitation cycle, historical [1970-2005] versus future [2006-2099] output, all stations average.

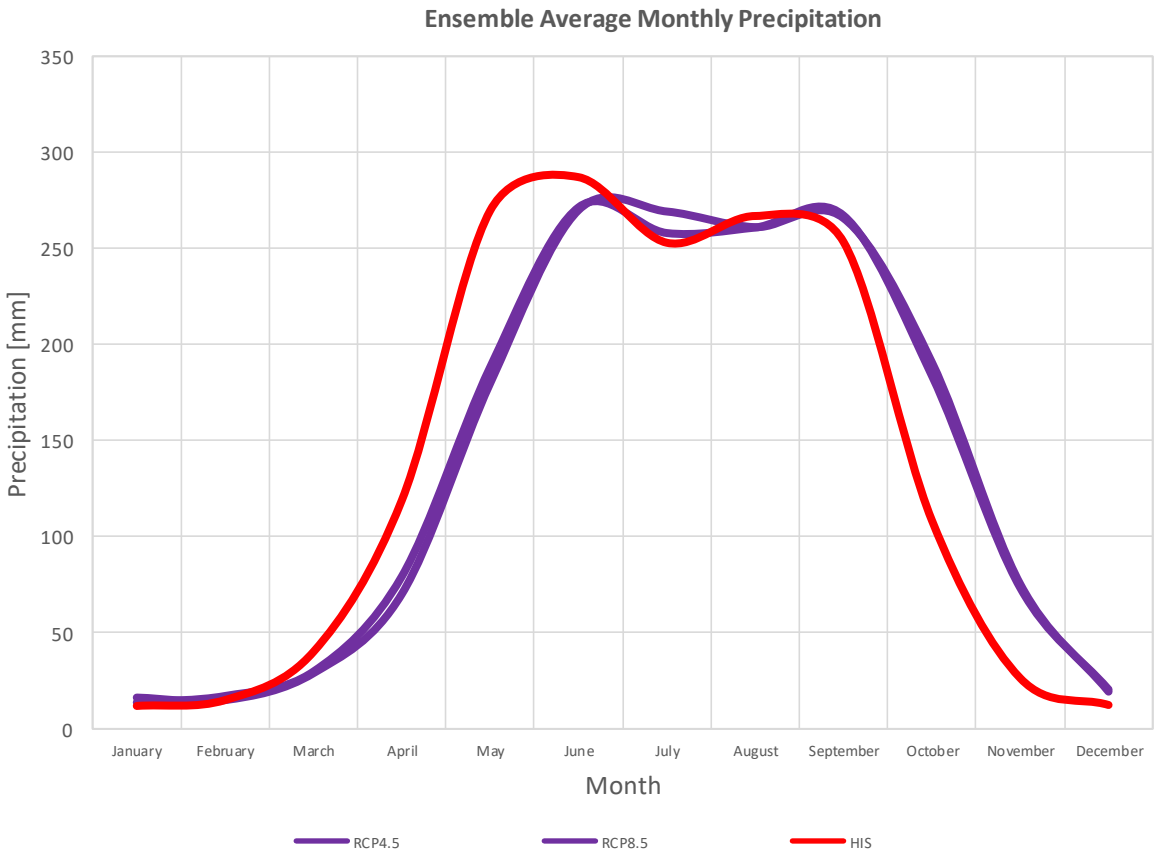

F3d: RCM Ensemble, seasonal precipitation cycle, historical [1970-2005] versus future [2006-2099] output, all stations average.

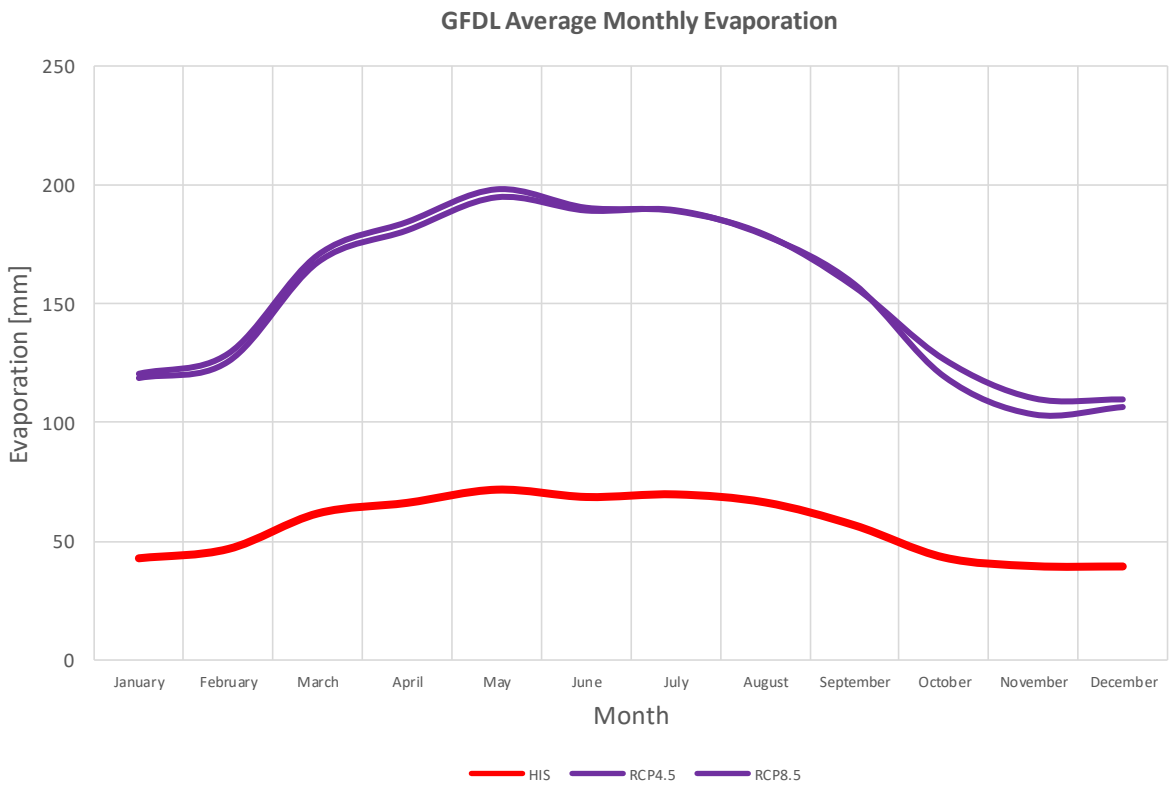

F4a: RCM GFDL, seasonal evaporation cycle, historical [1970-2005] versus future [2006-2099] output, all stations average.

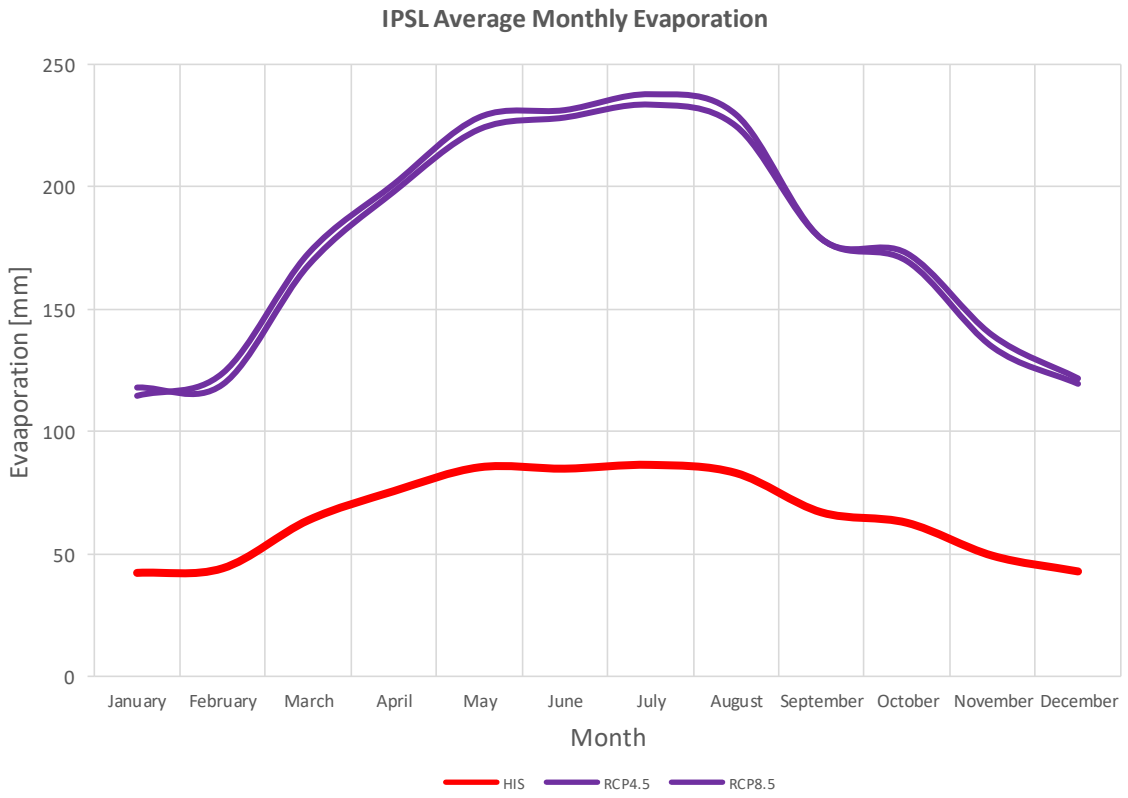

F4b: RCM IPSL, seasonal evaporation cycle, historical [1970-2005] versus future [2006-2099] output, all stations average.

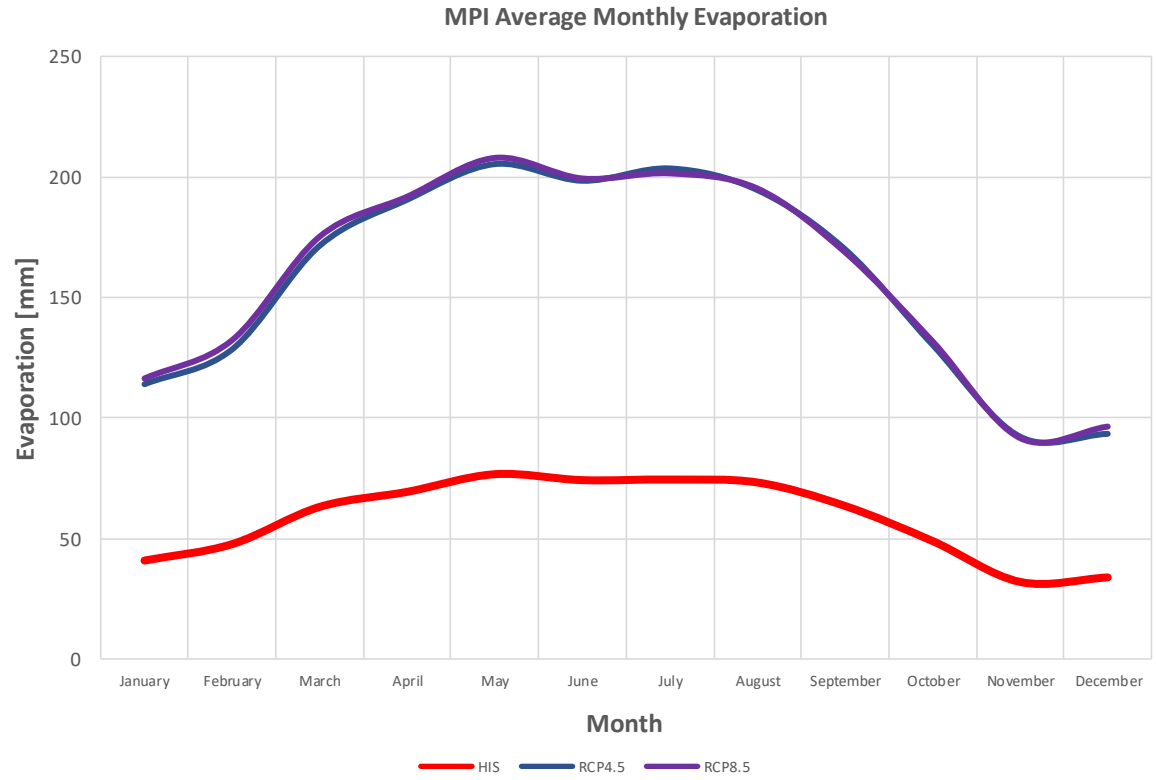

F4c: RCM MPI, seasonal evaporation cycle, historical [1970-2005] versus future [2006-2099] output, all stations average.

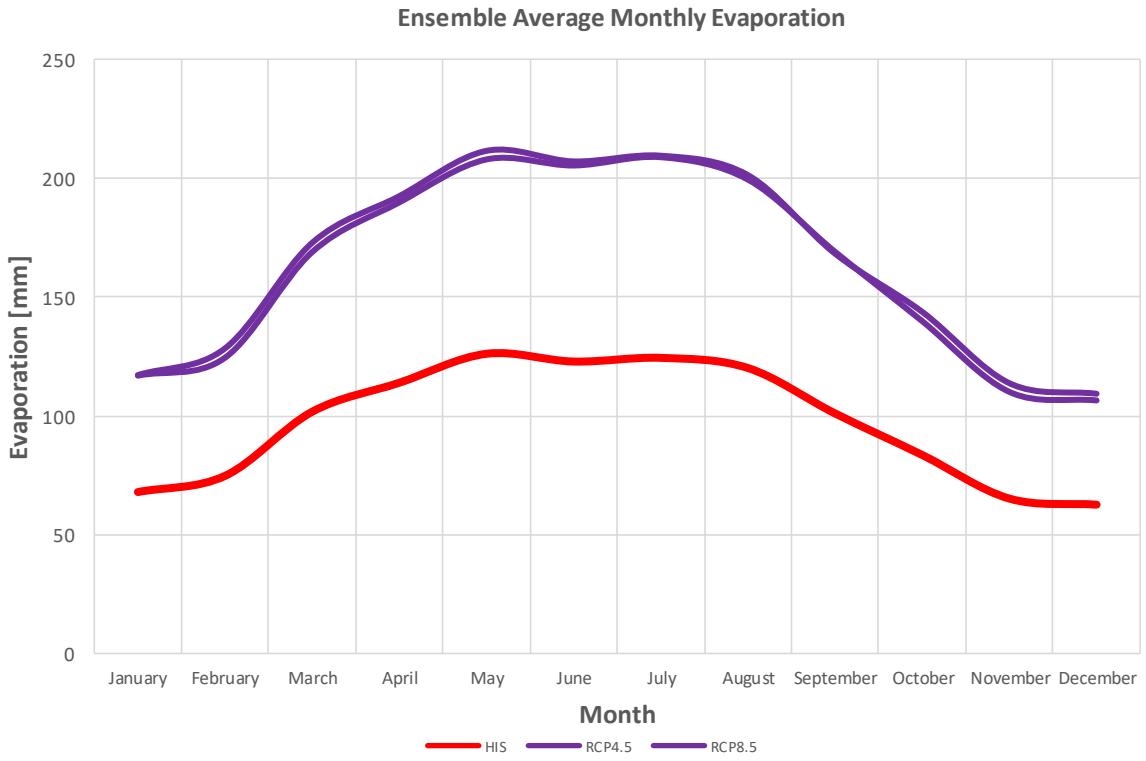

F4d: RCM Ensemble, seasonal evaporation cycle, historical [1970-2005] versus future [2006-2099] output, all stations average.

Appendix G: Meteorological model input

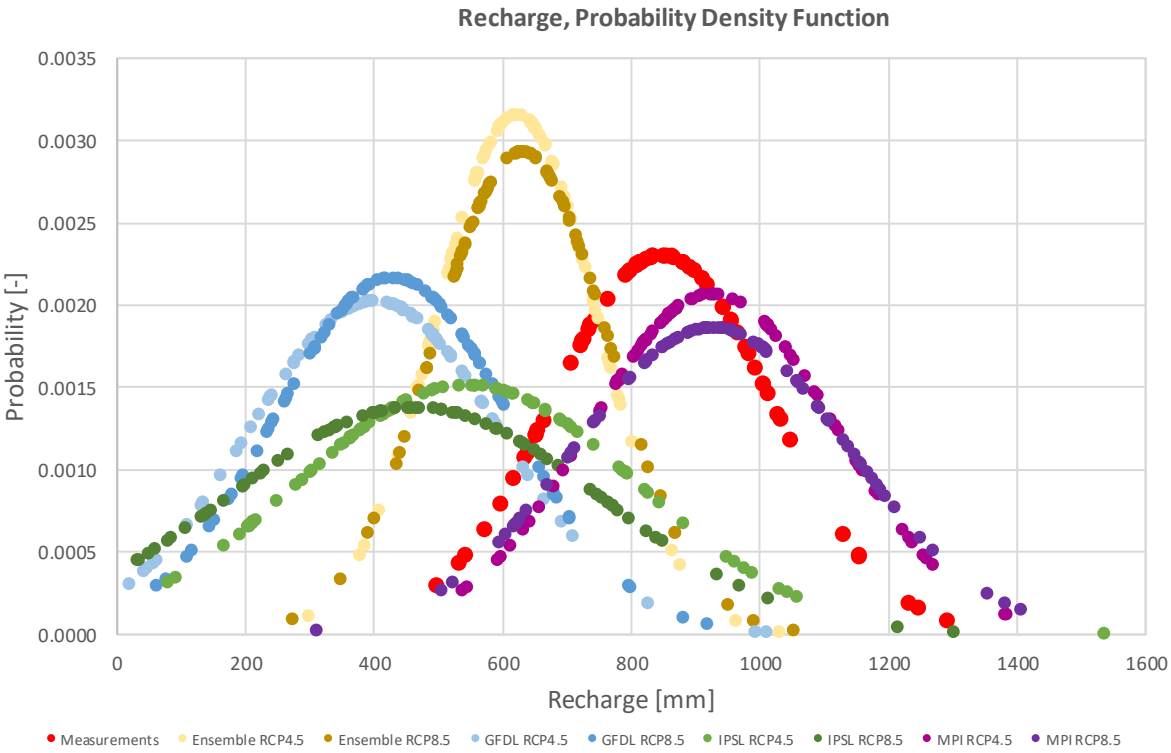

G1a: Probability density function, recharge, measurements [1951-2017] versus RCP4.5 & RCP8.5 [2018-2099].

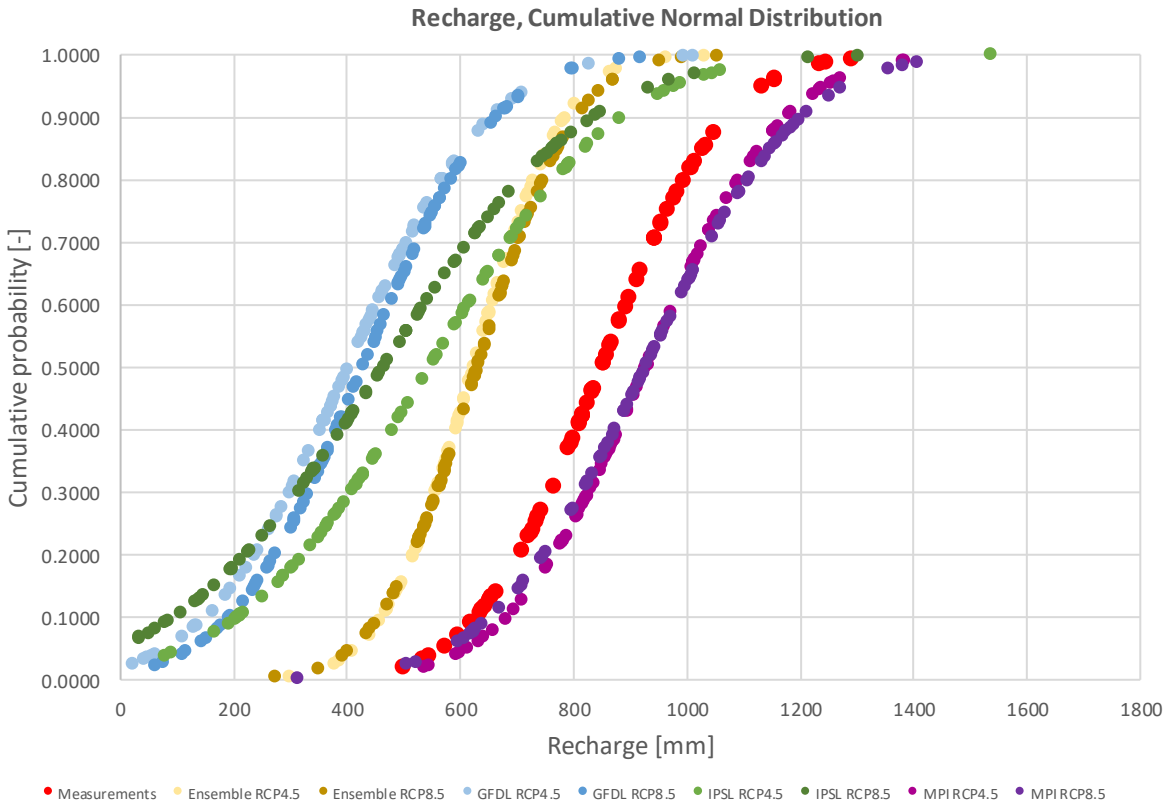

G1b: Cumulative normal distribution, recharge, measurements [1951-2017] versus RCP4.5 & RCP8.5 [2018-2099].

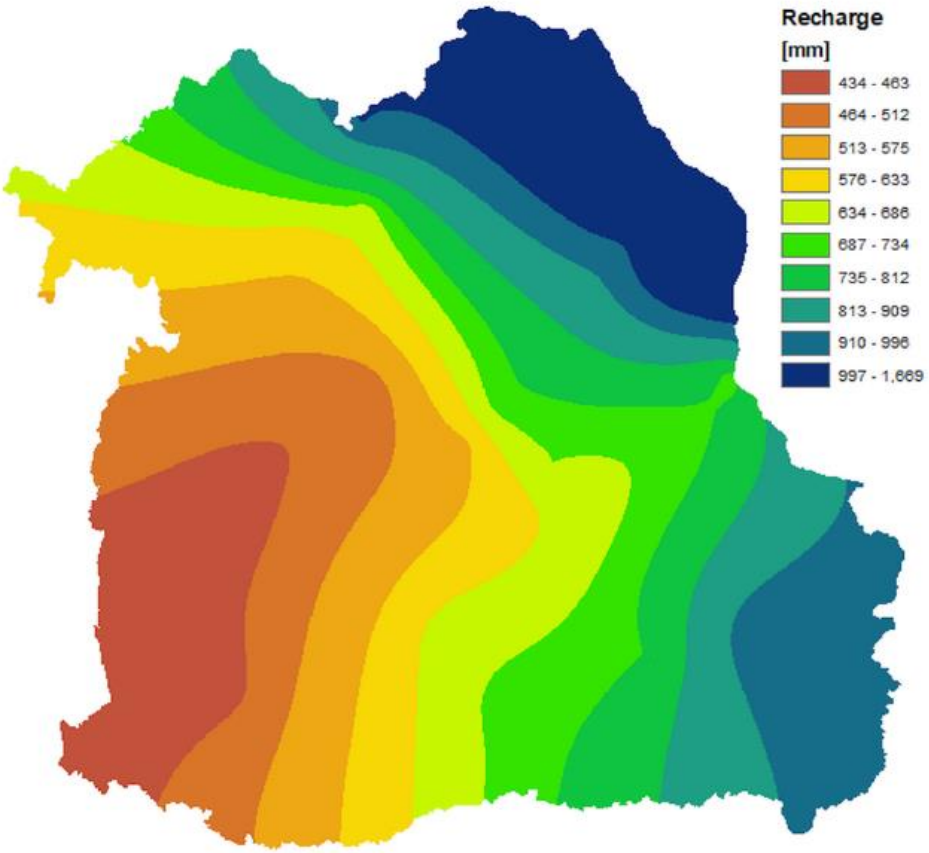

G2a: Spatial representation of recharge throughout Isan for RCP4.5, 2050.

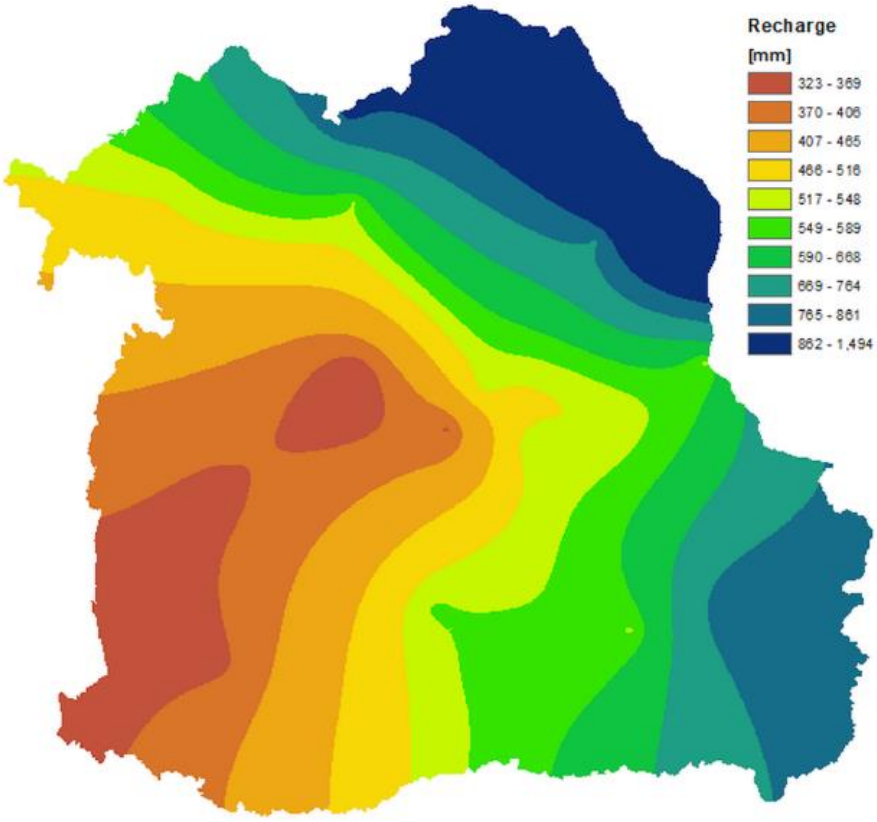

G2b: Spatial representation of recharge throughout Isan for RCP4.5, 2100.

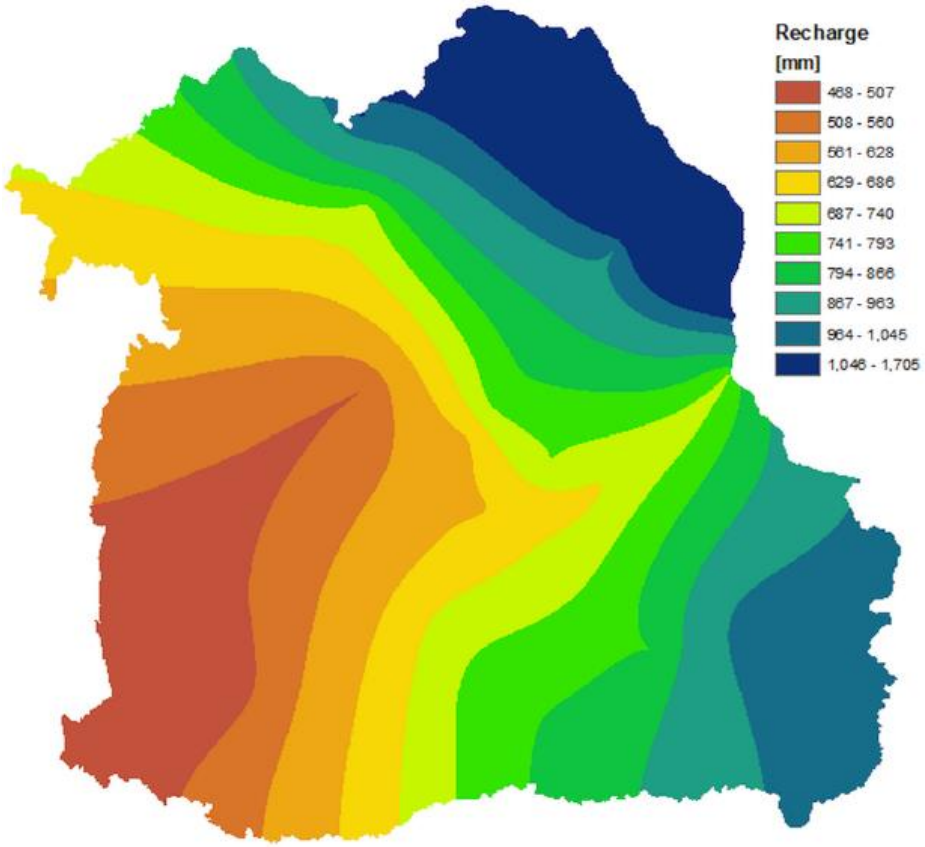

G2c: Spatial representation of recharge throughout Isan for RCP8.5, 2050.

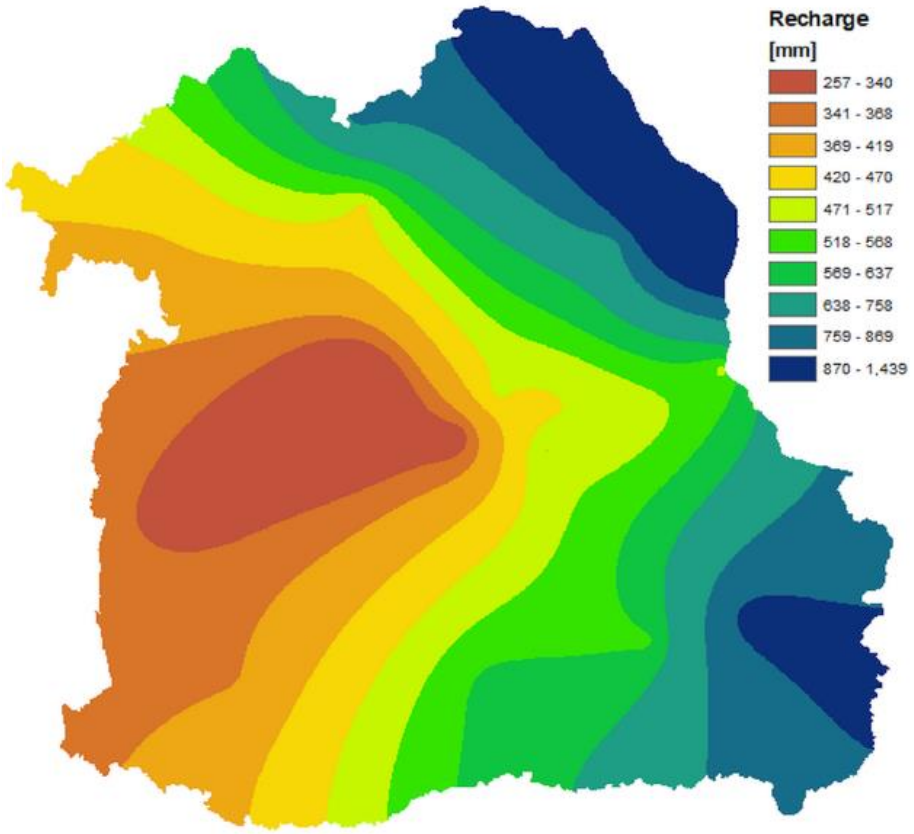

G2d: Spatial representation of recharge throughout Isan for RCP8.5, 2100.

	GFDL						IPSL						MPI						Ens					
RCP	4.5			8.5			4.5			8.5			4.5			8.5			4.5			8.5		
Location	1951 - 2001	2002 - 2050	2051 - 2099	1951 - 2001	2002 - 2050	2051 - 2099	1951 - 2001	2002 - 2050	2051 - 2099	1951 - 2001	2002 - 2050	2051 - 2099	1951 - 2001	2002 - 2050	2051 - 2099	1951 - 2001	2002 - 2050	2051 - 2099	1951 - 2001	2002 - 2050	2051 - 2099	1951-2001	2002 - 2050	2051 - 2099
Surin	733	533	247	733	612	373	733	640	402	733	693	269	733	1020	943	733	1080	1010	733	700	558	733	788	599
Ubon Ratchathani	1062	939	784	1062	1027	897	1062	1085	961	1062	1090	916	1062	1025	863	1062	1043	908	1062	993	854	1062	1044	936
Roi Et	858	571	393	858	641	407	858	667	412	858	676	260	858	836	765	858	882	715	858	688	548	858	743	520
Mukdahan	822	566	378	822	608	383	822	821	622	822	842	386	822	807	694	822	858	634	822	689	530	822	733	489
Kalasin	790	600	356	790	661	341	790	690	374	790	713	196	790	904	810	790	958	744	790	729	540	790	786	490
Khon Kean	599	329	123	599	375	89	599	504	280	599	509	126	599	634	607	599	687	517	599	462	323	599	507	257
Mahasarakham	661	429	176	661	482	156	661	539	237	661	537	80	661	712	638	661	776	566	661	547	360	661	600	308
Buriram	847	481	247	847	544	240	847	655	402	847	697	318	847	910	943	847	996	889	847	671	558	847	719	491
Nakhon Ratchasima	542	304	138	542	329	146	542	490	432	542	506	447	542	623	638	542	660	594	542	440	357	542	468	356
Sisaket	892	553	297	892	619	334	892	856	620	892	902	511	892	913	799	892	969	780	892	732	537	892	794	541
Sakon Nakhon	832	824	622	832	873	594	832	822	496	832	842	267	832	1023	912	832	1070	848	832	918	743	832	962	683
Nakhon Phanom	1679	1497	1281	1679	1558	1246	1679	1512	1112	1679	1515	846	1679	1885	1810	1679	1900	1768	1679	1670	1495	1679	1706	1440
Udon Thani	718	480	282	718	543	205	718	564	322	718	544	87	718	873	909	718	957	835	718	648	540	718	711	449
Loei	675	481	250	675	533	219	675	607	321	675	541	164	675	881	912	675	943	774	675	653	520	675	696	434
Chaiyaphum	496	182	0	496	229	0	496	530	435	496	571	423	496	800	937	496	877	880	496	434	360	496	488	329
Nong Khai	945	815	626	945	870	560	945	915	619	945	852	359	945	1272	1283	945	1325	1198	945	1015	896	945	1056	802
Nong Bua Lamphu	N/A	367	249	N/A	442	201	N/A	448	296	N/A	432	123	N/A	913	945	N/A	1045	868	N/A	590	525	N/A	674	451
Average	822	585	378	822	644	374	822	726	491	822	733	340	822	943	906	822	1002	855	822	740	603	822	793	563

G3: Recharge averages used for interpolation.

Appendix H: Hydrological model results

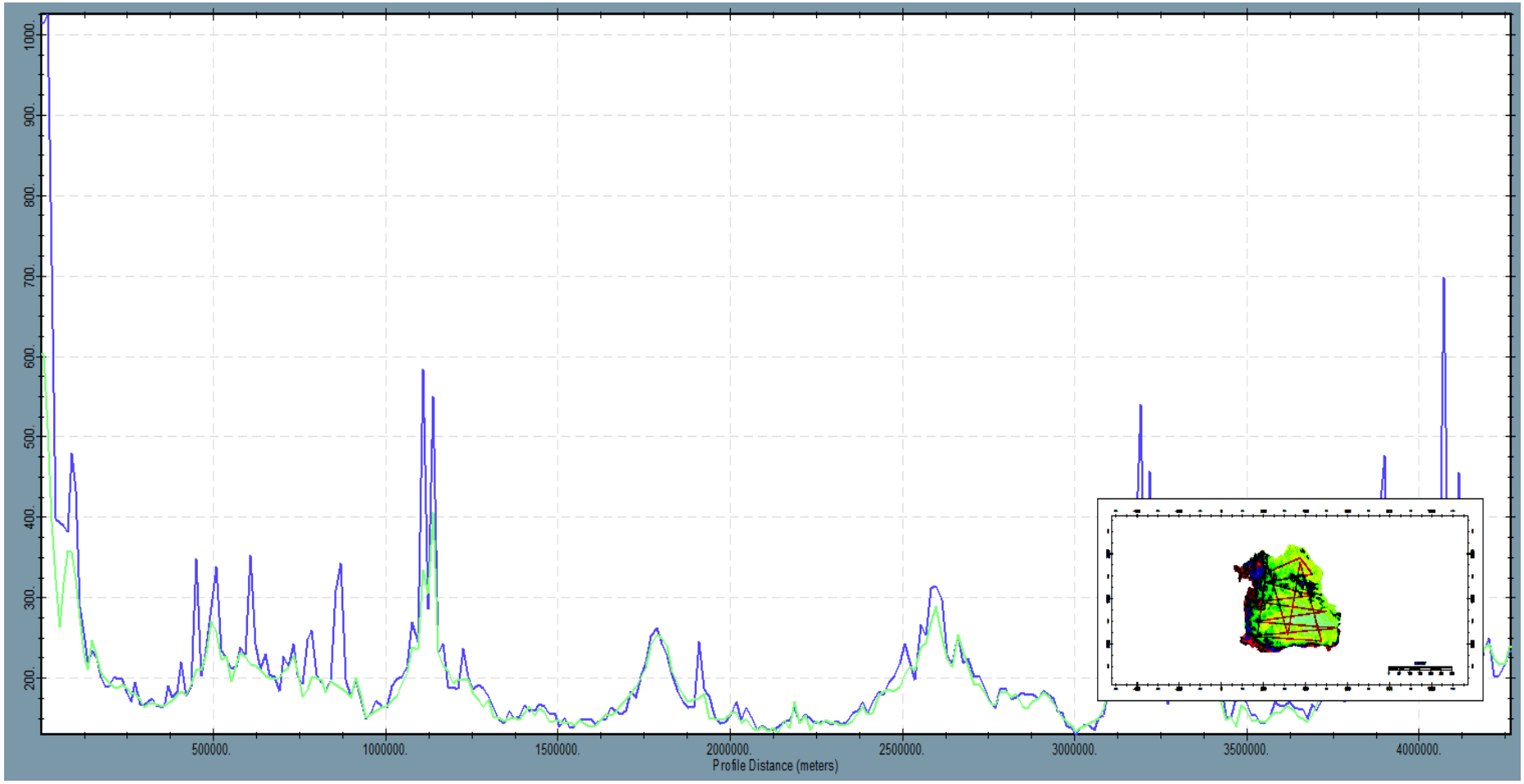

H1: DEM (blue) compared to measured hydraulic head (green); cross section covering the entire research area, units in meters.

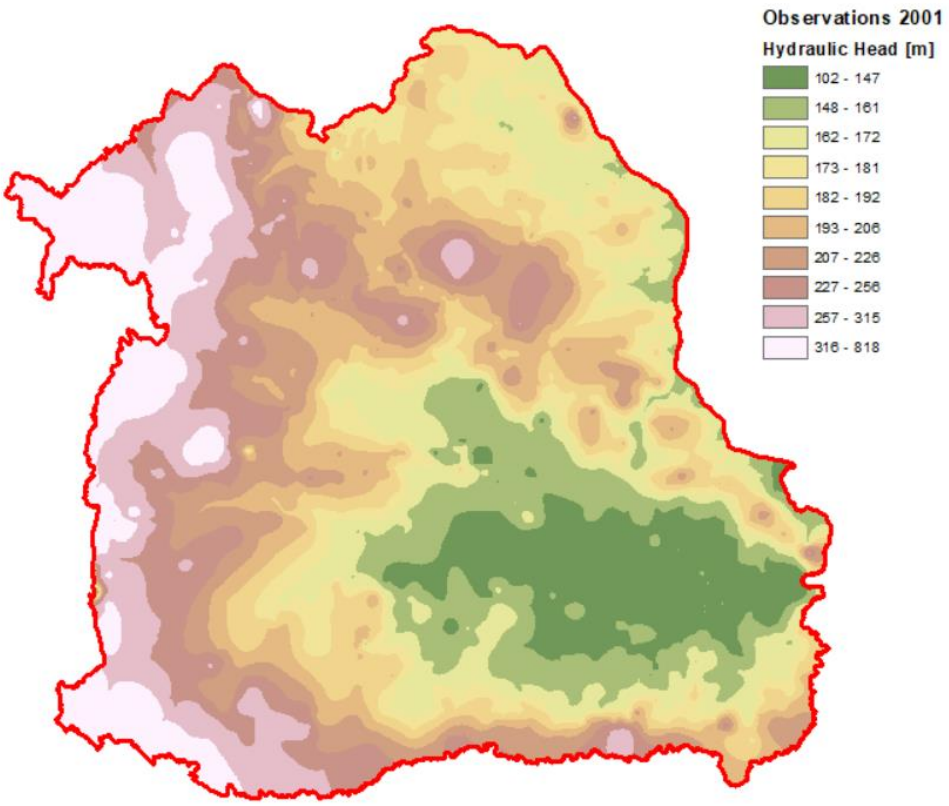

H2a: Observed hydraulic head, 2001.

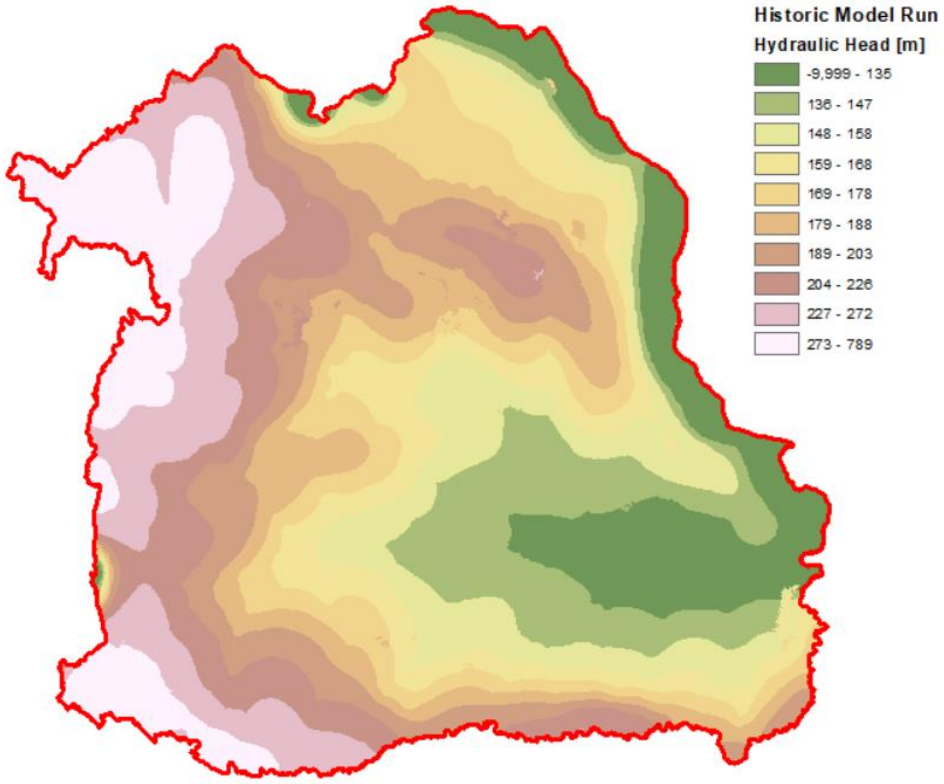

H2b: Modelled hydraulic head, 2001.

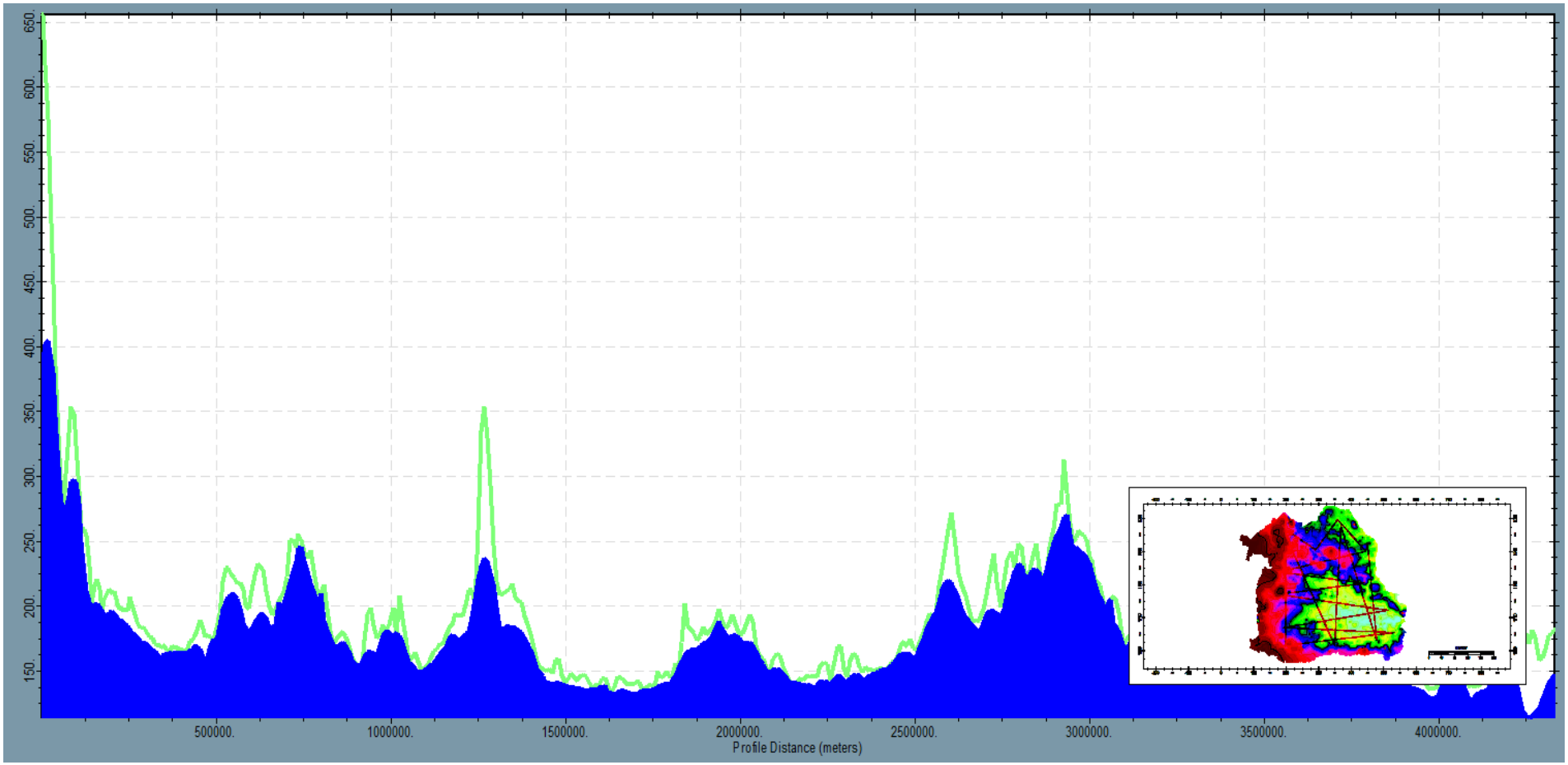

H3: Hydraulic head (m), historic model run (blue) versus measurements (green); cross section covering the entire research area.

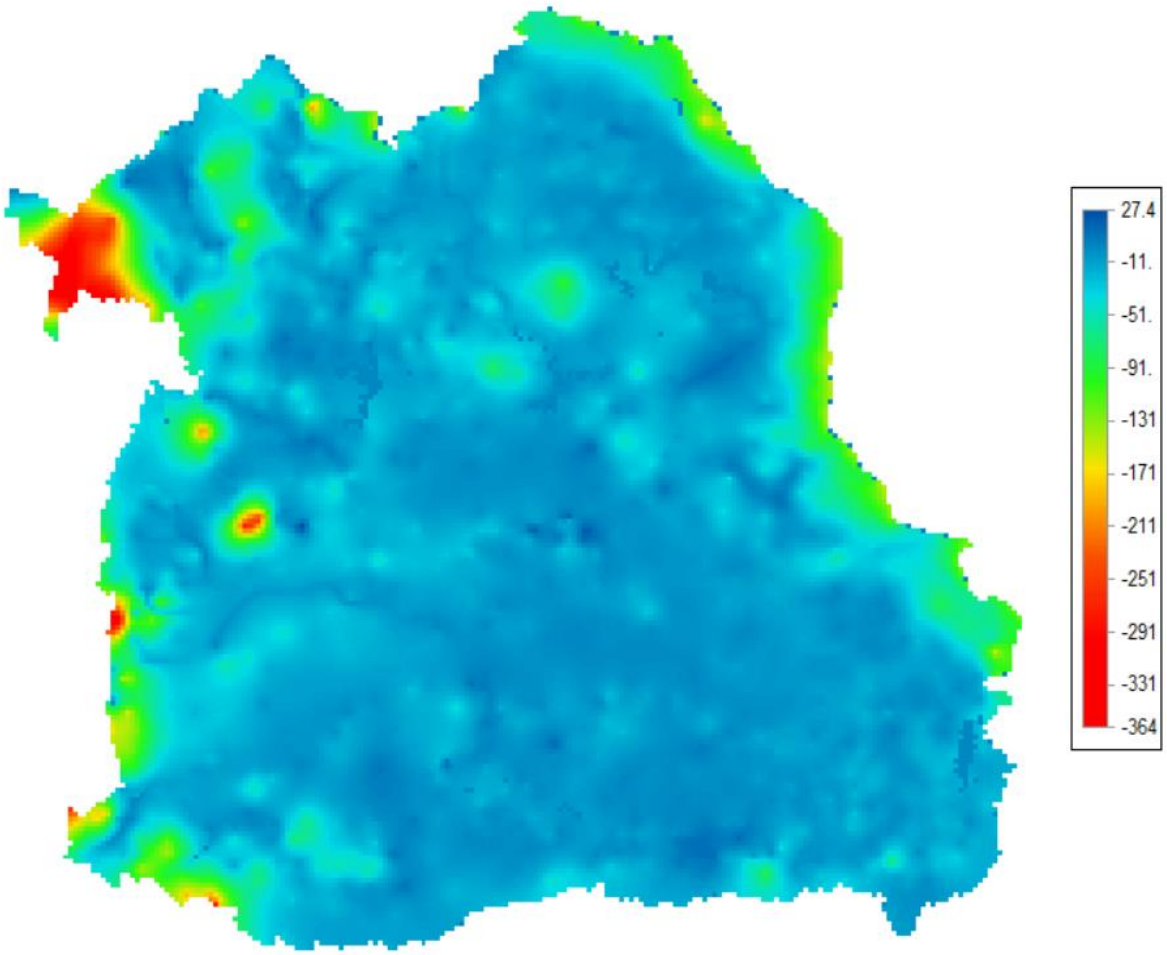

H4a: Relative difference in head between the historic model run and measurement data, in meters.

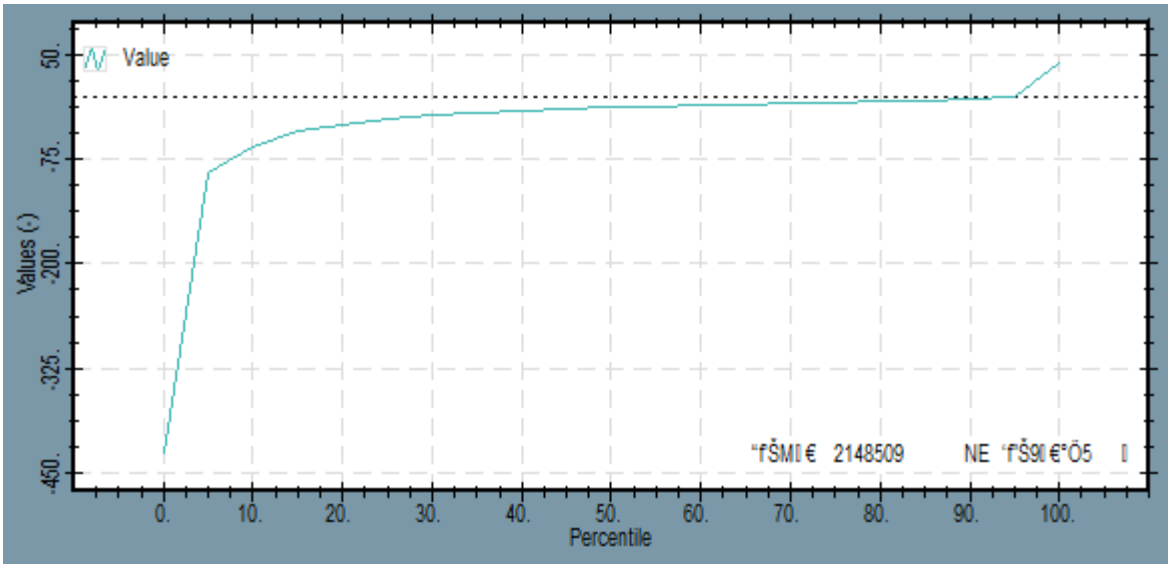

H4b: Cumulative distribution for the relative difference in head (m) between historic model run and measurement data.

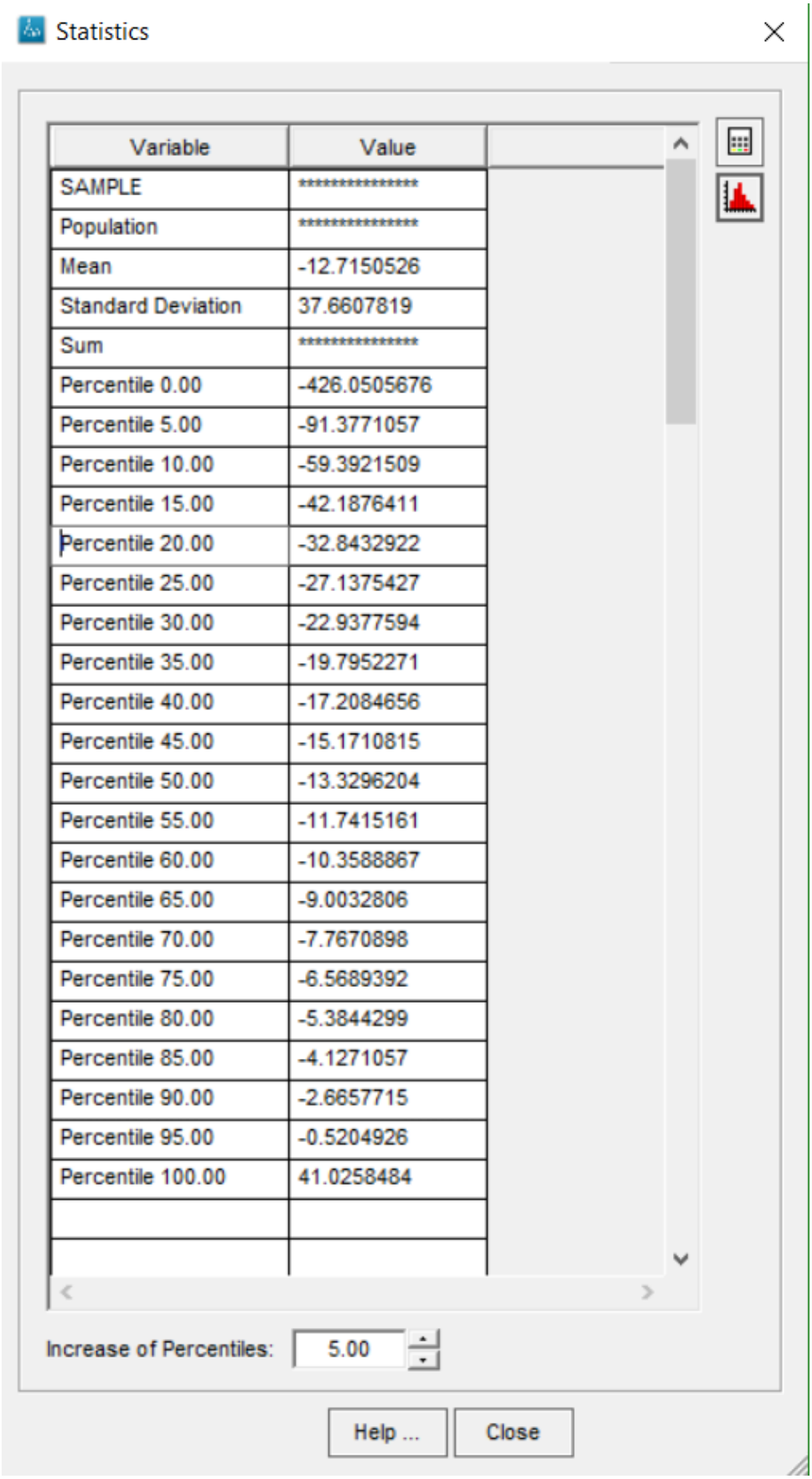

H4c: Mean, standard deviation and percentile distribution, in meters, for the relative difference in head between historic model run and measurement data.

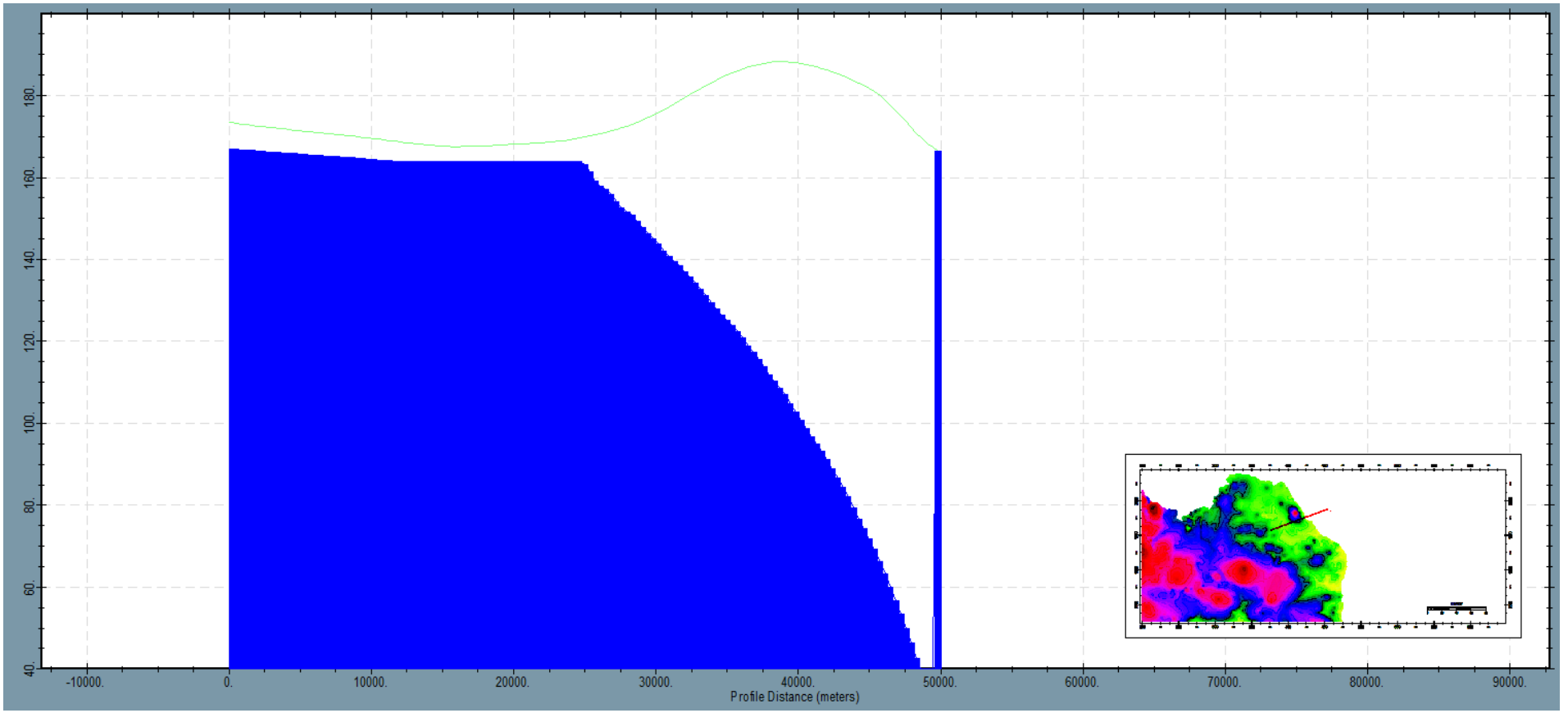

H5: The modelled hydraulic head (blue) versus the measured hydraulic head (green), in meters, showing an unlikly drop in head along the fringes of the Mekong boarded part of Isaan.

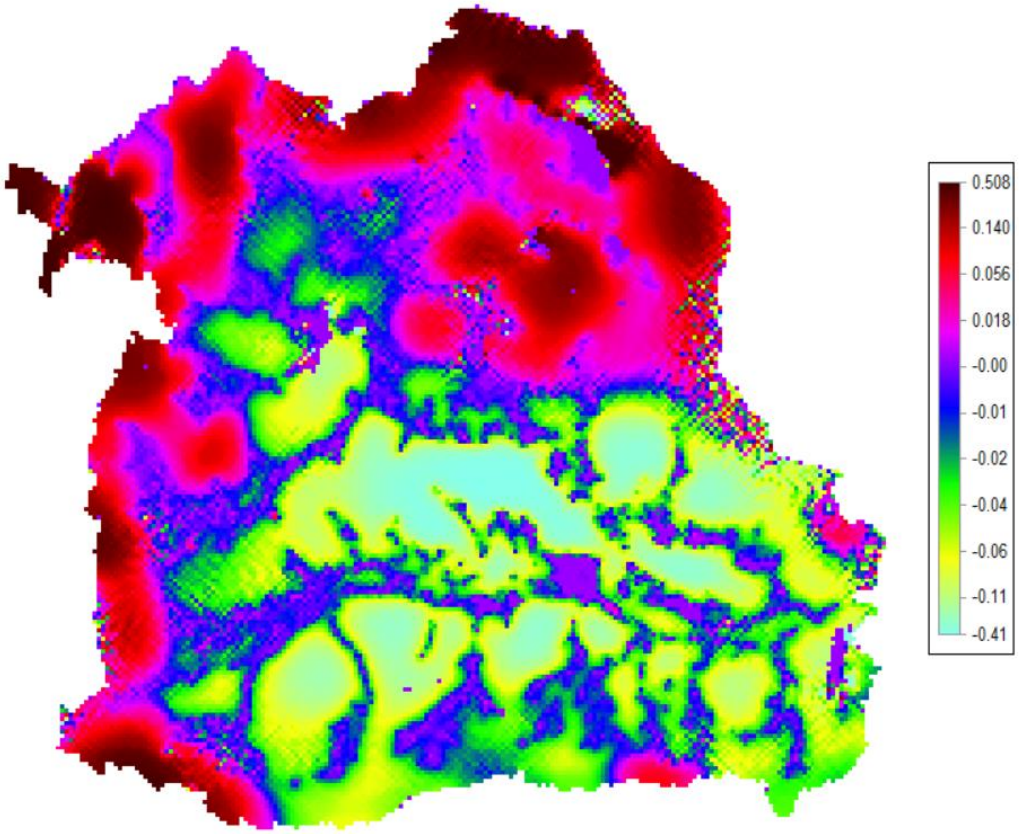

H6a: Difference historic run and Ensemble RCP4.5, 2050, in meters.

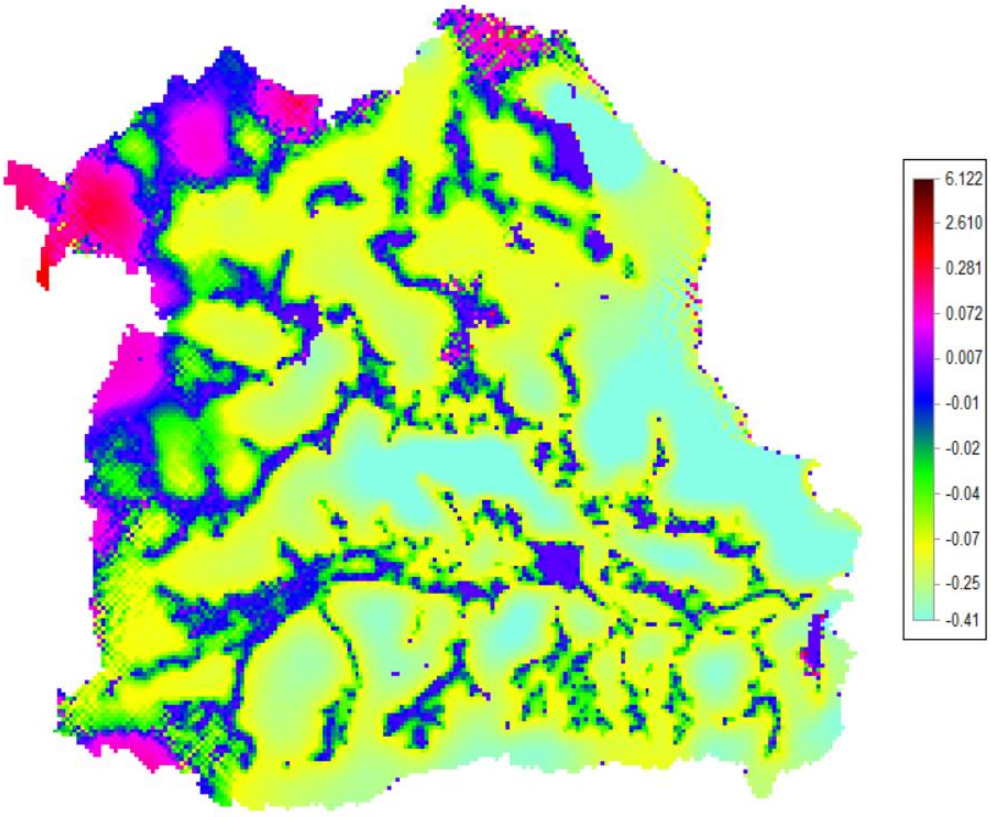

H6b: Difference historic run and Ensemble RCP4.5, 2100, in meters.

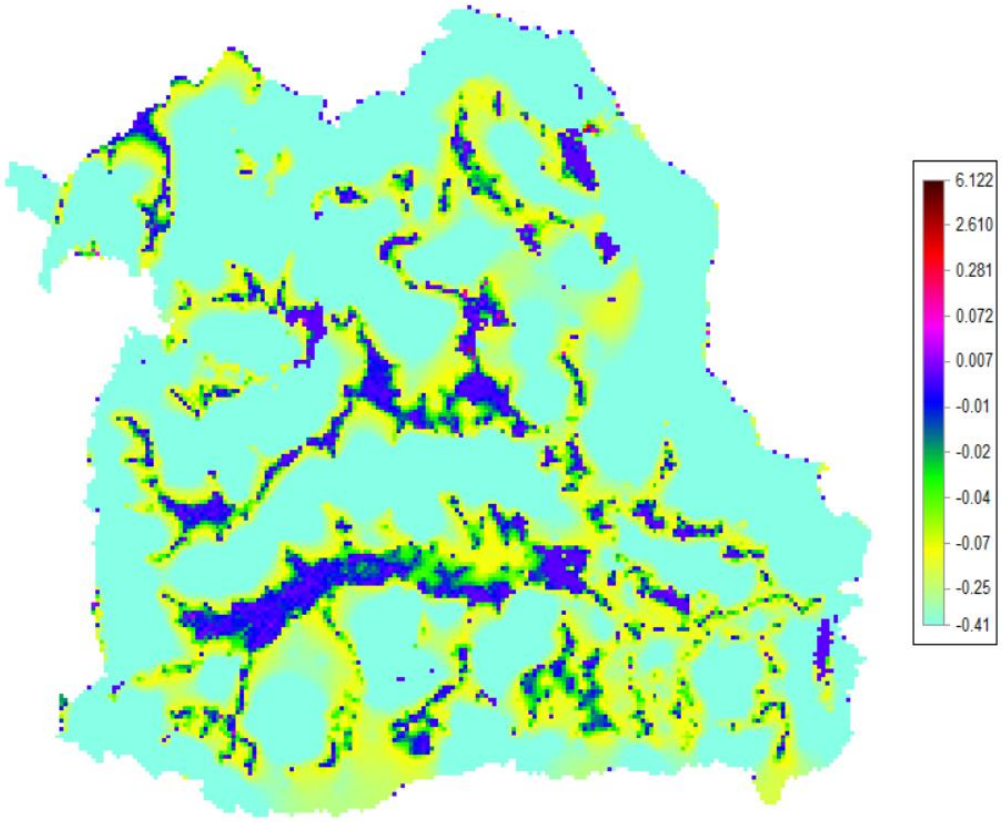

H7a: Difference historic run and Ensemble RCP8.5, 2050, in meters.

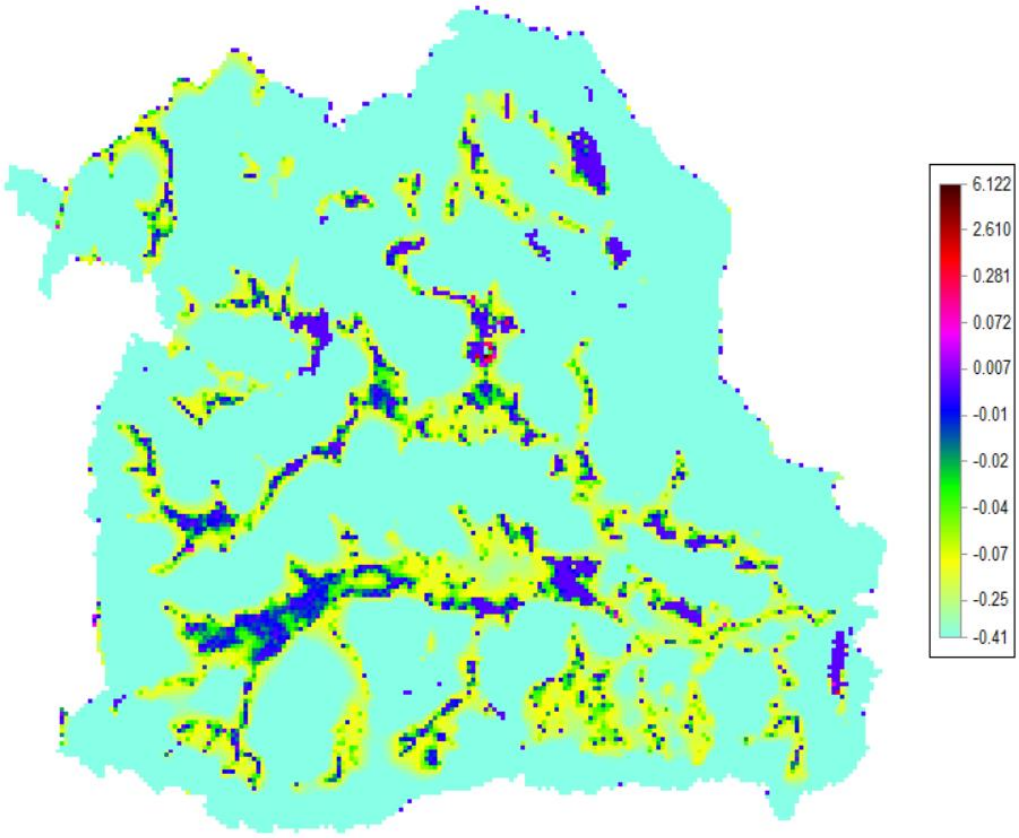

H7b: Difference historic run and Ensemble RCP8.5, 2100, in meters.

Lecture VI - P.G.W.F - 29/09/2017 - Ruud Schotting

Unconfined aquifer

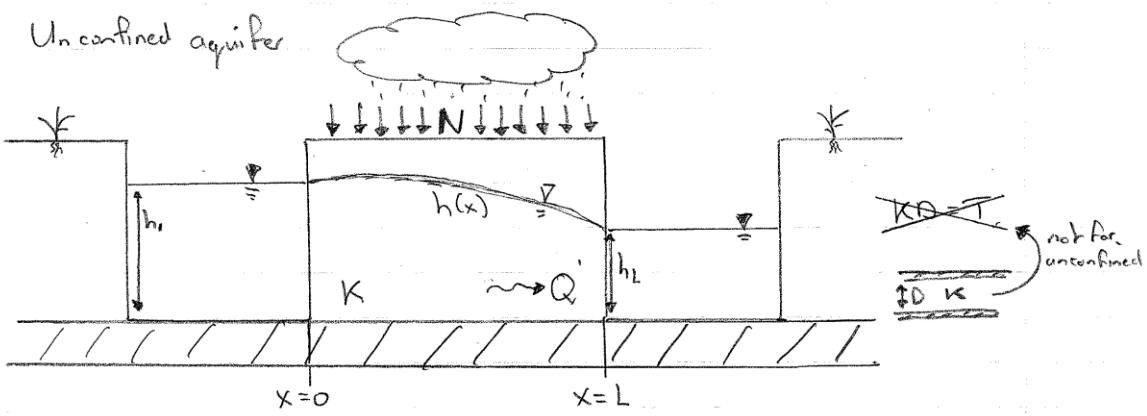

1.) $Q = D \cdot q \rightarrow Q = hq$
D = not constant = height water table (h)

2.) $\frac{dQ'}{dx} = N$

3.) $q = -K \frac{dh}{dx}$

$Q' = -Kh\left(\frac{dh}{dx}\right)$

$\frac{d}{dx}\left(-Kh\left(\frac{dh}{dx}\right)\right) = N$

$-K \frac{d}{dx}\left(h \frac{dh}{dx}\right) = N$

$\frac{d}{dx}\left(h \frac{dh}{dx}\right) = -N/K$

* Intermezzo:

$h \frac{dh}{dx}$ = product $\rightarrow h \frac{d}{dx}\left(\frac{dh}{dx}\right) + \frac{dh}{dx}\left(\frac{dh}{dx}\right) \rightarrow h \frac{d^2h}{dx^2} + \left(\frac{dh}{dx}\right)^2$ (2de graads dev) (1ste graads dev^2)

* $\frac{d}{dx}\left(h \frac{dh}{dx}\right) = \frac{d}{dx}\left(\frac{1}{2} \frac{dh^2}{dx}\right)$; $h\,dh/dx = \frac{1}{2} \frac{dh^2}{dx}$ (d integreren, d differ.)

$dx\left(\frac{d}{dx}\left(h \frac{dh}{dx}\right)\right) = \left(-\frac{N}{K}\right) dx \rightarrow \int d\left(h \frac{dh}{dx}\right) = \int -\frac{N}{K}\,dx$

$h \frac{dh}{dx} = -\frac{N}{K} x + C_1$

$dx\left(h \frac{dh}{dx} = -\frac{N}{K} x + C_1\right) \rightarrow \int h\,dh = \int -\frac{N}{K} x\,dx + \int C_1\,dx$

$\frac{1}{2} h^2 = -\frac{1}{2} \frac{N}{K} x^2 + C_1 x + C_2$

$\downarrow$

$\boxed{h^2 = -\frac{N}{K} x^2 + 2C_1 x + 2C_2}$ g.s.

B.C. ①: $h(0) = (h_0) \rightarrow h_0^2 = 0 + 0 + 2C_2 \rightarrow C_2 = \frac{1}{2} h_0^2$

②: $h(L) = h_L \rightarrow h_L^2 = -\frac{N}{K} L^2 + 2C_1 L + h_0^2 \rightarrow C_1 = \frac{(h_L^2 - h_0^2)}{2L} + \frac{N}{2K} \cdot L$

thus: $\boxed{h^2(x) - h_0^2 = -\frac{N}{K}(x^2 - xL) + \frac{(h_L^2 - h_0^2)}{L} x}$

26

H8: Derivation of Hooghoudt's empirical equation for the calculation of the change in hydraulic head with a specified recharge input for unconfined aquifers.

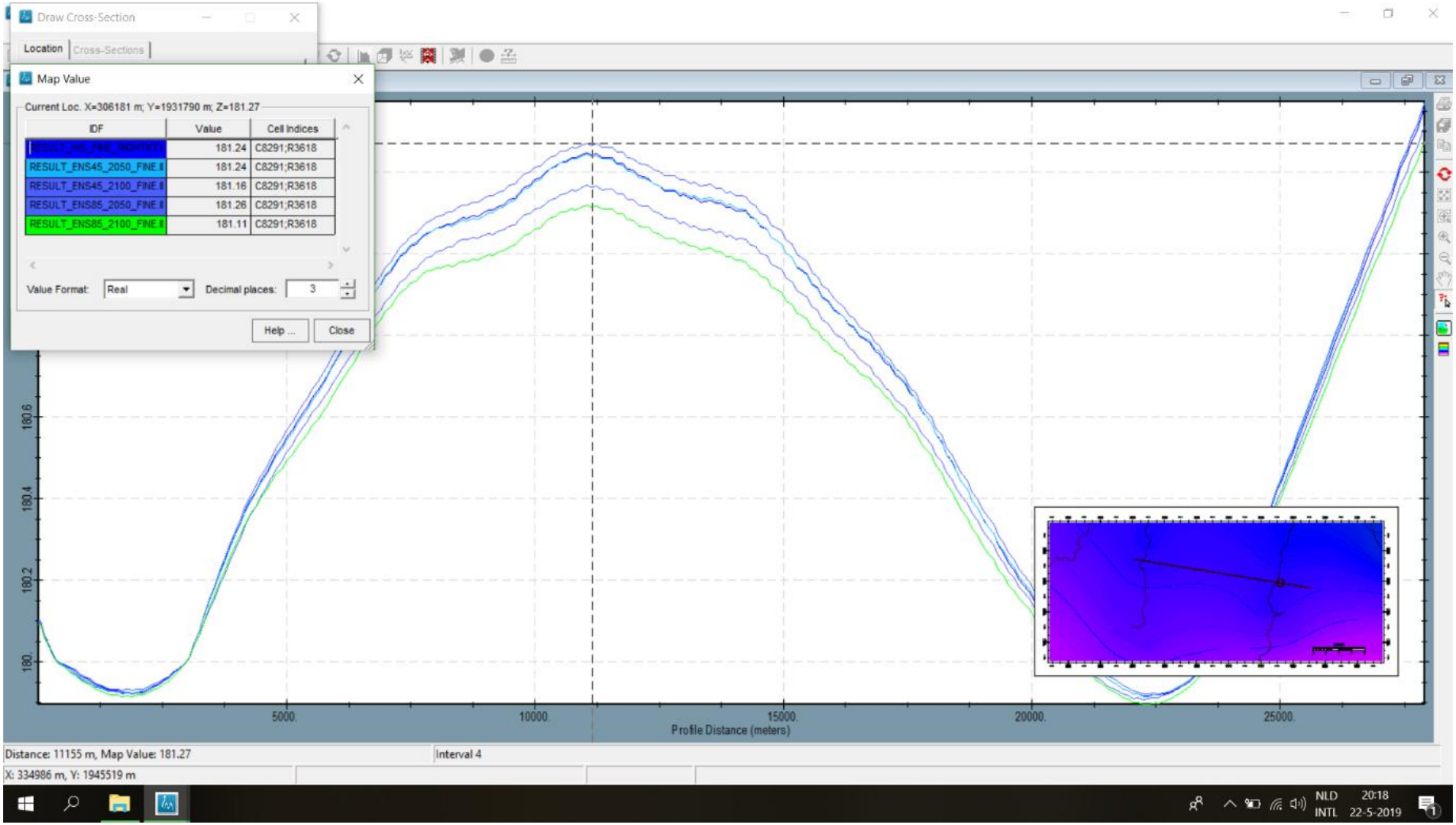

H9a: Random cross-section between two river tributaries showing values for the modelled historic hydraulic head (m) and all RCP scenarios.

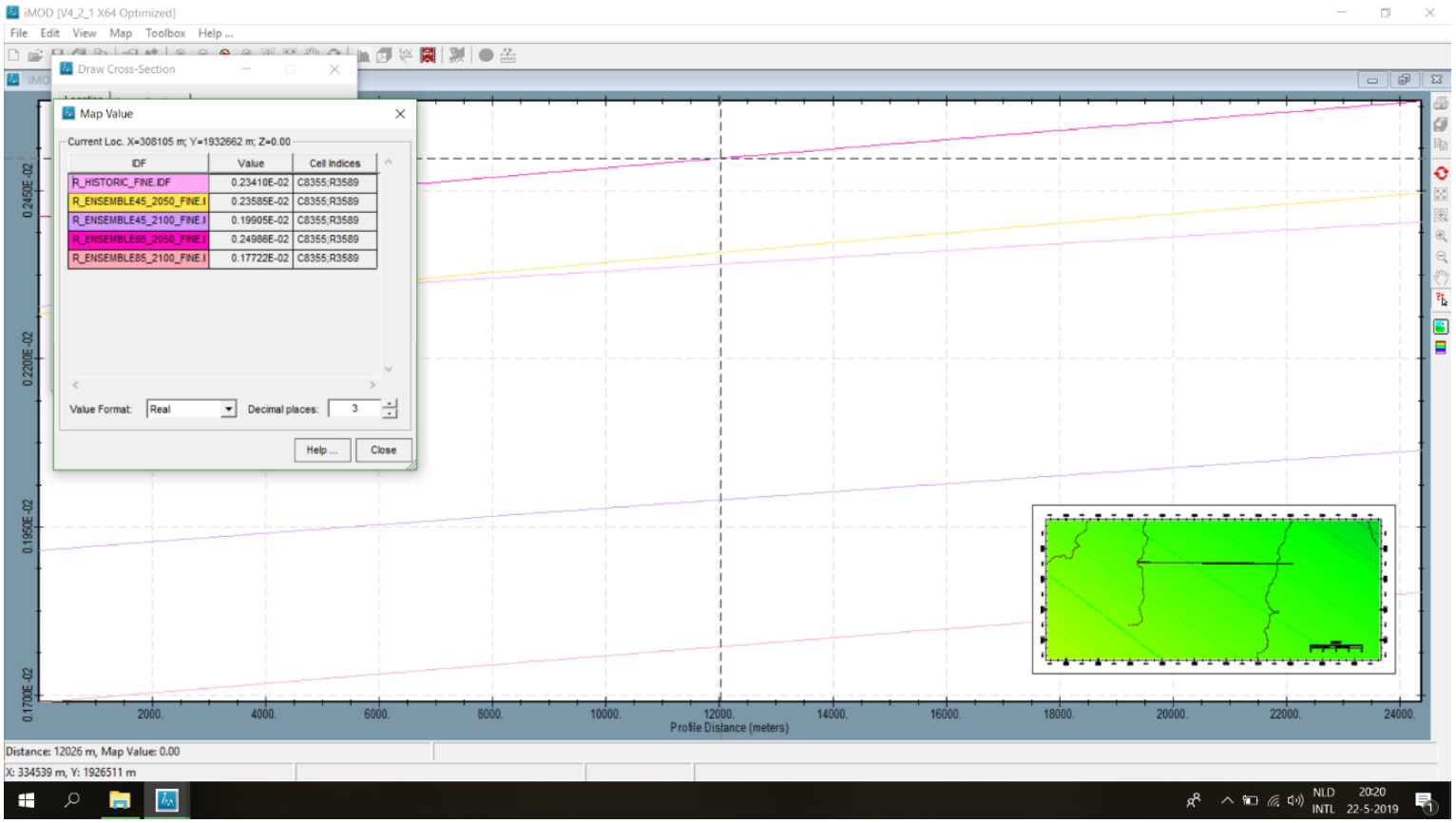

H9b: For the same cross-section as presented in G9a, the change in recharge (m/day) for the modelled historic period and all RCP scenarios.

		Historic	RCP4.5		RCP.8.5				
x	**L**	**N (2001)**	**N (2050)**	**N (2099)**	**N (2050)**	**N (2099)**	**h_L**	**h_0**	**k**
[m]	**[m]**	**[m/d]**	**[m/d]**	**[m/d]**	**[m/d]**	**[m/d]**	**[m]**	**[m]**	**[m/d]**
10313	20625	0.0023	0.0024	0.0020	0.0025	0.0018	179.9	179.9	1.215

H9c: Parameter input used to calculate the hydraulic head using Hooghoudt's empirical equation.

Appendix I: A-0 map

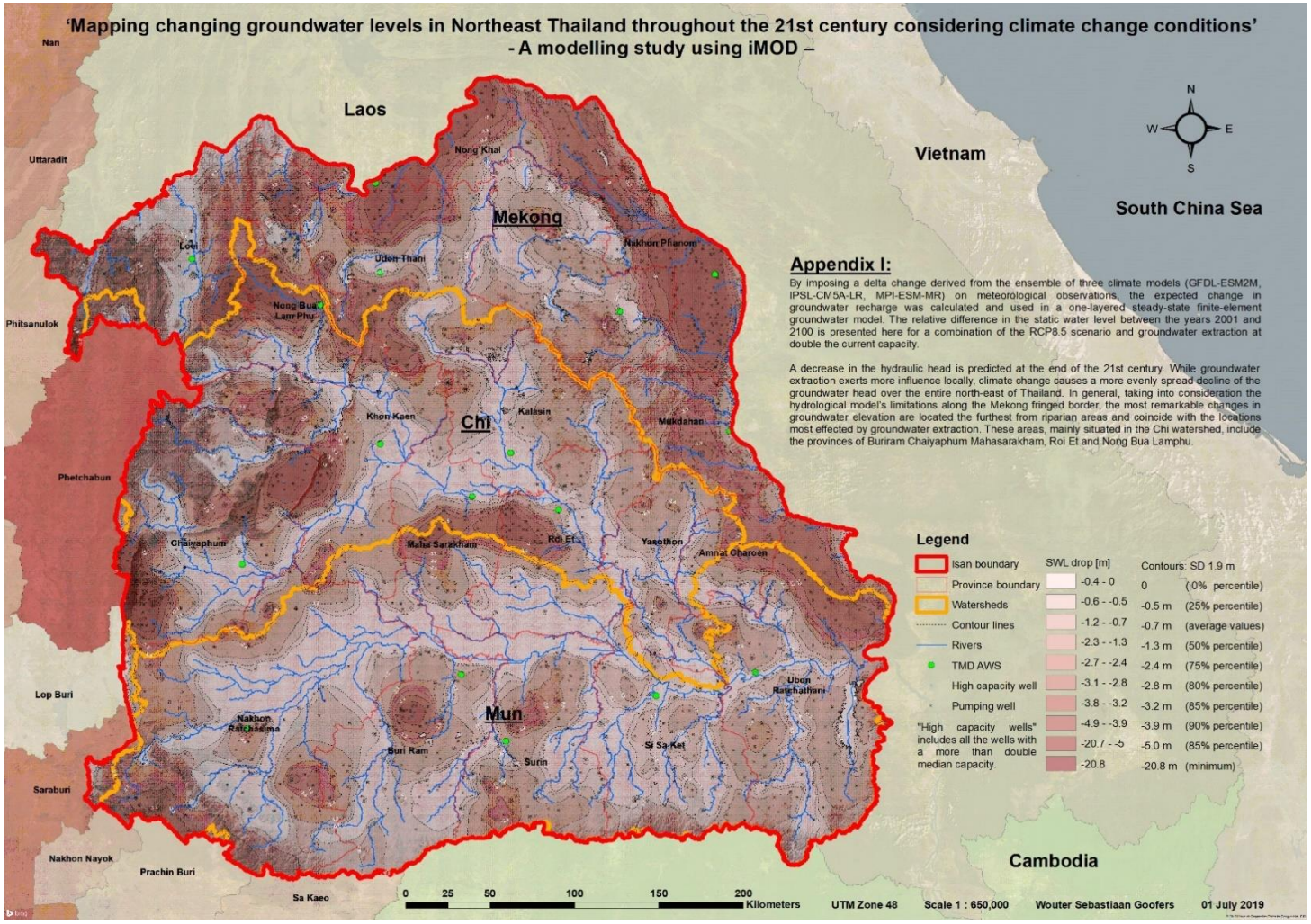

I: Thumbnail of the A0-poster showing the combined impact of pumping at double capacity and climate change scenario RCP8.5.

Appendix J: Discussion

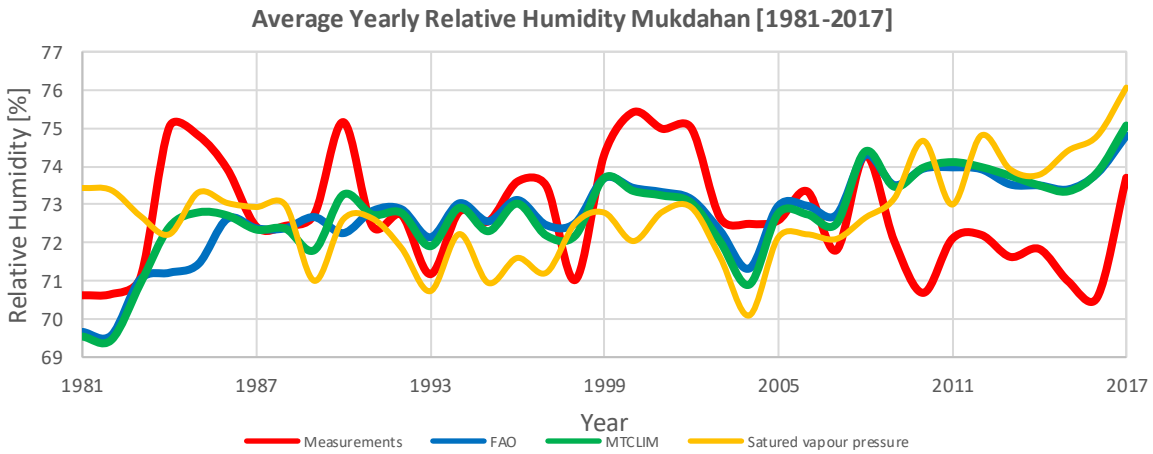

J1: FAO, MTCLIM and E_s output for the reconstruction of relative humidity, example site Mukdahan.

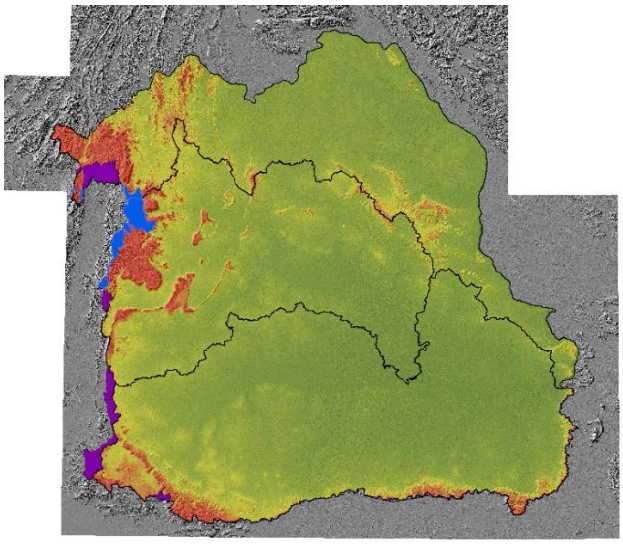

J2: Areas that contribute to the watersheds but are outside of the research area (blue) and areas that are part of the research area, but do not contribute to the watersheds (purple).

Rainy season: 1st of April until the 31st of October. Dry season: 1st of November until the 31st of March.

Average river discharge Mun-Chi: rainy season (7 months) average: 959 x 7 = **6713 m³/s.**

Average river discharge Mun-Chi: dry season (5 months) average: 367 x 5 = **1837 m³/s.**

Yearly average: (6713+1837) / 12 = **712.5 m³/s**

$$\frac{(712.5 * 60 * 60 * 24 * 365 = 22.469 \text{ MCM})}{(49.480+69.700 = 119.180 \text{ km}^2)} = 0.1885 * 1000 = \mathbf{188.5\ mm}.$$

Applying the same ratio between the Mekong and Chi/Mun watershed for river discharge as for potential runoff, then for the Mekong basin:

$$\frac{551}{(287+359)} = 0.85 * \frac{(6713+1837)}{12} = 608\ {}^{m^3}/_{s} * 60 * 60 * 24 * 365 = \frac{19174 \text{ MCM}}{46.460 \text{ km}^2} = 0.413 \text{ m} * 1000 = \mathbf{413\ mm}$$

J3: Average yearly river discharge calculation for the Mun-Chi and Mekong Watershed, data from Toda et al. (2004).